

The role of soil heterogeneity on field scale evapotranspiration: 3D integrative modelling and upscaling of root water uptake

Dissertation

zur

Erlangung des Doktorgrades (Dr. rer. nat.)

der

Mathematisch-Naturwissenschaftlichen Fakultät

der

Rheinischen Friedrich-Wilhelms-Universität Bonn

vorgelegt von

Katrin Huber

aus

Ingolstadt

Bonn 2014

Angefertigt mit Genehmigung der Mathematisch-Naturwissenschaftlichen Fakultät der Rheinischen
Friedrich-Wilhelms-Universität Bonn

1. Gutachter: Prof. Harry Vereecken
2. Gutachter: Prof. Bernd Diekkrüger

Tag der Promotion: 29.04.2015

Erscheinungsjahr: 2015

ABSTRACT

Background and Motivation: Hydrological models mainly rely on empirical functions to describe root water uptake. However, in case of water limitation due to either scarce or heterogeneously distributed soil water, plants have developed strategies to adapt. One short-term strategy is the regulation of stomatal aperture either by plant hydraulics or phyto-hormones. The latter are thought to act as a kind of sensor for dry soil. It can be assumed that hormones are produced locally in single root segments as function of low root water potentials. After being transported with the xylem stream they become effective in stomatal closure. Long-term adaptation strategies are mostly related to changes in carbon allocation within the plant and result in growth adaptations. Both strategies often remain insufficiently represented in hydrological models.

Methods: R-SWMS, a mechanistic soil and root water flow model that operates at the scale of a single root system was used to conduct a variety of virtual experiments. The model simulates three dimensional water flow through the soil, to, and within the roots. It was extended by a module to account for additional hormonal signalling, subsequently testing its influence in virtual split-root experiments. In a next step, direct mathematical relationships that link effective soil water potential and transpiration were derived. Considering the long-term adaptation strategies, the numerical model was modified to incorporate measured dynamic root architectures.

Results: Measured hormone concentrations in the leaves and some phenomena, like e.g. oscillations in stomatal aperture, were reproduced by the model. The direct relationships between soil water potential and transpiration showed that the stomatal behaviour depends on the underlying control and its parameterization. Experimental data, visualizing root systems over a 30 day growth period, were obtained from UFZ Halle, Germany, by CT scans. This dataset showed that plants grown under permanently limited water supply were considerably smaller with correspondingly less total water uptake compared to plants with initially unrestricted water resources. In combination with the numerical model, the flow dynamics in the soil-root system were resolved. The predicted location of root water uptake was found to be different from the measured zone of water depletion.

Conclusion: The implementation of bio-physical relationships into a mechanistic root soil model resulted in a powerful tool to identify key processes for plant water use in agricultural environments. This work provided new direct relationships between the effective soil water potential and transpiration rate in case stomata are controlled by hormones. In combination with an experimental dataset it gave new insights into water pathways within the soil-plant continuum.

ZUSAMMENFASSUNG

Hintergrund und Motivation: Hydrologische Modelle beschreiben Wurzelwasseraufnahme meist auf Basis von empirischen Funktionen. Für den Fall einer limitierten Bodenwasserverfügbarkeit, entweder durch Knappheit oder durch heterogene Verteilung, haben Pflanzen jedoch Strategien entwickelt, die es ihnen ermöglichen sich anzupassen. Eine kurzfristige Strategie ist die Regulierung der stomatären Leitfähigkeit entweder als Funktion des Pflanzenwasserpotentials oder von Phytohormonen. Letztere können als eine Art Sensor für trockenen Boden betrachtet werden. Man kann annehmen, dass Hormone lokal in einzelnen Wurzelsegmenten als Funktion eines niedrigen Wurzelwasserpotentials produziert werden. Nach dem Transport der Hormone im Xylem zu den Blättern können sie dort die stomatäre Leitfähigkeit beeinflussen. Langfristige Anpassungsstrategien sind meist mit einer Veränderung in der Kohlenstoffverteilung innerhalb der Pflanze verbunden, was wiederum in eine Anpassung des Pflanzenwachstums resultiert. Beide Strategien sind oftmals nicht hinreichend in hydrologischen Modellen repräsentiert.

Methodik: Mithilfe von R-SWMS, einem mechanistischen Boden-Wurzel Modell, welches für die Skala einer einzelnen Pflanze ausgelegt ist, wurden eine Reihe von virtuellen Experimenten durchgeführt. Das Modell beschreibt den Bodenwasserfluss, die Wurzelwasseraufnahme und den Wassertransport in der Wurzel und wurde mit einem Modul zur hormonellen Signalübertragung erweitert und dessen Einfluss an virtuellen ‚split-root‘ Experimenten getestet. Als nächstes wurden direkte, mathematische Relationen für hydraulische und/oder hormonelle stomatäre Kontrolle entwickelt, welche den Zusammenhang zwischen effektivem Bodenwasserpotential und Transpirationsrate beschreiben. In Anbetracht der langfristigen Pflanzenstrategien wurde das numerische Modell erweitert um gemessene, dynamische Wurzelarchitekturen berücksichtigen zu können.

Ergebnisse: In Blättern gemessene Hormonkonzentrationen sowie einige Phänomene, wie z.B. oszillierende stomatäre Leitfähigkeit, konnten vom Modell reproduziert werden. Die direkten Relationen zwischen Bodenwasserpotential und Transpiration konnten zeigen dass das Verhalten der Stomata von dem jeweiligen Kontrollmechanismus und seiner Parametrisierung abhängt. Experimentelle Daten, welche die Entwicklung von Wurzelarchitekturen über einen Zeitraum von ca. 30 Tagen zeigen, wurden am UFZ in Halle mit Hilfe eines CT Scanners erhoben. Diese Daten zeigten, dass Pflanzen unter permanent limitierter Wasserversorgung, im Vergleich zu Pflanzen mit anfangs uneingeschränktem Wasserangebot, erheblich kleiner mit dementsprechend geringerer Wasseraufnahme waren. In Kombination mit dem numerischen Modell wurde die Fließdynamik des

Boden-Wurzelsystems detailliert dargestellt. Der errechnete Ort der Wurzelwasseraufnahme stimmte demnach nicht mit dem Bereich der gemessenen Wassergehaltsminderung überein.

Schlussfolgerung: Die Implementierung von biophysikalischen Beziehungen in ein mechanistisches numerisches Boden-Wurzel Modell ergab einen interessanten Ansatz zur Identifizierung von Schlüsselprozesse für Pflanzenwassernutzung im landwirtschaftlichen Kontext. Die vorliegende Arbeit konnte, im Fall einer hormonellen Signalübertragung, neue, direkte Relationen zwischen effektivem Bodenwasserpotential und Transpirationsrate ermitteln. Die Kombination zwischen experimentellen Daten und numerischem Modell ergab des Weiteren neue Aufschlüsse von Wasserflüssen im Boden-Pflanze Kontinuum.

LIST OF PUBLICATIONS

1. **Huber, K.**, J. Vanderborght, M. Javaux, N. Schröder, I. Dodd, and H. Vereecken (2014), Modelling the impact of heterogeneous rootzone water distribution on the regulation of transpiration by hormone transport and/or hydraulic pressures, *Plant and Soil*, 1-20.
2. **Huber, K.**, J. Vanderborght, M. Javaux, and H. Vereecken, Transpiration reduction due to hydraulic versus chemical signalling from a partially dry root zone - a simulation study, *Plant and Soil* (submitted).
3. Koebernick, N., **K. Huber***, E. Kerkhofs, J. Vanderborght, M. Javaux, H. Vereecken, and D. Vetterlein, Measuring and modeling three-dimensional water uptake of growing broad beans (*Vicia faba* L.) within split-soil columns, *Frontiers in Plant Science* (in preparation).
* shared first co-authorship
4. Koebernick, N., U. Weller, **K. Huber**, S. Schlüter, H.-J. Vogel, R. Jahn, H. Vereecken, and D. Vetterlein (2014), In Situ Visualization and Quantification of Three-Dimensional Root System Architecture and Growth Using X-Ray Computed Tomography, *Vadose Zone Journal* (8).
5. Dodd, I. C., J. Puertolas, **K. Huber**, J. G. Pérez-Pérez, H. Wright, and M. Blackwell, The importance of soil drying and re-wetting in crop responses to deficit irrigation, *Journal of Experimental Botany* (submitted).

TABLE OF CONTENTS

Abstract	i
Zusammenfassung	ii
List of Publications	v
Table of Contents	vii
List of Abbreviations	xi
CHAPTER 1	1
General Introduction and Objectives	1
1.1 Soil water flow	2
1.2 Plant water uptake	3
1.3 Modelling soil water flow and root water uptake	5
1.4 Root architecture	7
1.4.1 Observation of root architectures	7
1.4.2 Root architectural modelling	8
1.5 Motivation and objectives	8
1.5.1 Short-term adaptation – modelling stomatal closure	8
1.5.2 Long-term adaptations – observing and modelling root architecture	9
CHAPTER 2	11
Modelling the impact of heterogeneous rootzone water distribution on the regulation of transpiration by hormone transport and/or hydraulic pressures	11
2.1 Introduction	12
2.2 Model approach	15

TABLE OF CONTENTS

2.2.1 Definition of water potential, water pressure, and pressure head.....	15
2.2.2 Concept of stomatal conductance.....	15
2.2.3 Hydraulic signalling.....	17
2.2.4 Chemical signalling.....	19
2.3 Materials and Methods.....	22
2.3.1 Virtual experiments.....	22
2.3.2 Soil Domain.....	22
2.3.3 Root System.....	24
2.3.4 Boundary and Initial conditions.....	25
2.3.5 Definition of effective rootzone pressure head.....	26
2.4 Results and Discussion.....	27
2.4.1 Influence of stomatal regulation mechanisms.....	27
2.4.2 Effect of chemical signal concentration and linkage to soil pressure head.....	29
2.4.3 Effects of signal transport.....	30
2.4.4 Sensitivity analysis.....	31
2.4.5 Alternated partial rootzone drying.....	33
2.5 Conclusions.....	37
CHAPTER 3.....	39
Transpiration reduction due to hydraulic versus chemical signalling from a partially dry root zone – a simulation study.....	39
3.1 Introduction.....	40
3.2 Methods.....	42
3.2.1 Numerical mechanistic model, R-SWMS.....	42
3.2.2 Direct relation between transpiration and root zone water distribution including chemical signalling.....	44
3.2.3 Model setup.....	49

TABLE OF CONTENTS

3.2.4 Scenarios	55
3.3 Results and Discussion	56
3.3.1 Comparison of the direct and the numerical relations	56
3.3.2 Verification of the assumptions	60
3.3.3 Sensitivity analysis	63
3.3.4 Applicability of these approaches	64
3.4 Conclusion	67
CHAPTER 4	69
Measuring and Modelling three-dimensional water uptake of growing broad beans (<i>Vicia faba</i> L.) within split columns	69
4.1 Introduction	70
4.2 Materials and Methods	73
4.2.1 Experiments	73
4.2.2 Modelling of RWU	77
4.3 Results	82
4.3.1 Experimental results	82
4.3.2 Simulation results	86
4.4 Discussion	96
4.4.1 Influence of paraffin layers on plant growth	96
4.4.2 Relation between measured water loss and RWU	96
4.4.3 Predawn collar potential:	97
4.4.4 Determination of RSA with CT	98
4.4.5 Parameterization of root hydraulic conductivity	98
4.5 Conclusion and Outlook	99
CHAPTER 5	101

TABLE OF CONTENTS

General Conclusions and Outlook.....	101
5.1 Conclusion.....	101
5.2 Outlook.....	103
Acknowledgements	115
Bibliography.....	117
List of Tables.....	125
List of Figures	127
Curriculum Vitae.....	129

LIST OF ABBREVIATIONS

a	Production rate of hormones per dry mass of a root segment	$\text{N M}^{-1} \text{L}^{-1} \text{T}^{-1}$
A_r	Cross sectional area	L^2
A_x	Lateral surface area	L^2
c_d	Boolean variable	-
c_L, c_{leaf}	Concentration of hormones arriving in stomata	N L^{-3}
f_{dry}	Fraction of roots in dry soil	-
g	Gravitational acceleration	L T^{-2}
H	Total potential	L
h	Matric head	L
h_0	Threshold pressure head for onset of hormonal signal production	L
h_{crit}	Critical pressure head	L
$h_{s,eff}$	Effective soil pressure head	L
h_x	Xylem pressure head	L
i	Index for a root segment	-
J_r	Radial root flow	$\text{L}^3 \text{T}^{-1}$
J_x	Axial root flow	$\text{L}^3 \text{T}^{-1}$
K	Soil hydraulic conductivity	L T^{-1}
k	Index for a soil voxel	-
K_r^*	Radial conductivity	T^{-1}
K_x^*	Axial conductivity	L T^{-1}
K_{root}	Equivalent root hydraulic conductivity	$\text{L}^3 \text{P}^{-1} \text{T}^{-1}$
K_{sat}	Saturated soil hydraulic conductivity	L T^{-1}
K_x	Axial root hydraulic conductance	$\text{L}^3 \text{T}^{-1}$
l	Length	L
LA	Leaf area	L^2
LW	Leaf width	L^2
m	Shape parameter of Van Genuchten equation	-
M	Hormonal signal mass	M
n	Shape parameter of Van Genuchten equation	-
P	Hydrostatic head	L
S	Sink term in Richards equation	T^{-1}
S	Degree of Saturation	-

LIST OF ABBREVIATIONS

s_c	Sensitivity parameter of stomata to chemical signal	$L^3 N^{-1}$
s_h	Sensitivity parameter of stomata to hydraulic signal	L^{-1}
s_p	Fitting parameter / Sensitivity parameter of stomata to hydraulic signal	P^{-1}
SSF, s	Standardized sink fraction	-
t	Time	T
T_{act}	Actual transpiration rate	$L^3 T^{-1}$
T_{pot}	Potential transpiration rate	$L^3 T^{-1}$
V_{buffer}	Volume of buffer for hormonal signal	L^3
z	Gravitational head	L
α	Inverse air entry value	L^{-1}
α	Relative stomatal aperture	-
α_R	Residual relative stomatal aperture	-
θ	Volumetric soil water content	$L^3 L^{-3}$
θ_r	Residual volumetric soil water content	$L^3 L^{-3}$
θ_s	Saturated volumetric soil water content	$L^3 L^{-3}$
ρ	Density	$M L^{-3}$
ψ_{leaf}	Leaf water potential	P
ψ_{lim}	Threshold water potential	P
$\psi_{root,dry}$	Soil water potential in dry or wet soil fraction	P
$\psi_{root,wet}$		

CHAPTER 1

GENERAL INTRODUCTION AND OBJECTIVES

With 85% of the total fresh-water use, agriculture has a higher water demand than any other sector on this planet [Foley *et al.*, 2005] and irrigation alone consumes 70% of the total withdrawn fresh-water [Foley *et al.*, 2011]. A considerable part of this water is taken up by plant roots. The quantity of water uptake is foremost dependent on the size of the plant and the atmospheric conditions (vapour pressure deficit, temperature, and wind speed). The location of water uptake is determined by the root morphology, the hydraulic properties of the roots, and the soil properties (texture) and state (soil moisture), which itself is inherently heterogeneous. Even if all these parameters could be measured at a single point in time, plants have the ability to adjust to changes in their environment with a multitude of different mechanisms [Lambers *et al.*, 2008]. This adjustment, with a focus on plant root systems, to soil heterogeneity will be the main topic of this thesis.

1.1 Soil water flow

Soil is a porous medium consisting of a composite of minerals and organic matter in different grain sizes and aggregates. The upper layers of the unsaturated or vadose zone, where plant roots are growing into, is characterized by a high temporal and spatial variability of the water content. The spatio-temporal distribution of water content is driven by soil boundary conditions (rainfall, aquifer level, lateral fluxes) and affected by hydraulic and structural soil properties. By extracting water out of the soil system, plants also impact soil water content distribution and fluxes.

Soil water redistribution fluxes take place when total water potential gradients exist. Total potential of soil water is defined as the sum of several components, but in this thesis the three principal components will be considered as driving forces of water flow:

$$H = h + z + P \quad 1.1$$

Where H [L] is the total potential head, h is the matric head, P [L] is the hydrostatic head and z [L] is the gravitational head. Soil water content is related to soil matric head through the soil moisture retention characteristic [Van Genuchten, 1980]. Together with the soil hydraulic conductivity curve, they characterize the soil hydraulic properties.

Soil hydraulic properties of natural soils are hardly uniform but heterogeneous in the lateral as well as the vertical direction. The most common heterogeneity is the stratification of soils with layers of different soil materials and properties (horizons). Even in managed and tilled agricultural fields the heterogeneity might be large due to different geomorphological features within one field. While there is a wealth of research concerning water movement within the soil [Vereecken *et al.*, 2008] it is still not well understood how plants adapt to this heterogeneity.

1.2 Plant water uptake

While plants use only a small amount of the water they take up for their metabolism, most of it is lost through the stomata, small apertures in the leaves, in exchange for CO₂ uptake. Even though there has been a scientific debate [Tyree, 1997; Zimmermann *et al.*, 2004], current consensus still refers to the cohesion-tension theory to describe water transport in plants. It was first proposed in 1894 by *Dixon and Joly* and regards the connection between soil, plant, and atmosphere as a continuum (SPAC) where root water uptake, ascension of water in plants and its subsequent transpiration into the atmosphere is passively driven by the vapour pressure deficit (VPD) between the water in the stomata and the relatively dry air. The VPD exerts a negative pressure in the plant and can be as high as 100 MPa (Figure 1.1 A) and drives water up in trees over 100 m high. The cohesion of the water to the xylem (water-conducting plant tissue) walls together with the tension of the water molecules prevents the water from cavitation above 10 m height.

For water to reach the atmosphere, it has to overcome several resistances. Water flow towards the roots is controlled by the hydraulic conductivity of the soil, which is itself a function of the soil water content [Mualem, 1976; Van Genuchten, 1980] (Figure 1.1 B). The driver is the water potential gradient between soil and root surface. Even though often neglected, the rhizosphere in the immediate vicinity of the roots, exhibits very own hydraulic properties that can result in higher or lower hydraulic rhizosphere conductivities, depending if the soil is drying or wetting [Zarebanadkouki and Carminati, 2014]. The radial uptake is driven by the water potential gradient between the soil surface and the root xylem. According to the composite model [Stedde, 2000; Stedde and Peterson, 1998], water can follow three different paths into the root (Figure 1.1 C): The apoplastic pathway along cell walls and within intercellular spaces [Eshel and Beeckman, 2013], the symplastic pathway through the symplastic continuum that connects individual cells and the transcellular pathway through the cell membranes. The permeability of the cell membranes depends on water channels (aquaporins), whose quantity and expression shows a high plasticity depending on environmental conditions [Parent *et al.*, 2009]. Before water reaches the xylem it has to overcome the Casparian band, which is a suberized ring around the xylem and phloem [North and Nobel, 1991], which can only be overcome by the symplastic or the transcellular pathway. Water will be taken up in varying ratios from each of these pathways, depending on the individual resistance of each way. When water is within the xylem, it is quickly transported upwards (with velocities between 1-10 m h⁻¹). The xylem conductivity is usually not limiting, only when embolization in the vessels occurs it can be significantly reduced (see review by Rockwell *et al.* [2014], Figure 1.1 D). In the leaves the water is pulled from the xylem into the mesophyll cells. It leaves the plant by the stomata. The largest gradients in water potentials are found between stomata and atmosphere. Thus opening and closing of stomata is a main regulator of the

pressures in the whole plant system. At last the water molecule has to overcome the boundary layer resistance, which is due to a layer of still air on the leaf surface. The thickness of this layer depends on wind-speed. These resistances are connected in series (some in parallel), so that the smallest resistance will eventually control the complete system. As the resistances are variable under different environmental conditions, the controlling resistance will change during the duration of a day, a season, and a plant life. Mathematical representations of these relationships can be used to set up models that describe basic soil-root systems.

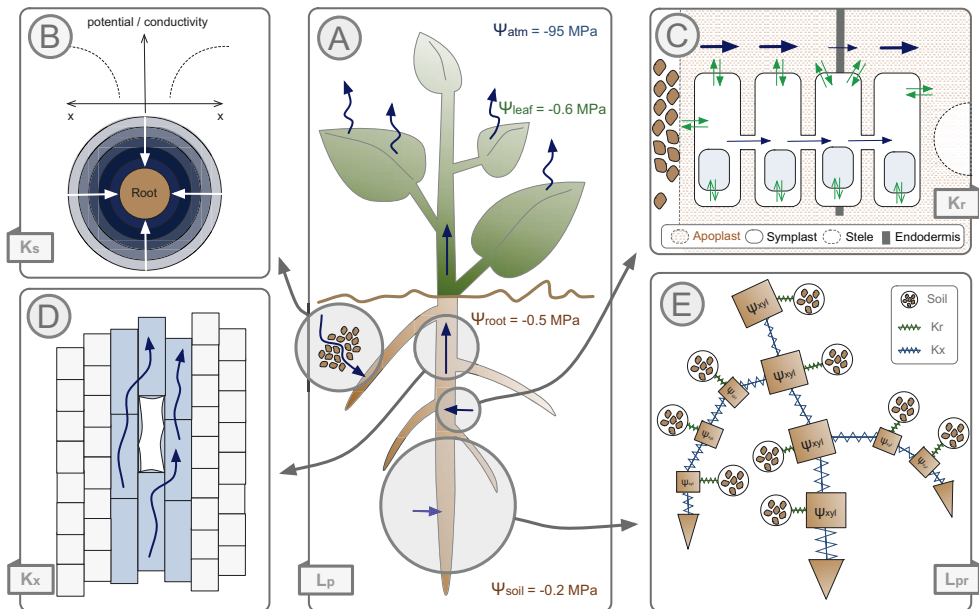


Figure 1.1 Water flow in the soil-plant-atmosphere continuum (SPAC). A. Cohesion tension mechanism. The water flows along the SPAC following the gradient of water potential between the different compartments. B. Water movement in the soil. The water flows in the soil following local gradient of matrix forces. Close to the root surface, the radial nature of the water flow induces a strong water potential gradient. C. Radial movement of water in the root. Water entering the roots has to traverse several cell layers using a combination of symplastic, cell to cell and apoplastic pathway. Blue arrows represent pressure-driven convection while green arrows represent osmotically-driven flow. D. Axial movement of water in the root. Water moves in xylem vessels following water potential gradients between roots and leaves. The path can be interrupted locally at embolized vessels (cavitation). E. Importance of the root system architecture as an integrative element. The analogy between the root system hydraulic architecture and an electric network makes it possible to predict the sites of water uptake within the root system. [modified from *Eshel and Beekman, 2013*]

1.3 Modelling soil water flow and root water uptake

The Richards equation [1931], which is derived from Darcy and the continuity equations, describes flow in variably saturated soils and is usually solved numerically. The Richards equation (Eq. 1.2) states in three dimensional notation:

$$\frac{\partial \theta}{\partial t} = \nabla \cdot [K(h)\nabla(h)] + \frac{\partial K(h)}{\partial z} + S(x, y, z, t) \quad 1.2$$

where $K [L T^{-1}]$ is the hydraulic conductivity of the soil, $x, y, z [L]$ are respectively the two horizontal dimensions and the elevation, and $S [T^{-1}]$ is the sink term. Depending on the extent of the problem, root water uptake is modelled in different dimensionalities. For field or larger scale problems, the soil is usually represented as a one dimensional soil column with the sink term as an empirical function that depends on the root length density distribution, a stress term to account for unfavourable water availability, and a compensation term [Javaux *et al.*, 2013]. Some physical processes, like compensation of water uptake, are not explicitly accounted for, but empirical functions have to be parameterized [Jarvis, 1989]. Especially in large scale simulations with small scale heterogeneity, this factor proves difficult [Kuhlmann *et al.*, 2012]. Explicit solutions of the sink term require, on the other hand, a larger set of parameters, including the age and root type dependent root hydraulic resistances, which are hard to measure. As this approach is computationally more expensive it is usually only applied either at a single root or at the single plant scale [Schneider *et al.*, 2010]. An explicit model on the other hand has the advantage to intrinsically account for compensation or water redistribution in the soil via the roots (hydraulic lift) [Caldwell *et al.*, 1998] by solving the soil and root equations. Recent developments allow to combine the advantage of both methods by taking into account the hydraulic architecture of the root system and then solving root water uptake via a macroscopic approach [Couvreur *et al.*, 2012].

For an explicit model, the root system, as explained in a previous paragraph, can be mathematically described by Ohm's analogy [Cowan, 1965; van den Honert, 1948] (Figure 1.1 E). The resulting equations for radial flow into the roots (Eq. 1.3) and axial flow through the root xylem (Eq. 1.4), as stated by Doussan *et al.* [2006] were combined with a numerical soil model [Simunek *et al.*, 1995] and named R-SWMS [Javaux *et al.*, 2008].

$$J_r = K_r^* A_r (h_{s,int} - h_x) \quad 1.3$$

$$J_x = -K_x^* A_x \left(\frac{dh_x(z)}{dl} + \frac{dz}{dl} \right) \quad 1.4$$

where J_r [$L^3 T^{-1}$] and J_x [$L^3 T^{-1}$] are the radial and the xylem flow, respectively, K_r^* [T^{-1}] is the radial conductivity, K_x^* [$L T^{-1}$] the axial conductivity, $h_{s,int}$ [L] the pressure head at the root interface, h_x [L] the xylem pressure head, l [L] the length of a single root segment, A_r [L^2] the lateral surface area, and A_x [L^2] the cross sectional area of a root segment.

The root and the soil water flow equations are coupled via the sink term of the Richards equation (Eq. 1.2) and the water potential at the soil-root interface for the Doussan equation, $h_{s,int}$ (Eq. 1.3). Both sets of equations are solved iteratively until the error between J_r and S is smaller than a threshold value. A typical setup for this model, which has been used throughout this thesis, is shown in Figure 1.2 with a tap root system located within an approximated cylindrical domain. An important input for this kind of models is a realistic root architecture.

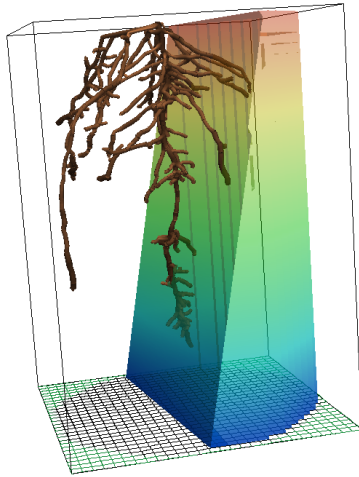


Figure 1.2 Typical R-SWMS setup with a root grown within a cylindrical domain. The soil is coloured according to its water content from dry (red) to wet (blue).

1.4 Root architecture

1.4.1 Observation of root architectures

Experimental observation of root system architecture and its development still proves challenging because roots are rendered invisible by the opaque growth medium. Probably the earliest architectural descriptions of root systems within their soil environment were made by *Weaver et al.* [1924] and perfected by *Kutschera* [1960]. They excavated the root system layer by layer in the field and subsequently depicted the root system by drawing. These works resulted in beautiful images and insights into the various types and adjustments of root systems (Figure 1.3 a). Nowadays non-destructive imaging techniques allow the direct observation of plant roots (and in some cases soil water) and their temporal development within soil. The most advanced techniques for imaging soil-grown roots include X-ray computed tomography [*Mooney et al.*, 2012] (Figure 1.3 b), neutron radiography [*Oswald et al.*, 2008], magnetic resonance imaging [*Pohlmeier et al.*, 2008], transparent soils [*Downie et al.*, 2012], or light transmission through a thin soil layer [*Garrigues et al.*, 2006]. However, these methods are hitherto either constrained to quasi two-dimensions (rhizotrons) or very small root systems. Reconstructions of these 3D root structures can be used as inputs for the simulations.

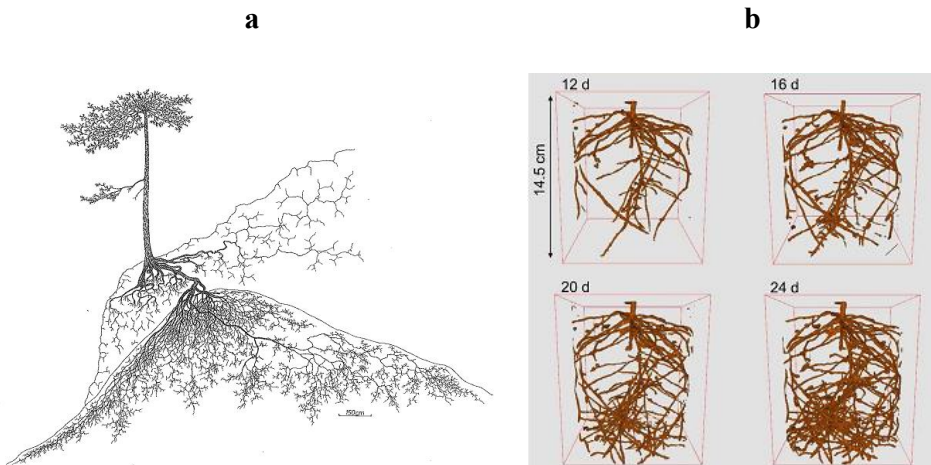


Figure 1.3 Root growth adaptations: a) *Pinus nigra (nigra)* with roots grown into two contrasting soil environments: fractured rock above an embankment of loose gravel [*Kutschera and Lichtenegger*, 2002]; b) μ -CT scans of *Vicia faba* after 12, 16, 20, and 24 days of growth in a sand-filled cylinder of 6.25 cm radius and 21.5 cm height [*Koebnick et al.*, 2014]

1.4.2 Root architectural modelling

Root system architectures can also be obtained by modelling. And, again, depending on the problem, the root structure can either be explicitly modelled in three dimensions or described as a continuous function in a single dimension [i.a. Dupuy *et al.*, 2010]. In the present work we mainly worked with architectural models. A recent review [Dunbabin *et al.*, 2013] showed the progress of root growth modelling from the 1970's to now. There are two main mathematical approaches to describe root growth at the system scale: L-systems [Leitner *et al.*, 2010b; Prusinkiewicz *et al.*, 1990], a string-based model that multiplies existing structures, and vector addition [Lynch *et al.*, 1997; Pagès *et al.*, 2004]. The model used in parts of this thesis was developed by Clausnitzer and Hopmans [1994] and is of the latter category. A single root branch consists of several connected nodes with a root segment attached to each root node. The branches are all connected and eventually converge to a single seed at the top of the root system. The root system grows by creating new segments at the root tips. Depending on the soil environment around the existing tips both, direction and length, of the new segments were adjusted. The influencing soil states for growth in this model are soil resistance, temperature and solute concentration. Together with soil and root water flow dynamics, as simulated with R-SWMS, it is possible to simultaneously describe root growth and water uptake, which is a major advantage of this model compared to others.

1.5 Motivation and objectives

The main objective of this thesis is to understand how root systems and consequentially plants react to and subsequently affect spatial heterogeneity of soil water distribution. We particularly look at short and long term reactions as a function of environmental conditions.

1.5.1 Short-term adaptation – modelling stomatal closure

For fast changes in soil water availability, e.g. higher transpirational demand during midday, stomata can close. In plant physiology a multitude of triggers are known for stomatal closure, but for hydrological models stomata usually only react to integrated soil water potential [Feddes *et al.*, 1978]. One, highly discussed [W Davies *et al.*, 2002; Holbrook *et al.*, 2002], strategy is the sensing of dry soil by plant roots, and a subsequent release of a chemical/hormonal signal from these roots. The hormones are then thought to be transported with the transpiration stream within the xylem to the plant leaves where they initiate stomatal closure.

In Chapter 2 the implementation of a hormonal signal, using a particle tracking algorithm, into the explicit soil and root water flow model R-SWMS is described. The signal is produced in the root segments as function of local xylem water potential. The subsequent convective transport within the xylem towards the leaves, where it triggers stomatal closure, initially leads to very strong oscillations in stomatal aperture. Even though this effect can be observed to various degrees in certain plant species, a buffer with a certain volume, representing the plant shoot, was added to the model to damp the signal. The modelled hormone concentrations arriving at the leaves were comparable to previously experimentally observed hormone concentrations. We set up virtual split-root experiments where one half of the root system was continuously irrigated and the other half subjected to drying. Hormonal signal could be entrapped on the way to the leaves as root water uptake ceased with continuous soil drying. After re-wetting of the dry soil, the trapped particles were flushed out and transpiration rate was temporally decreased. However, comparing the differences between hydraulic and/or hormonal stomatal control only showed slight discrepancies.

The aim of the third chapter was to derive simple relationships between available soil water, expressed as the fractions of roots in dry soil, to transpiration reduction. The commonly used hydraulic relationships were extended by a term to account for additional or exclusive hormonal stomatal control. To verify these simple relations virtual split-root experiments, with either horizontally or vertically split domains, were simulated with R-SWMS. The outputs from the numerical simulations were in good agreement with the theoretical relationships. Marked differences in stomatal behaviour depending on the control were found. Under certain conditions, leaf water potential is kept constant when transpiration is reduced over a wide range of effective soil water potentials (isohydric behaviour) in plants that are controlled by hydraulics. Contrary, leaf water potential of plants that are only controlled by hormones, varies with effective soil water potential (anisohydric behaviour). The latter behaviour can also be distinguished by a unique relationship between the ratio of actual to potential transpiration to the fractions of roots in dry soil.

1.5.2 Long-term adaptations – observing and modelling root architecture

For more persistent soil heterogeneities, e.g. due to soil morphology or structure, plants can adjust by changing their root and shoot architecture. By controlling this heterogeneity in split-root experiments the influences on root development and plant water use can be demonstrated.

In Chapter 4 an experimental data set was analysed and subsequently compared to 3D simulations of soil and root water flow. At UFZ in Halle, Germany, broad bean plants (*Vicia faba*) were grown in soil-filled cylinders with and without horizontal paraffin splits. While the paraffin layers restricted

vertical soil water redistribution within the separated compartments, root growth was not inhibited by the paraffin. The plants were exposed to a single drying period during which soil and plant water statuses were measured. The root systems of the bean plants were CT-scanned every second day and the resulting binary images of the consecutive root systems were reconstructed using a virtual reality system to obtain connected root architectures. Time series of the reconstructed root architectures were used in the detailed root and soil water flow model to simulate soil and root water potentials as well as individual fluxes through the roots and the soil. The plants grown in the split setup were overall smaller with less transpiration rates and lower stomatal conductance than the plants grown in vertically unrestricted soil. Comparison between simulated and measured soil water potentials revealed that in most cases the split layers were not completely hydraulically isolating. Nevertheless, the layers substantially restricted vertical flow through the soil, which led to lower predawn collar water potentials, which can in turn be associated with lower stomatal conductance and reduction of plant growth.

This thesis is a combination of work published and unpublished. Some passages within one chapter may be repeated in other chapters. I herewith apologize to the reader of the complete document.

CHAPTER 2

MODELLING THE IMPACT OF HETEROGENEOUS ROOTZONE WATER DISTRIBUTION ON THE REGULATION OF TRANSPIRATION BY HORMONE TRANSPORT AND/OR HYDRAULIC PRESSURES

This chapter is based on a journal article published as:

Huber, K., Vanderborght, J., Javaux, M., Schröder, N., Dodd, I. C., Vereecken, H. (2014) Modelling the impact of heterogeneous rootzone water distribution on the regulation of transpiration by hormone transport and/or hydraulic pressures, *Plant and Soil*, 1-20.

2.1 Introduction

Plants lose large amounts of water to the atmosphere through stomata that open for CO₂ uptake and carbon assimilation. This water loss is compensated by water uptake from the soil. When soil dries, there may be damaging effects of root shrinkage and subsequent loss of contact with the surrounding soil, and the low plant water potentials required to maintain soil water uptake may induce xylem cavitation [Barigah *et al.*, 2013]. However, effective stomatal regulation prevents excessive loss of water when the soil dries out [Brodribb and McAdam, 2011]. This mechanism represents the main short-term regulation of water flow between the soil and the atmosphere [Taiz and Zeiger, 2006].

In many experiments, leaf water potential is correlated with stomatal closure [Buckley, 2005]. One obvious strategy to avoid cavitation is to close stomata to maintain the leaf water potential (Ψ_L) at a certain level. This is called pressure homeostasis (isohydric behaviour). On the other hand, in some species, stomata are insensitive to changes in Ψ_L within a certain range, and their stomata remain fully open during soil drying and higher transpiration demand. Large diurnal variations of Ψ_L may occur, leading to so-called anisohydric behaviour [Franks *et al.*, 2007], in contrast to isohydric species where low soil water potentials cause stomatal closure which maintains Ψ_L . The hydraulics of the root and shoot system provide a direct link between root-zone water potential, transpiration flow and leaf water potential and may influence long-distance hydraulic signalling thereby linking plant water potentials and stomatal closure [Christmann *et al.*, 2013].

However, plants have also developed non-hydraulic strategies to regulate transpiration [Tardieu and Simonneau, 1998]. Experiments that split the roots between two soil compartments have suggested that hydraulics alone cannot explain certain stomatal responses. Although drying part of the root system decreases stomatal conductance in the absence of changes in leaf water potential, continued drying of parts of the rootzone actually increases stomatal conductance [Khalil and Grace, 1993; Stoll *et al.*, 2000]. These effects were proposed to result from the roots in drying soil synthesizing a chemical signal which is transported from the roots to limit stomatal conductance, but then stomata re-open when signal transport is restricted as the soil becomes too dry. These split-root experiments have been upscaled to implement partial rootzone drying as a water-saving irrigation technique to improve crop water use efficiency, with periodic alternation of wet and dry sides of the rootzone to ensure continued signal transport to the shoots [Bravdo, 2005; Dodd *et al.*, 2006; Kang, 2004; Stoll *et al.*, 2000].

The production, transport and release of chemicals such as the phytohormone abscisic acid (ABA) or hormone precursors such as 1-aminocyclopropane-1-carboxylic acid (ACC - the ethylene precursor) into leaves [Tardieu and Davies, 1993; Wan and Zwiazek, 2001] can be critical in stomatal regulation

[*W J Davies and Zhang, 1991*]. However, the source of chemical signals that are important for stomatal regulation is contentious. Early evidence for root ABA production [*Hartung and Aboumandour, 1980*] was supported by later observations that xylem ABA concentrations increase significantly under water stress conditions and correlate with stomatal closure [*Schurr et al., 1992*]. Furthermore, soil drying increases xylem sap pH, which enriches ABA in the leaf apoplast by decreasing ABA uptake by mesophyll cells [*Wilkinson and Davies, 1997*]. These mechanisms suggest that root sourced ABA can act as a long-distance signal initiating stomatal closure.

In contrast, other studies cast doubt on the hypothesis of root sourced ABA acting as a long-distance signal for stomatal closure. Reciprocal- and self-grafts of wild-type and ABA-deficient tomatoes demonstrated that stomatal regulation depends on the shoot genotype only, and is independent of the rootstock [*Dodd, 2009; Holbrook et al., 2002*]. Furthermore, osmotic stress applied to the roots reveals ABA-dependent reporter gene expressions only in the leaves [*Christmann et al., 2007*]. Those experiments suggest that leaves are the main source of ABA, and a subsequent basipetal transport of ABA via the phloem towards the roots, where the hormones are recycled to the xylem and transported upwards again. However, the proportional contributions of ABA recycling and root synthesis to xylem ABA concentration vary according to the root environment [*Wolf et al., 1990*]. Mechanistically, both sources of an additional chemical signal can be (mathematically) described by the same approach, namely a production or a release of the chemical within the roots into the xylem and a subsequent transport to the leaves.

In hydrological models, signalling between rootzone conditions and stomatal closure is not modelled explicitly but stomatal regulation in response to low soil water potentials is implicitly accounted for through “stress functions”. These functions relate the reduction of the potential transpiration rate directly to bulk soil water potential (instantaneous effect) thereby bypassing other variables that control stomatal conductance and root-to-shoot signalling mechanisms. An oft-used stress function is the Feddes function which describes the transpiration reduction factor as a piece-wise linear function of soil water potential [*Feddes et al., 1978*]. The decreasing part of the function for low soil water potential implicitly represents the effect of soil water potential on stomatal closure. However, this relationship is indirect and may therefore depend on other factors. For instance, for the same bulk soil water potential, lower leaf water potential may be expected with higher transpiration rates. On the other hand, when production rate of the hormonal signal is not a function of sap flow rate, a higher transpiration rate will dilute the signal, causing lower signal concentrations in the leaves. Depending on which mechanism relates soil water potential to stomatal conductance, the impact of higher transpiration rate on the onset of stomatal closure will be different.

As discussed above, several models link stomatal conductance to environmental factors. However, most of these models “*do not include satisfactorily the effects of drought, impairing our capacity to simulate plant functioning in conditions of limited water supply*” [Damour *et al.*, 2010]. Here, a new model is presented that combines both hydraulic and chemical signalling processes into a common modelling framework. A 3D model that explicitly solves the water flow equations in the root system [Javaux *et al.*, 2008] was coupled to a model that simulates signal production in the rootzone and transport through the root system to the leaves. Hereby, the stem and leaves were not explicitly considered but only modelled as an additional root segment with the same volume as the total root system. First, how the different signalling mechanisms are implemented in the model is discussed. Secondly, the effect of different signalling processes on the relation between soil water potential and transpiration is demonstrated and a sensitivity analysis presented. Finally, water and chemical flows from different parts of the rootzone of split-root plants, and whole plant transpiration were modelled during alternate partial rootzone drying. This study intends to (i) simulate observed plant behaviour during partial rootzone drying and (ii) show the impact of a chemical signal on the relation between soil water potential and transpiration reduction.

2.2 Model approach

2.2.1 Definition of water potential, water pressure, and pressure head

Plants take up water from the soil through their roots and transport it to the leaves where it is transpired through the stomata. The driver for this transport is the difference in water potential (a measure of the energy state of water) between the atmosphere and the soil. The energy of the plant (or soil) water or water potential can be either stated as *total* water pressure (ψ [Pa], energy per volume) or as hydraulic head (H [m], energy per weight). *Total* water pressure and hydraulic head can be converted using Eq. 2.1a. Gradients in *total* water pressure or hydraulic head are relevant for driving water flow. The *total* water pressure and hydraulic head represent the sum of different partial potentials, including the gravitation potential or the energy of water due to its elevation above a certain reference height.

$$H = \psi / (\rho g) \quad 2.1a$$

$$h = H - z \quad 2.1b$$

where ρ [kg m^{-3}] is the density of water assumed to be constant, g [m s^{-2}] the acceleration due to gravity, and z [m] is the height above a reference level. By approximating g as 10 m s^{-1} and ρ as 1000 kg m^{-3} , we can state that h [m] $\approx 10000 \psi$ [Pa] or that a pressure head of 1 cm approximates a pressure of $1 \cdot 10^{-4}$ MPa.

2.2.2 Concept of stomatal conductance

Stomatal closure is the main short-term control mechanism that decreases actual transpiration (T_{act}) as the soil dries. The potential transpiration (T_{pot}) represents the transpiration of the plant under the same climatic conditions but in a well-watered soil. Following *Tardieu and Simonneau* [1998], who classified stomatal sensitivities for different plant species, anisohydric behaviour refers to stomata that remain fully open during drying until the plant reaches its permanent wilting point. The leaf pressure head, h_L , of anisohydric plants thus shows strong fluctuations with changes in soil water availability and transpiration rates (e.g. diurnal or seasonal cycles). In contrast, isohydric plants try to regulate h_L and keep it higher than or equal to a certain threshold which is higher than the permanent wilting point

value, thereby reducing T_{act} when soil is drying. We chose an adapted version of the Tardieu and Davies (1993) model that describes stomatal conductance as a function of the internal plant variables h_L and concentration of chemical signal in the leaves.

Relative stomatal conductance α , relative to the maximum conductance under the same conditions but when water content is optimal, was calculated using:

$$\alpha = \alpha_R + (1 - \alpha_R)e^{-(1-c_d)s_c c_L - c_d} e^{-s_h (h_L - h_{crit})} \quad 2.2a$$

where α_R [-] is the residual relative stomatal aperture, c_L [nmol cm^{-3}] is the concentration of chemical signal in the leaf, h_L is the leaf pressure head and h_{crit} is a threshold pressure head in the leaf, s_h [cm^{-1}] and s_c [$\text{cm}^3 \text{nmol}^{-1}$] are fitting parameters for pressure head and signal concentration respectively. The variable c_d is a Boolean variable that either enables only pressure head regulation ($c_d = 1$) or an interaction between chemical and pressure regulation ($c_d = 0$). Equation 2a is valid for $h_L < h_{crit}$, otherwise

$$\alpha = \alpha_R + (1 - \alpha_R)e^{-s_c c_L} \quad 2.2b$$

where at concentration $c_L = 0$, α will be equal to 1. Note that α corresponds with the ratio of actual transpiration, T_{act} , to the potential transpiration, T_{pot} , with values between α_R (residual stomatal conductance) and 1. The effect of both hydraulic and chemical signalling ('H+C'= hydraulic and chemical control) on the transpiration reduction as described by Eq. 2.2a is illustrated (Figure 2.1). While keeping the concentration of the chemical constant, α is plotted versus h_L (parameters are detailed in Table 2.1. Different lines represent α for different signal concentrations. Lower leaf water potentials as well as higher chemical concentrations decrease transpiration. An anisohydric plant ('NR' = No Regulation) keeps the ratio α at 1 and thus actual transpiration equals potential transpiration until the permanent wilting point is reached (acc. Eq. 2.2a, this would correspond to $s_c = 0$ and $h_{crit} = h_{WP}$). For the case $s_h = 0$ and $s_c > 0$, the leaf conductance does not directly depend on h_L and reduces only with increasing concentrations ('C'= chemical control). With chemical control only, it should be noted that an indirect relation between stomatal conductance and leaf water potential follows from the fact that the chemical signal is produced as a function of root water potential which is hydraulically linked to leaf water potential.

Another extreme case would be a hydraulically controlled plant ('H' = hydraulic control) in which the leaf conductance remains constant as long as the leaf pressure head, h_L , stays above a critical pressure head, h_{crit} . When h_L equals h_{crit} , stomatal conductance is reduced until the transpiration from the leaves to the atmosphere matches the transpiration stream in the plant that is driven by the hydraulic head difference between the rootzone and the leaves where the pressure head equals h_{crit} . This corresponds with $c_d = 1$ and s_h equal to infinity so that Eq. 2.2a is a step function in terms of h_L . Such step functions are often used to describe stomatal closure in hydrological models [Feddes *et al.*, 1978].

In Figure 2.1, the curves shown represent lines on the $\alpha(h_L, c_L)$ surface that are obtained when the signal concentration c_L is kept constant. These curves demonstrate the behaviour of the $\alpha(h_L, c_L)$ function but do not represent a projection of the trajectory of $\alpha(h_L, c_L)$ on the h_L axis during a drying event, in which both h_L and c_L change over time. Thus these curves only represent the stomatal response for a single concentration value.

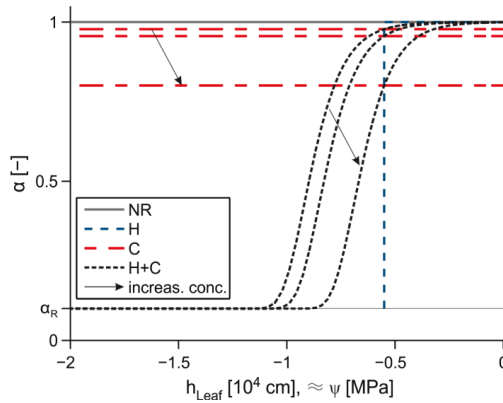


Figure 2.1 General behaviour of Eq. 2.2a over varying leaf water potentials, where multiple lines refer to different signal concentrations (arrows indicate towards higher concentrations; $(0.5, 1, 2) \cdot 10^{-3} \text{ nmol cm}^{-3}$). NR: No regulation, H+C: hydraulic and chemical control ($s_c = 5 \cdot 10^{10} \text{ cm}^3 \text{ mol}^{-1}$, $s_h = 1 \cdot 10^{-3} \text{ cm}^{-1}$, $a_R = 0.1$; $h_{crit} = -5500 \text{ cm}$); H: hydraulic control ($s_c = 0$; $s_h = 1 \cdot 10^{10}$; $a_R = 0.1$, $h_{crit} = -5500 \text{ cm}$), C: chemical control ($s_c = 5 \cdot 10^{10}$; $s_h = 0$, $a_R = 0.1$)

2.2.3 Hydraulic signalling

R-SWMS [Javaux *et al.*, 2008] calculates the pressure head in the leaves, h_L , by solving the hydraulic equations within the xylem network, between the xylem and the soil-root interface, and between the soil-root interface and the bulk soil. The water flow distribution in the soil and root systems can be predicted in 3-D by solving respectively the Richards [1931] and the equations from Doussan *et al.* [2006]. Radial uptake J_r [$\text{m}^3 \text{ s}^{-1}$] and axial flow within the root xylem, J_x [$\text{m}^3 \text{ s}^{-1}$] are defined for each root segment, i , by the equations from Doussan *et al.* [2006]:

$$J_r = K_r^* A_r (h_{s,int} - h_x) \quad 2.3a$$

$$J_x = -K_x^* A_x \left(\frac{\Delta h_x}{l_i} + \frac{\Delta z}{l_i} \right) \quad 2.3b$$

where K_r^* [s^{-1}] is the radial conductivity, A_r [m^2] the root outer surface, $h_{s,int}$ the soil pressure head at the root-soil interface and h_x the pressure head in the root xylem, K_x^* [$m s^{-1}$] the xylem hydraulic conductivity, A_x [m^2] the root cross-sectional area, Δh_x the difference in pressure head within the root segment, Δz [m] the difference in elevation, and l_i the length of the root segment. The R-SWMS model [Javaux *et al.*, 2008; N Schroder *et al.*, 2012; T Schroder *et al.*, 2009] was used to solve these equations numerically by coupling, on a voxel basis, the sink term of the Richards equation to the root water uptake ($\sum J_r$). Thus distributions of pressure heads within the soil and the root system and the root-water-uptake distribution within the soil could be predicted.

The shoot and leaves were effectively modelled with a segment connected to the root system collar. The length of this segment was relatively short so that the pressure head drop across this element was small. The simulated leaf pressure heads were therefore similar to the pressure heads at the root collar. By increasing the effective length or reducing the xylem conductivity of this segment, a larger pressure head difference between root collar and leaves can be simulated. However, accounting for an extra pressure drop between the root collar and the leaves will not influence the effect of different signalling mechanisms.

2.2.4 Chemical signalling

Chemical signalling refers to the loading of chemical signals into the xylem of plant roots as a function of rootzone water potential, their transport in the xylem to the shoot, and the regulation of stomatal conductance by their concentrations in the leaves. Thus production of chemicals in the leaves as a function of the leaf pressure head is not considered as chemical signalling between roots and leaves. Rootzone conditions and stomatal conductance are in this case related by hydraulic signalling. The concentration c_L in our model therefore only refers to the concentration of chemicals in the leaves that originate from the roots. This implies that the function $\alpha(h_L, c_L)$ cannot be parameterized based on chemical concentrations that are measured in the leaves.

Production of chemicals in the roots

The chemical production rate in a segment i , $M_{Signal,i}$ [mol d⁻¹], is modelled as a function of the pressure head in the root xylem, $h_{X,i}$, and the dry mass of the root segment m_i (g_{DM}) following *Dodd et al.* [2010] and [*Liu et al.*, 2005].

$$M_{Signal,i} = \begin{cases} 0 & \text{for } |h_{Root,i}| < |h_0| \\ a (|h_{X,i}| - |h_0|) m_i & \text{for } |h_{Root,i}| \geq |h_0| \end{cases} \quad 2.4$$

where a [mol g_{DM}⁻¹ m⁻¹ d⁻¹] is the production rate per dry mass of the root segment and pressure head, and h_0 [m] a threshold pressure head, below which production is started. This threshold was introduced to avoid hormone production for unstressed conditions and to lower computational costs for the particle tracking algorithm, as explained below. As ABA production was independent of root

type or age but dependent on root water potential [Simonneau *et al.*, 1998], a and h_0 are considered to remain constant in time.

Hormone transport to the leaves

Hormone transport in the root system was simulated using a particle tracking algorithm. At each time step, Δt , in any particular segment i , when $|h_{Root,i}| \geq |h_0|$, one particle with the mass $M_{signal,i} * \Delta t$ is generated. This particle is transported with the root water flow towards the leaves. By knowing the water flow through the root system, the xylem flow velocity $v_{R,i}$ in a given root segment, is calculated by Eq. 2.5.

$$v_{R,i} = \frac{J_{x,i}}{A_{x,i}} \quad 2.5$$

where $J_{x,i}$ [$m^3 d^{-1}$] is the axial water flow through the root segment i , and $A_{x,i}$ [m^2] is the cross section of the segment.

To account for particle mixing in the shoot, this segment was modelled as a perfectly mixed buffer with a volume, V_{Buffer} , that was a predefined multiple or fraction of the total root volume, V_{Root} (Eq. 2.6), representing the shoot volume. For herbaceous plants, the root:shoot ratio decreases with age and is strongly influenced by environmental conditions [Wilson, 1988]. Crop growth models (e.g. gecros) assume variations over a plant life from 0.5 to 2.0 [Yin and van Laar, 2005]. A reference buffer size, equalling the total root volume (root:shoot = 1.0), was assumed. A transpiration rate of $10 \text{ cm}^3 \text{ d}^{-1}$ and a buffer volume of around 1 cm^3 (plant age around 20 days) leads to an average residence time of the chemical in the buffer of around 0.1 days, within the range of previously observed half-life of ABA in stressed plants [Liang *et al.*, 1997]. The concentration in this uppermost segment, c_L at time $t_j + \Delta t$ was calculated from the concentration at time t_j as:

$$c_L(t_j + \Delta t) = c_L(t_j) + \frac{\Sigma mass - c_L(t_j)T_{act}\Delta t}{V_{Buffer}} \quad 2.6$$

where $\Sigma mass$ is the mass of all particles that arrive in the upper segment during time t_j and $t_j + \Delta t$.

To evaluate the impact of chemical transport from the roots to the leaves, a model in which root produced hormones are assumed to arrive instantaneously at the leaves ('H + C, i') was considered, so that c_L [nmol cm⁻³] can be calculated as the sum of the root tip production rates, $\Sigma M_{signal,i} = M_{signal,tot}$, divided by the actual transpiration (Eq. 2.7). In this approach it is not necessary to simulate transport through the root system.

$$c_L(t_j + \Delta t) = c_L(t_j) + \frac{M_{signal,tot}\Delta t - c_L(t_j)T_{act}\Delta t}{V_{Buffer}} \quad 2.7$$

2.3 Materials and Methods

2.3.1 Virtual experiments

First, a split root experiment in which one part of the rootzone was dried was simulated to compare different mechanisms that relate heterogeneous rootzone conditions to stomatal closure and transpiration reduction: hydraulic (H), chemical transport (C), the combination of both (H+C), and a hypothetical instantaneous chemical signal (H+C,i). Second, to evaluate the model's general behaviour and its response to changes in the parameters of the stomatal model (s_c , s_h , h_0) (Eq. 2.2a), a sensitivity analysis was carried out by varying each parameter by one order of magnitude. Additionally shoot buffer size was varied from 0.02 to $2*V_{Root}$ (see Appendix A.1). Third, the impact of chemical *versus* hydraulic signalling on transpiration when rootzone drying was alternated between the two soil compartments was tested for a constant and for a transient, diurnal, transpiration demand.

For all simulations, daily irrigation rates as well as the daily transpiration demand (T_{pot}) remained the same. Different responses were thus due to a different parameterization (sensitivity analysis) and/or due to different signalling mechanisms (H, C, H+C, H+C,i). Details of the soil compartments, root system and boundary conditions are given below. Parameterization of the setups and sensitivity analyses are given in Table 2.1 and Table 2.2 respectively.

2.3.2 Soil Domain

The soil domain (Figure 2.2) of $7 \times 3 \times 15.5 \text{ cm}^3$ was subdivided by a grid with voxel sizes of $0.25 \times 0.5 \times 0.5 \text{ cm}^3$. To simulate spatially variable water application leading to contrasting water distribution over the rootzone, the domain was split in two equal parts, separated by a non-conductive layer in the y-plane with a width of 4 voxels (

Table 2.3, #2). Soil parameters for the two compartments were set to a clay loam (

Table 2.3, #1) taken from *Carsel and Parrish* [1988].

Table 2.1 Parameters for Eq. 2.1a - 2.3a and root hydraulic conductivities (parameters in italic are for the transient simulations with diurnal variations in transpiration rate)

	H	C	H+C	H+iC
	hydraulic signaling	chemical signaling	hydr.+chem. signaling	hydr. + instantaneous chem. signaling
Chemical transport	no	yes	yes	no
$h_{crit}[cm]$			-5500 -8500	
$s_c[cm^3 mol^{-1}]$	0		$5*10^{10}$	
$s_h[cm^{-1}]$	$1*10^{100}$	0		$1*10^{-4}$
$a^a[mol g^{-1} cm^{-1} d^{-1}]$	-		$2.755*10^{-12}$	
$h_0 [cm]$	-		-4500 -7500	
$\alpha_R[-]$	-		0	
$V_{Buffer}[cm^3]$	0	$0.97 (= 1*V_{Root})$		0
$K_R [d^{-1}]$			$4.32*10^{-5}$ $1.728*10^{-4} **$	
$K_X^b[cm^3 d^{-1}]$			$4.32*10^{-2}$	

^afrom *Simonneau et al.* [1998], Fig.8

^bParameter from *Doussan et al.* [1998b]

Table 2.2 Parameters that were varied in the sensitivity analysis

	$s_c [cm^3 mol^{-1}]$	$s_h [cm^{-1}]$	$h_0 [cm]$	$V_{Buffer} =$ V_{Root}^*	Impact
Reference	$5*10^{10}$	$1*10^{-4}$	-4500	1	
$s_c *0.1$	$5*10^9$	$1*10^{-4}$	-4500	1	} <i>magnitude</i> <i>of</i> <i>transpiration</i> <i>reduction</i>
$s_c *10$	$5*10^{11}$	$1*10^{-4}$	-4500	1	
$s_h *0.1$	$5*10^{10}$	$1*10^{-5}$	-4500	1	
$s_h *10$	$5*10^{10}$	$1*10^{-3}$	-4500	1	
h_0+1000	$5*10^{10}$	$1*10^{-4}$	-3500	1	} <i>onset of</i> <i>transp. reduc.</i>
h_0-1000	$5*10^{10}$	$1*10^{-4}$	-5500	1	
$V_B *0.02$	$5*10^{10}$	$1*10^{-4}$	-4500	0.02	} <i>oscillations</i> <i>of</i> <i>the</i> <i>system</i>
$V_B *0.1$	$5*10^{10}$	$1*10^{-4}$	-4500	0.1	
$V_B *0.5$	$5*10^{10}$	$1*10^{-4}$	-4500	0.5	
$V_B *2$	$5*10^{10}$	$1*10^{-4}$	-4500	2	

Table 2.3 Soil hydraulic parameters of the Mualem van Genuchten equations [*Van Genuchten*, 1980]

Material Number	θ_{res} [-]	θ_{sat} [-]	α [cm ⁻¹]	n [-]	m [-]	l [-]	K_{sat} [cm d ⁻¹]
1	0.095	0.41	0.019	1.31	0.237	0.5	6.24
2	0.095	0.41	3*10 ⁻⁶	1.5	0.333	0.5	0

2.3.3 Root System

The root system was considered to be static (non-growing) during the simulation (25-40 days), to focus on non-growth related plant responses to water deficit. The split-root system was generated by using the root growth module within R-SWMS (Figure 2.2), as previously described [*Clausnitzer and Hopmans*, 1994; *Somma et al.*, 1998]. Both soil compartments have an equal number of root tips but root structures are not mirror images of each other as the growth model includes a random component. With the same input configuration, two subsequent runs of the growth model result in different root structures. Since the root surface in the two compartments differed by 1.8 % and the root length by 2.1 %, simulated root water uptake rates from the two compartments deviated by 1.2 % when uniform irrigation was supplied to both soil compartments.

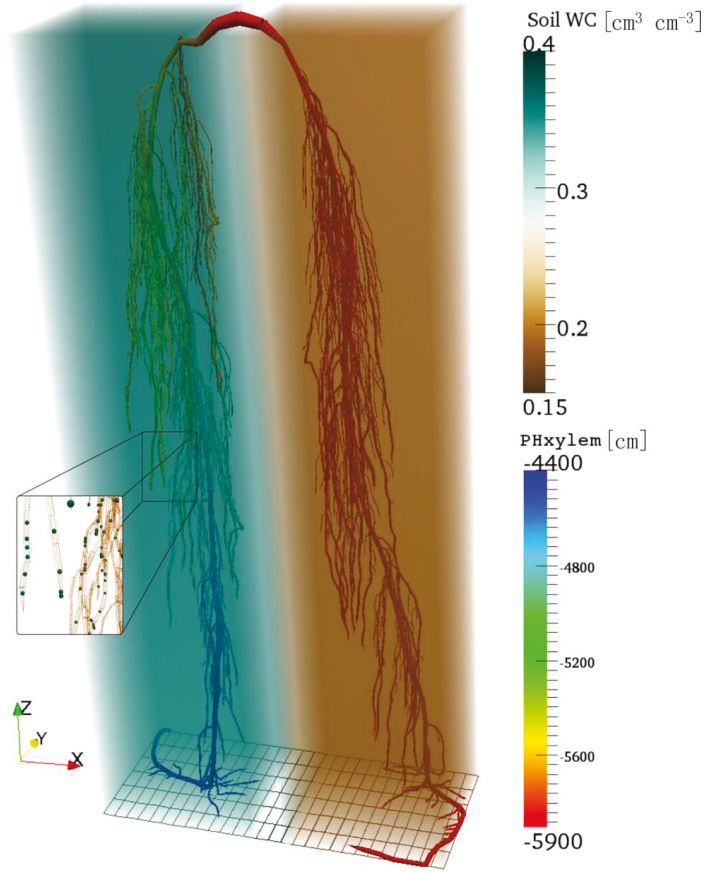


Figure 2.2 3D distribution of soil water content within the soil domain [$\text{cm}^3 \text{cm}^{-3}$] at Day 25, after stopping irrigation of the right compartment, together with distribution of water potential in the root xylem [cm] $\approx \psi$ [10^{-4} MPa]. The soil domain was $7 \times 3 \times 15.5 \text{cm}^3$. The detail shows the particles, representing a chemical signal, within the roots

2.3.4 Boundary and Initial conditions

The upper soil boundary condition was set to a flow boundary (Cauchy type). Both soil compartments were independently, uniformly irrigated during the first five days (each side received $5.85 \text{cm}^3 \text{d}^{-1}$, irrigation rate = 0.65cm d^{-1}). On subsequent days, one side of the root system received $11.7 \text{cm}^3 \text{d}^{-1}$ whereas the other compartment was not irrigated. Irrigation of the two soil compartments was sometimes alternated, as in PRD experiments under field conditions. Lateral walls of the soil domain were set to a no-flow condition and the bottom to free drainage, i.e. $dh/dz = 0$.

To solve the flow equations in the root system, the transpiration rate, $T_{act} = \alpha T_{pot}$ was set as a flow boundary condition at the upper segment connected to the root network. The potential transpiration rate was either kept constant over time with $T_{pot} = 10 \text{ cm}^3\text{d}^{-1}$ or transient with a diurnal cycle that was modelled as a truncated sine with zero transpiration during night (12 h). For the C, H+C and H+C,i scenarios, the relative stomatal conductance α was derived from the pressure head and chemical signal concentration in the leaves. For the H scenario, a flow boundary condition was used with $\alpha = 1$ for $h_L > h_{crit}$. When $h_L = h_{crit}$, the boundary condition was switched to a so-called Dirichlet condition for which h_L was kept at a constant pressure head h_{crit} .

The steady state water pressure heads obtained under uniform irrigation were used as initial condition. Simulation durations, with varying irrigation regimes and stomatal regulation, ranged from 25 to 40 days.

2.3.5 Definition of effective rootzone pressure head

Typically in hydrological models a piece-wise linear relation between rootzone pressure head and transpiration rate [Feddes *et al.*, 1978] is used to relate the reduction of transpiration and soil water potential. To investigate the effect of chemical signalling on this relationship, we calculated averaged rootzone pressure heads in the entire rootzone and in each of the two compartments of the split root experiment.

Couvreur *et al.* [2012] derived a procedure to define an effective rootzone hydraulic head $h_{S,eff}$ that takes the root architecture into account by only considering soil voxels that are affected by root water uptake:

$$h_{S,eff} = \frac{\sum_{k=1}^n (h_k + z_k) s_k}{\sum_{k=1}^n s_k} \quad 2.8$$

where the subscript k stands for the k^{th} soil voxel and s_k [-] is the standardized sink fraction (SSF [-]) that corresponds to fraction of root water uptake from this voxel for the case that the hydraulic heads ($h+z$) are uniformly distributed in the rootzone [Couvreur *et al.*, 2012].

2.4 Results and Discussion

2.4.1 Influence of stomatal regulation mechanisms

Initially, the effect of different mechanisms (NR, H, C, H+C) that relate the rootzone water pressure head with stomatal conductance on the pressure head in the leaves and on transpiration rate were simulated (Figure 2.3). During the first five days, when irrigation was applied uniformly to both soil compartments, the plant was unstressed ($T_{act} = T_{pot}$, Figure 2.3 b). After switching to non-uniform irrigation (Day 5), while keeping the amount of applied water constant, the pressure head at the leaves started to drop (Figure 2.3 a). Until approximately Day 9, the pressure heads for the different mechanisms are similar and actual transpiration rates equal potential transpiration rates. Water uptake from the drying compartment progressively decreased until it ceased around Day 18, when the irrigated compartment alone supported transpiration (Figure 2.3 d).

For the NR case, after Day 9 transpiration remained constant over time but the pressure head at the leaves declined until about Day 20 when it reached a steady state (ca. $-6400 \text{ cm} \approx -0.64 \text{ MPa}$, Eq. 2.1a). When only one compartment is irrigated, the same volume of water must be taken up and transported to the leaves through fewer roots, thus the pressure head drop between the soil and leaves becomes larger and the pressure head at the leaves smaller (Figure 2.3 c).

For the H case, stomatal conductance regulates the pressure head in the leaves and keeps it constant when $h_{crit} = -5500 \text{ cm}$ is reached. Thus the pressure head at the leaves cannot decrease to the value (-6400 cm) required to maintain a steady transpiration rate when only one compartment of the rootzone is irrigated. Consequently, transpiration starts to decrease when the pressure head at the leaves becomes -5500 cm , until it reaches a new steady value after around 25 days.

For two of the chemical signalling cases (C, H+C), transpiration was reduced earlier than in purely hydraulic regulation (H). Since chemicals were produced at pressure heads in the rootzone below -4500 cm (Table 2.1, h_0), chemical signalling started to decrease stomatal conductance and transpiration for leaf pressure heads slightly smaller than -4500 cm in the case of instantaneous transport (H+C,i) and more negative values when convective transport in the plant root system was considered. Although there are some differences between chemical (C and H+C) and hydraulic (H) controls, the transpiration rate as well as the pressure head at the leaves were similar when steady state was reached (data not shown). Responses to an instantaneous chemical signal (H+C,i, Eq. 2.6) were comparable to hydraulic only signalling (H) but with a higher steady state pressure head of around -4800 cm .

Generally, simulated transpiration rate evolved similarly with time for the different cases. However, transpiration rate monotonically declines for the H and H+C,i cases whereas for C and H+C cases it starts to gradually increase again at around Day 15 (Figure 2.3 b). This recovery of transpiration during uninterrupted drying of one part of the root system was previously reported from split-root experiments [Khalil and Grace, 1993; Stoll *et al.*, 2000]. Our simulations indicate that it could be explained by the decline in water uptake from the drying compartment (Figure 2.3 d) and, for the C and H+C case, the corresponding decrease in transport of chemicals produced in the drying compartment. After reaching a peak at Day 14, the mass flux of chemical signals from the dry root system to the leaves declines again (Figure 2.4), as demonstrated experimentally [Dodd *et al.*, 2008b]. When comparing transpiration rates (Figure 2.3 b), transport limitation of chemical signals produced in the drying roots (H+C) leads to 50% less transpiration reduction than in the case of instantaneous chemical signal transfer to the shoot (H+C,i).

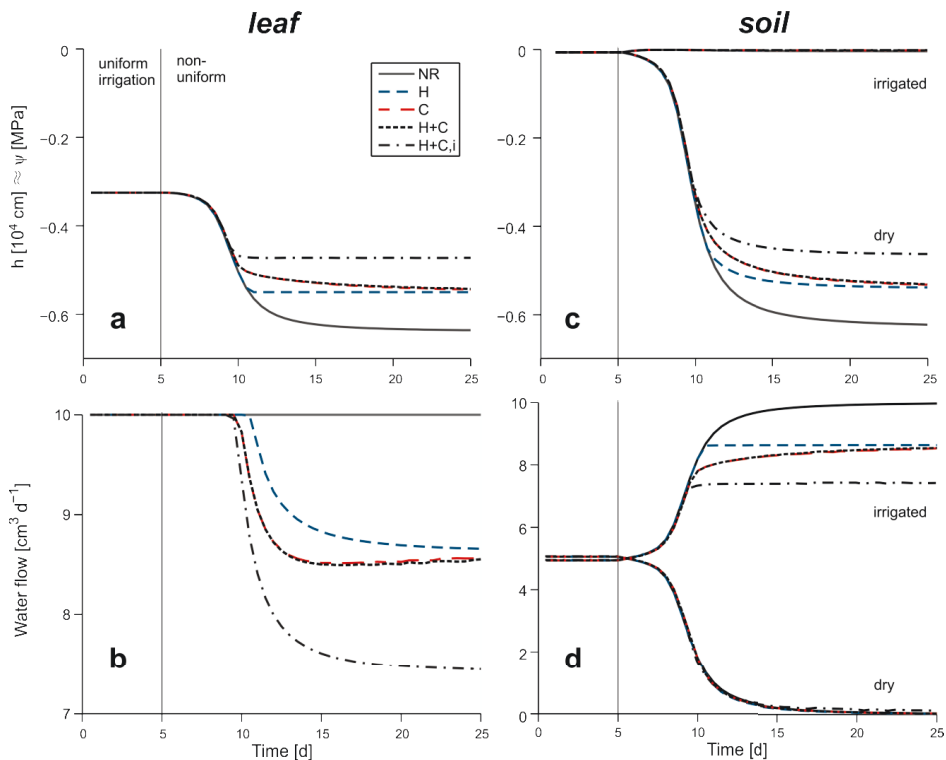


Figure 2.3 Responses of the soil-root system: a) leaf water potential and b) transpiration rate, and c) effective soil water potential and d) water uptake from the two soil compartments for different mechanisms that link rootzone water potential with stomatal conductance and transpiration: NR = no reduction of transpiration, H = hydraulic control, C = Chemical control, H+C = hydraulic and chemical control, and H+C,i = hydraulic and instantaneous chemical signalling

2.4.2 Effect of chemical signal concentration and linkage to soil pressure head

These simulations allow chemical signal concentrations and mass fluxes coming from the two parts of the split root system and arriving at the shoot to be examined (Figure 2.4). A signal concentration range between $1 \cdot 10^{-4}$ and 1 nmol cm^{-3} ($1 \text{ nmol cm}^{-3} = 1 \mu\text{M}$ or 1000 nM) matches the observed concentration ranges of ABA in xylem sap [Li *et al.*, 2011; Martin-Vertedor and Dodd, 2011; Stoll *et al.*, 2000]. Signal concentration in the transpiration stream arriving from the dry side is nearly three orders of magnitude higher than the concentration coming from the irrigated side (Figure 2.4). Ranges of two orders of magnitude were observed experimentally [Dodd *et al.*, 2008b]. However, the mass flow of chemical arriving from the dry compartment is only about twice as high as the flow from the irrigated compartment, due to limited transport of chemical signals out of roots in dry soil (Figure 2.4 a). The model also simulated chemical signal production in the irrigated rootzone, which considerably contributed (ca. 30 %) to the total mass that arrived in the shoot (Figure 2.4 a).

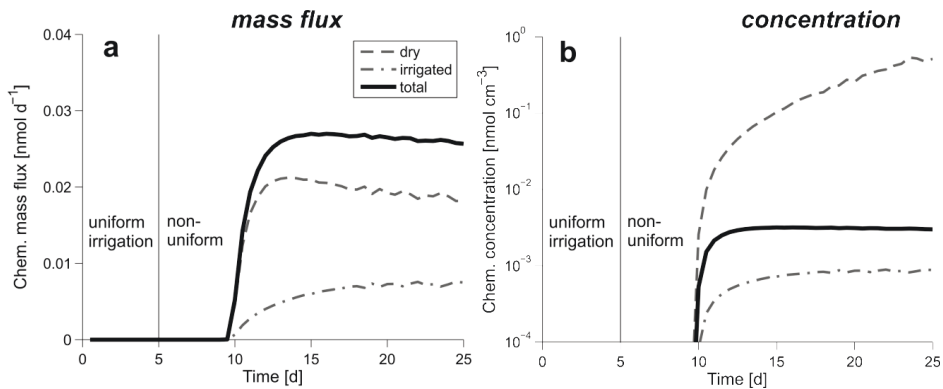


Figure 2.4 Concentration effect: Chemical signal arriving at the leaves from the dry (dashed line) and the irrigated (dash-dotted line) compartment and total (solid line). a) Comparison of mass fluxes and b) concentrations of chemical signal for the H+C case

The distribution of pressure heads in the root xylem and in the soil voxels where water is taken up for a uniform hydraulic head distribution ($SSF > 0$) is shown before and after the partial irrigation started for the H+C scenario (Figure 2.5). Since root water uptake in the irrigated part increased, the pressure difference between soil and root xylem increased and the pressure head in the roots decreased in the irrigated part of the rootzone even though the effective soil water pressure head increased. Furthermore, the pressure heads in the roots varied considerably so that the root pressure head decreased below h_0 in parts of the irrigated root system (Figure 2.5 a) and thus chemical signal was

produced. This illustrates that, for this study, signal production in the irrigated part of the rootzone, which is related to the local water pressure head in the roots, cannot be directly linked to the effective soil water pressure in that part. This missing link was previously observed in an experimental study [Puértolas *et al.*, 2013]. Since the flow from the non-irrigated part ceased, the pressure heads in the non-irrigated part converged to the leaf pressure heads (Figure 2.5 b, see also Figure 2.3 a, c).

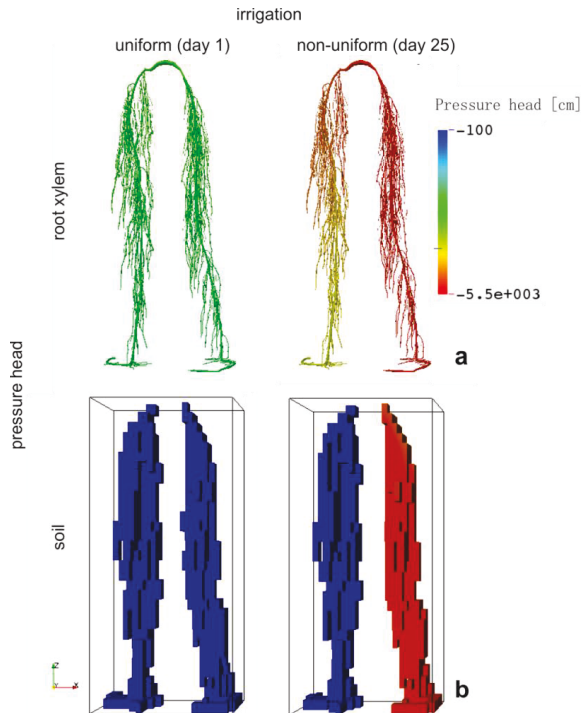


Figure 2.5 Comparison of root xylem and soil water pressure heads (only soil voxels where $SSF > 0$) for H+C at uniform irrigation (Day 1, left side) and for non-uniform irrigation (Day 25)

2.4.3 Effects of signal transport

Several authors attempted to link soil water content to xylem ABA concentrations [Dodd *et al.*, 2008b; Liu *et al.*, 2008] by assuming that soil water content was the driver for ABA production. Thus signal concentration in the shoot was plotted against the degree of (soil water) saturation ($S = (\theta - \theta_R) / (\theta_S - \theta_R)$) of the drying compartment (Figure 2.6). For comparison, signal concentrations were calculated by injecting all rootzone produced chemicals instantaneously into the

shoot. In this case, signal concentration continuously increased and was consistently one order of magnitude higher. When transport of the chemical signal with xylem water flow in the root system was simulated, a peak concentration was reached at a relative saturation of around 0.27, as in split-root experiments demonstrating a peak shoot hormone concentration at an intermediate soil water content of the drying compartment [Dodd *et al.*, 2008b; Liu *et al.*, 2008]. Thus linearly relating hormone production to root pressure head may lead to this type of behaviour when transport of chemical signals from a drying part of the rootzone becomes limiting.

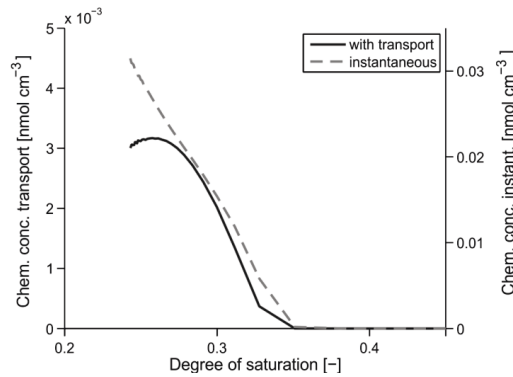


Figure 2.6 Transport effect: Concentrations of the chemical signal in the leaves versus the degree of saturation of the drying compartment for the case that the rootzone produced chemicals are transported with the water flow from root system to the leaves ('with transport') and for the case that the rootzone produced chemicals are instantaneously injected in the shoot ('instantaneous') (Eq. 2.7)

2.4.4 Sensitivity analysis

Stomatal conductance and resulting actual transpiration rate was modelled versus time and versus the effective soil water pressure head for different values of parameters used in Eq. 2.2a (Figure 2.7). Both sensitivities of this equation, s_h and s_c influence the magnitude of the transpiration reduction but not when transpiration is reduced (Figure 2.7 a). A higher sensitivity of stomatal conductance to chemical signal concentration (larger s_c) decreases transpiration to a greater degree. The sensitivity to the pressure head is smaller and the influence of the pressure term in Eq. 2.2a is negligible when s_h becomes smaller than $1 \cdot 10^{-4} \text{ cm}^{-1}$. The onset of reduction is related to the threshold for the release or production of chemical signals in the roots, h_0 . This parameter also influences the magnitude of transpiration reduction since it determines the chemical production rate as function of the root water pressure head.

When a threshold pressure in the leaves is maintained (H case), linear piece-wise relations (step functions) between transpiration reduction and the effective soil water pressure head as defined in Eq. 2.1a, which represents a soil water pressure head sensed by the roots, are obtained for a given potential transpiration rate [Couvreur *et al.*, 2012; Javaux *et al.*, 2013]. This agrees with the functions typically used in soil water flow models to describe the reduction of transpiration as a function of soil water pressure head [Molz, 1981]. If an additional chemical signal is considered, similar piece-wise linear relations between transpiration reduction and effective soil pressure head are obtained (Figure 2.7 b). The slope of the $\alpha(h_{s,eff})$ increases with increasing s_c and s_h and the onset of the transpiration reduction shifts towards lower effective soil water pressures for smaller s_h values. These results suggest that the effect of chemical signalling may be approximated by functions that relate transpiration reduction directly to soil water pressure head and that similar functions are obtained when only hydraulic signalling is considered. However, despite their similarity to piece-wise linear functions, the relationships obtained for chemical signalling (when soil pressure head is related to transpiration reduction) show some peculiarities when transport of chemicals produced in dry rootzones becomes limited. As observed experimentally, the relationship loses its linearity and transpiration recovers when chemicals produced in the dry rootzone are no longer transported to the shoot [Dodd *et al.*, 2008a; Liu *et al.*, 2008], thus increasing total root water uptake with decreasing effective soil water pressure head.

The influence of shoot volume on transpiration is explored in Appendix A.1.

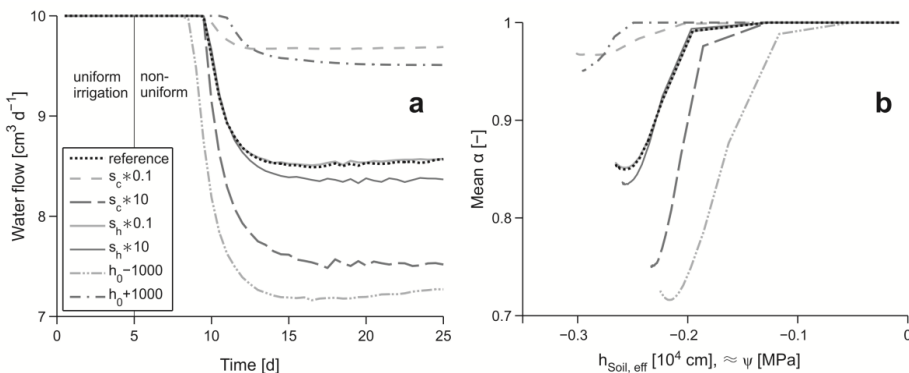


Figure 2.7 Sensitivity analysis of the parameters of Eq.2.2a: a) Transpiration rate over time and b) transpiration reduction ($\alpha = T_{act}/T_{pot}$) over effective soil water potential

2.4.5 Alternated partial rootzone drying

Constant transpiration demand

When irrigation was alternated between wet and dry soil compartments after 15 days, Simulation 1 regulated stomata only as a function of leaf pressure head (H) while Simulation 2 included an additional chemical signal (H+C). Additional simulations of C and H+C_i were not included as responses were similar to the H+C and the H case, respectively (see also Figure 2.3). During the first five days, when irrigation was applied uniformly to both soil compartments, actual transpiration equalled the potential transpiration (Figure 2.8 a) in both simulations. Transpiration began to decline about four days after changing to partial irrigation. The general course of transpiration is similar for the H and H+C cases, even though transpiration was less in the H+C case, indicating that both hydraulic and chemical signalling can produce similar plant responses during alternate PRD.

However, immediately after alternating irrigation at Day 20, the transpiration rate of H+C sharply decreased, associated with an increased signal concentration in the shoot (Figure 2.8 c, black solid line). After an initial drop, signal mass flux from the previously non-irrigated root system showed a distinct peak for about a day. With continued re-wetting of this compartment (Figure 2.8 b) and increased water uptake from roots contained therein, chemicals accumulated in the roots can again be transported to the shoot. Interestingly, signal mass flux from the now-drying compartment is reduced. As this compartment still contains water from the previous irrigation cycle, and the other compartment is now irrigated, a larger part of the root system can contribute to water uptake (Figure 2.8 b). This leads to a more homogeneous distribution of soil water pressures and thus a relaxation of the total root system with higher root water potentials than under stress conditions.

Increased transport of chemical signals upon rewetting part of the rootzone (presumably originating from previously stressed parts of the rootzone) was observed in field experiments with grapevine in the morning shortly after the onset of transpiration [Romero *et al.*, 2012] and in pot-grown tomato plants for 8 hours after alternating irrigation [Dodd *et al.*, 2006]. Production and accumulation of chemical signals during periods without root water uptake (e.g. during night or in non-irrigated parts of the rootzone) and subsequent transport when root water uptake starts again (e.g. in the morning or re-wetting of roots in dry soil) may be critical in regulating transpiration of plants exposed to PRD, and may contribute to the agronomic advantages of alternated partial rootzone drying over deficit irrigation [Dodd, 2009].

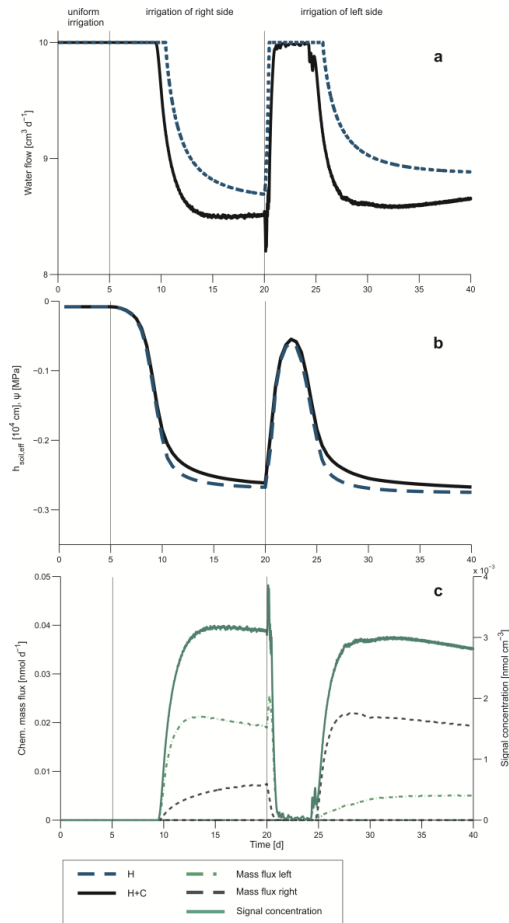


Figure 2.8 Partial rootzone drying with constant transpiration demand: a) Actual transpiration rate for regulation as a function of hydraulic signalling (H) and of hydraulic + chemical signalling (H+C), T_{pot} remained at $10 \text{ cm}^3 \text{ d}^{-1}$. Irrigation was either applied uniformly or partially at the right or the left compartment. b) Effective soil water pressure head for the total soil domain for H and H+C. c) Concentration of chemical signal in the shoot and mass flux of chemical arriving at the shoot from both compartments. Values are averaged over 0.1 days

Transient transpiration demand

To obtain more realistic conditions, the previously described scenario was modified by applying a diurnal, sinusoidal transpiration demand and an alternating irrigation cycle with a frequency of five days. Irrigation was only applied during day time at a constant rate of 2.6 cm d^{-1} ($= 11.7 \text{ cm}^3 \text{ d}^{-1}$), when plants transpired. Again, during the first five days, irrigation was uniform and the actual transpiration equalled the potential daily averaged transpiration of 10 cm^3 (Figure 2.9 b). About three days after changing to partial irrigation, transpiration declined. Unlike simulations with constant transpiration demand, transpiration rate did not recover immediately after alternating irrigation but remained low for another day until it recovered again. Here, the transpiration reduction was slightly higher for the purely hydraulic case (H) due to parameterization of either h_{crit} or the parameters of Eq. 2.2a (see the section ‘Sensitivity’). Generally, transpiration was similar with and without additional chemical signalling, suggesting it could be described by a hydraulic signal alone.

Effects of an alternation event on the daily courses of transpiration and chemical signalling were examined in more detail (Figure 2.9 b). Initially, actual transpiration follows potential transpiration (light grey) and as maximum transpirational demand at midday approaches, both cases start to reduce their transpiration rate. T_{act} equals T_{pot} again in the ‘evening hours’. Thus, both cases reproduce the well-known midday depression in transpiration and its subsequent recovery. Before switching the irrigation, the drying side of the root system provides most of the chemical signal that decreases transpiration. This is maintained for 2 days after the irrigation was alternated, reflecting a lag phase of the system due to the time it takes to re-wet the previously dry soil, and dry out the previously irrigated rootzone.

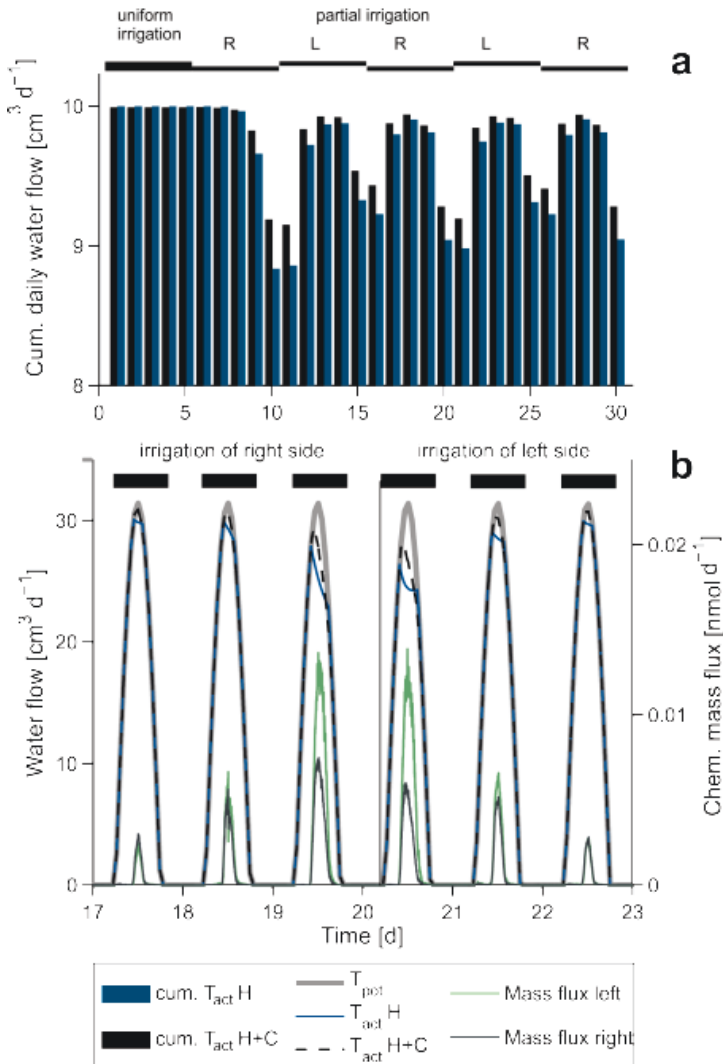


Figure 2.9 Partial rootzone drying with transient transpiration demand: a) Cumulated actual daily transpiration for regulation as a function of hydraulic signalling (H) and of hydraulic + chemical signalling (H+C), T_{pot} remained at $10 \text{ cm}^3 \text{ d}^{-1}$. Irrigation was either applied uniformly or partially at the right (R) or the left side of the compartment (L). Amount of irrigation per day remained constant. b) Daily course of mass flux of chemical signal arriving at the leaves from each compartment and of the actual transpiration for H and H+C in comparison to potential transpiration (light grey). Irrigation was only applied during day (indicated by black bars)

2.5 Conclusions

We developed a model that simulates the effect of a root-produced chemical signal on stomatal regulation, transpiration and root water uptake. This model evaluated the impact of different regulatory mechanisms on plant transpiration when the root system is in a soil with spatial variations in soil water potentials. The model reproduced some experimental observations such as absolute xylem ABA concentrations, transient effects of root-produced chemical signals on transpiration, a transpiration restriction when previously dried roots re-commence water uptake, and transpiration oscillations (see Appendix A.1). Those effects are attributed to transport limitations of the chemical signal from the roots that emerge when parts of the root zone dry out strongly so that there is no uptake and water flow from these regions. Transport limitation leads to a reduction of the stomatal regulation that may result in an increase in transpiration during a drying process. This phenomenon cannot be reproduced by classical root water uptake models that describe relative root water uptake (relative to potential transpiration) only as a function of rootzone water potential. Another transport related example is that of the flushing of chemical signals from a dry rootzone upon rewetting. This flush may lead to a temporal decrease in transpiration rate but may as well have other plant physiological effects. However, effects of chemical signals on modulating tissue hydraulic conductivity (e.g. via altering aquaporin expression in the leaves) that may enhance the impact of hydraulic signals on stomatal closure [Pantin *et al.*, 2012] were ignored in this study.

Alternatively, chemical signalling seems less important over longer time scales, since models that predicted root water uptake based only on hydraulic signalling adequately simulated plant responses to drying soil. However, a detailed soil and root water uptake model shows that soil moisture heterogeneity influences plant hydraulics. Contrary to current assumptions, simulations indicate that effects of heterogeneous distribution of rootzone soil water potential and alternate partial rootzone drying on stomatal conductance can largely be explained by hydraulic signalling. This suggests that the spatial dynamics of root water uptake from soils with temporally varying spatial distributions of water content may be described by models that consider only the hydraulics of the soil-root system, even when the mechanism that relates transpiration to soil water potential is chemical signalling.

Furthermore, the model allows the effects of a simultaneously increasing rate of signal production and a decreasing water uptake rate on signal concentration in PRD plants to be quantified. While the mass fluxes from the dry side were about twice as high as those from the irrigated side, the concentration difference was three orders of magnitude. Therefore, measuring signal concentrations from roots in drying soil [Dodd *et al.*, 2008a; b] may overestimate effects of chemical signalling on transpiration, as water (and signal) transport out of these roots decreases. Chemical signal fluxes cannot be linked directly to bulk nor effective soil water potentials (see also Eq. 2.8), as the heterogeneous distribution

of soil and root water potential might initiate chemical signalling in only parts of the root system. To verify this model, experiments should simultaneously measure chemical signalling (concentrations and mass fluxes) as well as soil and root water potentials in both soil compartments of plants exposed to PRD.

The sensitivity analysis showed that the fitting parameters for hydraulic and chemical signalling s_h and s_c both influence the magnitude of transpiration reduction while the threshold pressure head for chemical signal production h_L affects the onset of transpiration reduction. Although the relationship between soil water pressure and regulation of transpiration became non-linear for chemical signalling alone, further investigations are needed in relation to the distribution of soil moisture heterogeneity and to soil and root hydraulic properties.

In conjunction with experiments, the model might prove useful to further investigate the influence of soil properties (e.g. soil water holding capacity) on root water uptake patterns, chemical signalling and stomatal regulation. Being able to simulate chemical signalling between root and shoot may allow simulation of other physiological effects related to shoot growth and assimilate redistribution, that may be important for optimizing irrigation strategies such as PRD.

CHAPTER 3

TRANSPIRATION REDUCTION DUE TO HYDRAULIC VERSUS CHEMICAL SIGNALLING FROM A PARTIALLY DRY ROOT ZONE – A SIMULATION STUDY

This chapter is based on a journal article submitted as:

Huber, K., Vanderborght, J., Javaux, M., Vereecken, H. Transpiration reduction due to hydraulic versus chemical signalling from a partially dry root zone – a simulation study, *Plant and Soil*, (submitted).

3.1 Introduction

Plants subjected to low soil water availability have developed different strategies to cope with drought. One of these is stomatal closure to minimize water loss to the atmosphere. Experimentalists observed two types of plant stomatal reaction to low water availability: isohydric, when leaf water potential was kept constant at a certain threshold, or anisohydric, when large fluctuations in leaf water potential were observed under different water statuses [Tardieu and Simonneau, 1998]. The control of leaf water potential on stomatal closure has been known for decades [Gardner and Ehlig, 1963]. More recently, chemical signals by plant hormones originating from plant roots or other plant tissues that control stomatal closure, e.g. abscisic acid (ABA), were discovered [Gowing *et al.*, 1990; Stoll *et al.*, 2000].

Although there is a multitude of models that describe stomatal conductance in relation to environmental factors [Damour *et al.*, 2010], there still remains a need to understand whether the current approaches that link stomatal conductance to soil water availability are valid if transpiration is regulated by chemical signalling [Javaux *et al.*, 2013]. Furthermore, the observed stomatal behaviour (anisohydric or isohydric) does not necessarily imply a priori a specific control mechanism. For instance, depending on hormone production and corresponding stomatal sensitivity, a chemical signalling could either result in iso- or anisohydric behaviour [Tardieu and Simonneau, 1998].

Two types of models were proposed to simulate stomatal regulation induced by drought. On one hand, empirical models try to relate stomatal closure directly to soil water potential and/or root zone soil moisture content. These relations were obtained from experiments, which have proven since decades the link between transpiration reduction and low soil water content. Eco-hydrological models compute stomatal regulation often as a function of lumped soil water content [Rodriguez-Iturbe and Porporato, 2005]. In hydrological models stomatal regulation is implicitly accounted for through stress functions, which relate the reduction of the potential transpiration rate to bulk soil water status. There are functions that link the reduction factor linearly to the soil water potential [Feddes *et al.*, 1978] or to the matric flux potential [van Lier *et al.*, 2006]. In addition to soil water potential, these stress functions also depend on the transpiration rate with a stronger reduction in transpiration rate for the same soil water potential when the transpiration rate is higher.

On the other hand, mechanistic models aim at linking stomatal regulation to plant variables triggering or controlling the stomatal aperture in a more direct way. These models use functional relationships between hormone concentrations, plant hydraulic variables like leaf water potential and stomatal resistance [Tardieu *et al.*, 1993]. In order to further link plant variables (e.g. leaf water potential and leaf hormone concentrations) with soil environmental variables (e.g. soil water potentials in the root

zone), meteorological conditions (e.g. potential transpiration rate or the transpiration rate when stomata are fully opened), but also plant properties (e.g. root hydraulic architecture, hydraulic conductivities of roots, production of hormones as a function of root water potentials), eco-physiological models have been developed [*Rodriguez-Iturbe et al.*, 2001].

For the case that stomatal regulation is only a function of the leaf water potential (i.e. fully hydraulic control) and that this function is a step function (i.e. stomata are not closed when the leaf water potential is above a critical threshold value and adjust their aperture to keep a constant leaf water potential), a hydraulic model of the soil-plant system can be used to describe the transpiration fluxes [*Doussan et al.*, 2006; *Javaux et al.*, 2008]. Direct relations between hydraulic properties of the root system, the spatial distribution of the soil water potentials, the maximal possible transpiration rate, and the distribution of the water uptake in the root zone emerged from a theoretical analysis of such a system [*Couvreur et al.*, 2012; *Javaux et al.*, 2013].

However, such relations have not been established for the case that chemical signalling by plant hormones also plays a role. In order to bridge the gap between models and observations we included a module, which explicitly accounts for chemical signalling, to a numerical mechanistic root and soil water flow model. Recent attempts to model both hydraulic and chemical control of stomata showed promising results to reproduce experimental observations [*Huber et al.*, 2014]. Therefore, in this manuscript, we use simulations with this model to investigate the relation between transpiration reduction, water potential distribution in the root zone, and potential transpiration rate for different signalling mechanisms: hydraulic versus chemical signalling. We set up a series of virtual split root experiments with vertical and horizontal splits to further evaluate the influence of soil water heterogeneity on transpiration regulation. In addition, similar to what was done by *Couvreur et al.* [2012] for the hydraulically controlled soil-plant system, we did a theoretical system analysis of the chemically controlled and chemically-hydraulically controlled systems from which novel direct relations emerged. These relations, which might be useful in larger scale models to describe stomatal closure in a quantitative and mechanistic but simple way, were evaluated by simulations with the numerical model. In the following text we will refer to signalling by chemicals as ‘C’, and by both hydraulics and chemicals as ‘H+C’. We hypothesise that H+C controlled plants result in apparent isohydric behaviour, while C controlled plants lead to apparent anisohydric behaviour.

3.2 Methods

3.2.1 Numerical mechanistic model, R-SWMS

Soil-root water flow model and water potentials

R-SWMS (Root-Soil Water Movement and Solute transport modelling) is a coupled soil and root water flow model that computes water fluxes through the soil-plant-atmosphere continuum as a function of the hydraulic gradients in the system [Javaux *et al.*, 2008]. The Richards equation [Richards, 1931] is solved for a three-dimensional regular soil grid. The root architecture is explicitly represented in three dimensions. The water flow into the root xylem is governed by the pressure gradient between the soil root interface and the xylem pressure. The resulting radial flow is equal to the sink term of the Richard's equation. Flow through the roots towards the shoot is explicitly modelled and is driven by pressure gradients within the root system [Doussan *et al.*, 2006].

The total water potential is expressed as the energy per volume of water, which is equivalent to a pressure. The total water potential consists of different partial potentials. In the R-SWMS simulations, the partial potentials related to the elevation and to the water pressure are considered. For the water pressures, the difference to the atmospheric pressure is considered so that negative water pressures refer to pressures that are smaller than the atmospheric pressure. Partial potentials related to the osmotic potential can also be included [Schröder *et al.*, 2013], but were not considered in this study.

Chemical Signalling

In R-SWMS an additional chemical signalling was implemented [Huber *et al.*, 2014] using a particle tracking algorithm that generates during each time step and in each root segment a particle with a mass that is proportional to the duration of the time step and that depends on the local xylem water pressure. If the xylem water potential is lower (more negative) than a threshold water pressure, ψ_{lim} , particles are created.

The production rate of chemical in a root segment, M_i , (N T^{-1}) is given by Simonneau *et al.* [1998]:

$$\begin{aligned} M_i &= a m_i |\psi_{x,i} - \psi_{lim}| && \text{for } \psi_{x,i} < \psi_{lim} \\ M_i &= 0 && \text{for } \psi_{x,i} \geq \psi_{lim} \end{aligned} \quad 3.1$$

where a ($\text{N P}^{-1} \text{T}^{-1} \text{M}^{-1}$) is the production rate per root mass, m_i is the mass of segment i and $\psi_{x,i}$ is the xylem water pressure in segment i . The particles are further transported via the xylem water flow calculated by the root water flow model upwards towards the shoot, which is represented by a single segment with a volume, V_{buffer} [L^3]. This shoot segment acts as a mixing bucket or buffer and was introduced to suppress oscillations in stomatal regulation [Huber *et al.*, 2014]. The total mass of chemical signal in the shoot volume is calculated by adding the newly arrived chemical mass to and subtracting the mass that flows out from the prevalent mass in the shoot. The concentration is obtained by dividing the total mass by the volume of the shoot. The resulting concentration affects stomatal closure.

Tardieu and Davies [1993] proposed the following relation between stomatal aperture, signal concentration, and leaf water pressure, Eq. 3.2:

$$T_{act} = T_{pot} \left\{ \alpha_r + (1 - \alpha_r) \exp[-s_c c_{leaf} \exp(s_p |\psi_{leaf}|)] \right\} \quad 3.2$$

where T_{act} ($\text{L}^3 \text{T}^{-1}$) is the actual transpiration, T_{pot} ($\text{L}^3 \text{T}^{-1}$) is the potential transpiration, i.e. the transpiration when stomata are fully open, α_r (-) is the residual stomatal aperture, c_{leaf} is the chemical concentration in the leaves [N L^{-3}], $|\psi_{leaf}|$ [P] is the absolute value of the leaf water potential, and s_c ($\text{L}^3 \text{N}^{-1}$) and s_p (P^{-1}) are fitting parameters.

In R-SWMS, an H+C scenario is modelled using Eq. 3.2 with $s_p \neq 0$ and Eq. 1 $\psi_{lim} < 0$, and the C scenario using Eq. 3.2 with $s_p = 0$ and Eq. 3.1 with $\psi_{lim} = 0$. For the H scenario, Eq. 3.2 is not used directly but a critical water pressure $\psi_{lim,H}$ is defined in the shoot/leaves. As long as $\psi_{leaf} > \psi_{lim,H}$, T_{act} is equal to T_{pot} . When $\psi_{leaf} = \psi_{lim,H}$, the water potential in the leaves is kept constant and the water flow from the soil to the root and the shoot is calculated from the difference between the soil water pressure and $\psi_{lim,H}$ considering the soil and root resistances to flow in the system.

Although R-SWMS can be used to simulate the behaviour of single plants in which transpiration is controlled by chemical signalling, simpler models are needed to get insight into fundamental differences of the plant stomatal regulation by chemical or hydraulic signalling. Such models are also potentially useful for large scale system models (crop models), in which stress prediction is crucial but still poorly estimated.

3.2.2 Direct relation between transpiration and root zone water distribution including chemical signalling

In order to assess the regulation of transpiration by chemical signalling directly, a simple relation based on the following assumptions was developed (Figure 3.1): (i) soil is constituted of two isolated compartments, (ii) the wet part is constantly irrigated and the water pressure at the root-soil interface in the wet part, $\psi_{root,wet}$ remains close to zero, (iii) soil water pressure and root xylem water pressure in the dry parts of the root zone $\psi_{root,dry}$ is equal to the leaf water pressure ψ_{leaf} and differences in total water potential due to differences in elevation are neglected, (iv) chemical signal is only produced in the dry part of the root zone and is a linear function of the water pressure in the root, (v) the produced chemical signal is instantaneously effective in the stomata (no transport limitations considered), and (vi) the fraction of the water uptake from a compartment to the total water uptake by the entire root system when water pressure in both compartments is equal, is equal to the root mass fraction in the compartment. The last assumption implies that the distribution of fine and coarser roots and roots segments with different hydraulic conductivities is the same in the different compartments.

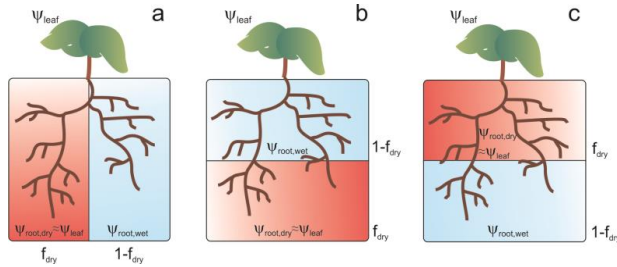


Figure 3.1 Schemes of the different split-root setups at steady state, where water uptake is only maintained by the wet (blue) part: vertical split (a), horizontal split with irrigation from the top (b) and from the bottom (c).

According to the third, fourth, and fifth assumption, dividing the production of signal by the actual transpiration results in the signal concentration in the leaves c_{leaf} ($N L^{-3}$), Eq. 3.3:

$$c_{leaf} = \frac{f_{dry} a^* |\psi_{root,dry} - \psi_{lim}|}{T_{act}} = \frac{f_{dry} a^* |\psi_{leaf} - \psi_{lim}|}{T_{act}} \quad 3.3$$

where a^* ($\text{N P}^{-1} \text{T}^{-1}$) is the signal production rate of the total root system which is multiplied by f_{dry} , representing the mass fraction of the roots in the dry compartment, to account for the fact that only roots in the dry compartment are producing the signal.

With the assumption that stomata close completely during night ($\alpha_s = 0$) and that the pressure difference between the dry and the wet soil compartment is large enough ($\psi_{root,wet} \approx 0$), combining Eq. 3.2 and 3.3 becomes (H+C) for $\psi_{leaf} < \psi_{lim}$:

$$T_{act} = T_{pot} \exp \left[\frac{-s_c f_{dry} a^*}{T_{act}} |\psi_{leaf} - \psi_{lim}| \exp(s_p |\psi_{leaf}|) \right] \quad 3.4$$

This equation relates T_{act} to ψ_{leaf} and T_{pot} but does not include the effect of the water flow in the soil root-plant system on the water pressure differences between the soil and the leaves. Based on the second and third assumption, it can be stated that the plant-soil system is in a steady state and that the actual transpiration is maintained only from the wet part of the soil and thus driven by the water pressure gradient between the leaf ψ_{leaf} (P) and the root-soil interface in the wet soil compartment $\psi_{root,wet}$ Eq. 3.5:

$$T_{act} = (1 - f_{dry}) K_{root} (\psi_{root,wet} - \psi_{leaf}) \quad 3.5$$

or

$$\psi_{leaf} = \psi_{root,wet} - \frac{T_{act}}{(1 - f_{dry}) K_{root}}$$

where K_{root} ($\text{L}^3 \text{P}^{-1} \text{T}^{-1}$) is the effective hydraulic conductivity of the entire root system. According to assumption (vi), f_{dry} can be either the mass fraction of roots in the dry compartment or the fraction of water that would be taken up from the dry compartment when it is equally wet as the wet compartment.

Based on this assumption and since water uptake only occurs from the wet part, the effective conductivity of the root system in the wet part is a fraction ($1-f_{dry}$) of the conductivity of the entire root system, K_{root} . Combining Eqs. 3.4 and 3.5 and assuming $\psi_{root,wet} \approx 0$ leads to:

$$T_{act} = T_{pot} \exp \left[\frac{-s_c f_{dry} a^*}{|(1-f_{dry})K_{root}|} \left| 1 - \frac{\psi_{lim}}{\psi_{leaf}} \right| \exp(s_p |\psi_{leaf}|) \right] \quad 3.6$$

This relation can be further rewritten as:

$$T_{act} = T_{pot} \exp \left\{ -s_c f_{dry} a^* \left[\left| \frac{1}{(1-f_{dry})K_{root}} \right| - \frac{|\psi_{lim}|}{T_{act}} \right] \exp \left[s_p \left| \frac{T_{act}}{(1-f_{dry})K_{root}} \right| \right] \right\} \quad 3.7$$

Eq. 3.7 provides an indirect relation between T_{act} , T_{pot} , plant parameters (s_c , s_p , a^* , ψ_{lim} , K_{root}), and the fraction of roots in dry soil which can be solved for T_{act} iteratively.

Once T_{act} is known, ψ_{leaf} can be calculated from Eq. 3.5 so that the effective soil water pressure $\psi_{soil,eff}$ (P) can be described according to *Couvreur et al.* [2012]:

$$\psi_{soil,eff} = (1-f_{dry})\psi_{root,wet} + f_{dry}\psi_{leaf} \quad 3.8$$

Where according to assumption (vi) ($1-f_{dry}$) and f_{dry} take up the role of the standard sink term fractions in the wet and dry parts of the root zone respectively. Plugging Eq. 3.8 into Eq. 3.5 leads to:

$$T_{act} = K_{root}(\psi_{soil,eff} - \psi_{leaf}) \quad 3.9$$

which is exactly the same equation as derived by *Couvreur et al.* [2012] to assess the effect of the soil water pressure and its spatial distribution on the transpiration rate. However, in contrast to *Couvreur et al.* [2012], who consider a isohydric plant behaviour with a constant $\psi_{leaf} = \psi_{lim,H}$ for $T_{act} < T_{pot}$, according to Eq. 3.6, ψ_{leaf} changes with T_{act} .

Apparent isohydric behaviour

Through inspection of Eq. 3.6, conditions or plant properties or parameters that lead to an isohydric plant behaviour can be inferred. In isohydric plants, leaf water potential is kept larger than or equal to a fixed value: $\psi_{leaf} \geq \psi_{lim,H}$. According to Eq. 3.6, such a behaviour can be obtained for $s_p > 0$ since stomatal conductance decreases sharply with $|\psi_{leaf}|$ when $|\psi_{leaf}| > 1/s_p$ so that $\psi_{lim,H} \approx 1/s_p$. Also for $s_p = 0$, when only chemical signalling is considered or active, apparent isohydric behaviour may emerge. When the sensitivity of the stomatal conductance to the chemical signal is sufficiently large, i.e. for a relatively large $\frac{s_c f_{dry} a^*}{(1 - f_{dry}) K_{root}}$, the actual transpiration rate decreases sharply within a relatively narrow range of $\psi_{leaf} \approx \psi_{root,dry} < \psi_{lim}$ so that $\psi_{lim,H} \approx \psi_{lim}$.

Apparent anisohydric behavior

When s_p is close to zero, i.e. $|\psi_{leaf}|$ must be very large before the stomatal conductance starts to decrease drastically with increasing $|\psi_{leaf}|$, the leaf water potentials can vary over a large range before a pronounced effect on the stomatal closure arises. For chemically controlled plants (C) with $\psi_{lim} = 0$ and $s_p = 0$, and for $|\psi_{root,wei}| \ll |\psi_{leaf}|$, Eq. 3.6 simplifies to:

$$T_{act} = T_{pot} \exp \left[\frac{-s_c f_{dry} a^*}{(1 - f_{dry}) K_{root}} \right] \quad 3.10$$

This equation illustrates that the relation between T_{act}/T_{pot} and f_{dry} neither depends on ψ_{leaf} nor on $\psi_{soil,eff}$.

Further the three parameters s_c , a^* , and K_{root} can be grouped in a dimensionless factor so that a change in one of these parameters can be compensated by a change in the other parameter without any effect on the relation between T_{act} and f_{dry} . Eq. 3.10 implies that for chemically controlled plants, the relation between the water pressure in the root zone and the transpiration rate is fundamentally different from the relation for hydraulically controlled plants. For a given f_{dry} , the ratio of T_{act}/T_{pot} is constant and therefore independent of T_{pot} . According to Eq. 3.9, this implies that for a given f_{dry} , the difference between effective soil water and leaf water pressure will be larger for a larger T_{pot} which implies in turn that for larger T_{pot} , ψ_{leaf} will be smaller, even when $T_{act} < T_{pot}$. In other words, the control exerted on stomatal closure in C plants cannot maintain a critical threshold leaf water pressure that is independent of the atmospheric demand for water or T_{pot} leading to apparent anisohydric behaviour.

For H or H+C plants, the leaf water pressure varies within a small range when $T_{act} < T_{pot}$. According to Eq. 3.9, this implies that for a given $\psi_{soil,eff}$, T_{act} is independent of T_{pot} (when $T_{act} < T_{pot}$).

In the following, relations between ψ_{leaf} , $\psi_{soil,eff}$ and T_{act} for chemically controlled plants are derived. With assumption (ii) $\psi_{soil,eff} \approx f_{dry}\psi_{leaf}$ and for $s_p = 0$ and $\psi_{lim} = 0$, T_{act} can be written for C plants in terms of $\psi_{soil,eff}$ as:

$$T_{act} = T_{pot} \exp \left[\frac{-s_c a^* \psi_{soil,eff}}{T_{act}} \right] \quad 3.11$$

Using Eq. 3.8 with assumption (ii) $|\psi_{root,wet}| \ll |\psi_{leaf}|$ and Eq. 3.5, ψ_{leaf} can be related to T_{pot} and f_{dry} for C plants as:

$$\psi_{leaf} = -\frac{T_{pot}}{(1-f_{dry})K_{root}} \exp \left[\frac{-s_c f_{dry} a^*}{(1-f_{dry})K_{root}} \right] \quad 3.12$$

Eq. 3.12 shows that ψ_{leaf} does not remain constant when T_{act} (for a constant T_{pot}) decreases due to an increasing f_{dry} .

The direct relations given above hinge on several assumptions. By comparing relations obtained from numerical simulations of 3-D flow and transport in the soil-plant system with the relations given above the validity of these assumptions and approximations for isohydric and anisohydric behaviour will be assessed. Further the comparison between the H (Eq. 3.9 with $\psi_{leaf} = \psi_{lim,H}$) and the H+C model (Eq. 3.6) will indicate if the simple hydraulic approach is valid to describe stomatal regulation or in which cases an additional hormonal signal is needed. A sensitivity analysis will show to which extent variations of s_c and K_{root} influence the stomatal regulation mechanism.













3.2.3 Model setup

Numerical model

Soil

We set up a cubical domain with 20 cm side lengths, z_{tot} , and a uniform discretisation of 0.5 cm and either one horizontal or two vertical, hydraulically impermeable, split layers (Table 3.1) with a width of two voxels. Soil hydraulic parameters for the bulk soil were set to those of a clay loam (Table 3.2, #1) [Carsel and Parrish, 1988] and for the impermeable layers to a non-conductive material (Table 3.2, #2).

Table 3.1 Model setups, the sketches for the setup show the irrigated compartments (in blue).

	<i>horizontal split</i>								<i>vertical split</i>			
												
<i>Fraction of irrigated soil domain</i>	0.25	0.5	0.75	0	0.75	0.5	0.25	0	0.25	0.5	0.75	0
<i>Fraction of root length in dry soil, f_{dry}</i>	0.95	0.68	0.22	0	0.05	0.32	0.78	0	≈0.75	≈0.5	≈0.25	0
<i>Water input: top (T) or bottom (B)</i>	T	T	T	T	B	B	B	B	T	T	T	T
<i>top boundary condition ^a:</i>	WP	WP	WP	WP	NF	NF	NF	NF	F	F	F	F
<i>bottom boundary condition ^a:</i>	NF	NF	NF	NF	WP	WP	WP	WP	D	D	D	D

^a flow (F), water potential (WP), no flow (NF), free drainage (D)

For the horizontal setup one thin impermeable layer was inserted at one of three soil depths (0.25, 0.5, or $0.75 * z_{tot}$) to divide the domain in two compartments. Boundary conditions were set to a constant water pressure either at the bottom (0 hPa) or at the top (-20 hPa). The remaining boundaries were defined as no flow. The vertical split was arranged by two thin impermeable perpendicular vertical layers that divided the simulation domain into four equal compartments (Figure 3.2, insets). The top boundary conditions of each of these compartments could be set individually to a flow condition. Either 25, 50, 75, or 100 percent of the top surface was irrigated but the amount of water that was applied, Q_{irr} ($L^3 T^{-1}$), was always larger than the pre-defined transpiration demand, T_{pot} . The bottom boundary was set to free drainage.

As initial conditions the water pressure for the horizontal split was in a hydrostatic equilibrium with a bottom water pressure of 0 hPa. The vertical split setup started initially with steady state flow conditions in the entire domain, which were obtained in a separate, preliminary run under uniform irrigation.

Table 3.2 Soil hydraulic parameters of the Mualem van Genuchten equation [*Van Genuchten*, 1980]

Material number	θ_R [cm ³ cm ⁻³]	θ_S [cm ³ cm ⁻³]	α [cm ⁻¹]	n [-]	l [-]	K_{sat} [cm d ⁻¹]
1	0.095	0.41	0.019	1.31	0.5	6.24
2	0.095	0.41	$3 * 10^{-6}$	1.5	0.5	0

Root

Two static (non-growing), fibrous root systems: one for the vertical and one for the horizontal splits were generated with the R-SWMS root growth model [*Clausnitzer and Hopmans*, 1994] and used for the simulations (Figure 3.2). The root systems varied slightly in their root length density distributions. Root fractions in the vertical split setup were equally distributed over the four compartments, while for the horizontal split the fraction of roots did not equal the fraction of the soil domain that was irrigated. The fraction of roots, f_{dry} , was defined equal to the relative root length per compartment. For the vertical split the resulting maximum difference in water uptake from each compartment was lower than 0.4 % under uniform irrigation. The uptake from the horizontal split roots followed the root length density distribution in case of hydrostatic equilibrium.

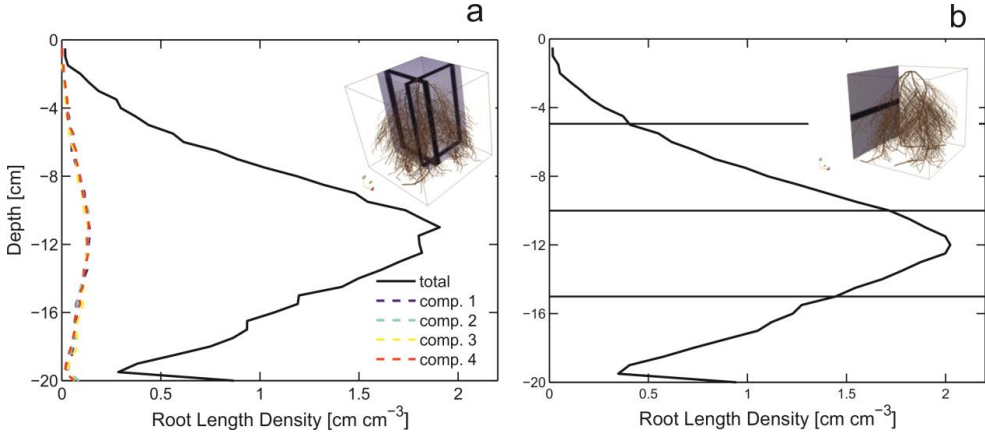


Figure 3.2 Root length densities over depth of the domain for (a) the vertical and (b) the horizontal split setup, where the horizontal lines represent the individual height of the split layer. The insets show the root architectures within the soil domains.

Root hydraulic parameters for radial conductivity and axial hydraulic conductance were chosen from a data set for maize plants [Doussan *et al.*, 1998b] and kept uniform and constant for all root segments.

According to Couvreur *et al.* [2012], the system hydraulic conductivity, K_{root} , can be derived directly from the simulated water uptake by the system for a uniform soil water pressure distribution and a given leaf water pressure. The water uptake that is simulated for this case in a single voxel and divided by the total water uptake represents the so-called standard sink fraction, SSF. The SSF distribution in the soil is subsequently used to calculate the effective soil water pressure $\psi_{soil,eff}$ as:

$$\psi_{soil,eff} = \sum_i SSF_i \psi_{soil,i} \quad 3.13$$

where i refers to the i^{th} soil voxel. It should be noted that when ψ_{soil} is uniform in a soil compartment and when the sum of the SSFs in the dry and wet compartments equal f_{dry} and $(1-f_{dry})$, respectively, Eq. 3.8 is obtained.

To root water pressure in the dry and wet compartments respectively were calculated from the simulated water potentials in the dry and wet compartments using:

$$\psi_{root,dry} = \frac{\sum_{i \in dry} SSF_i \psi_{soil,i}}{\sum_{i \in dry} SSF_i} \quad 3.14$$

and analogous for the wet compartment.

In Table 3.3, the parameters used for the simulations and the different types of control (H+C, C) are given.

Table 3.3 Parameterization for C and H+C controlled stomata

	<i>C</i>	<i>H+C</i>
T_{pot} [$cm^3 d^{-1}$]	30, 50, 100	
K_{root} [$cm^3 hPa^{-1} d^{-1}$]	0.0085	
s_c [$cm^3 mol^{-1}$]	$5*10^7$	$5*10^{10}$
s_p [hPa^{-1}]	0	$1*10^{-4}$
Ψ_{lim} [hPa]	0	-6000
$\alpha^* - DIRECT.$ [$mol hPa^{-1} d^{-1}$]	$3.0*10^{-11}$	$2.7*10^{-13}$
<i>RSWMS parameterization</i>	$a - RSWMS$ [$mol g^{-1} hPa^{-1} d^{-1}$]	$2.75*10^{-12}^a$
	Lr [d^{-1}]	$1.78*10^{-5}^b$
	Kx [$cm^3 d^{-1}$]	$4.32*10^{-2}^b$
	V_{buffer} [cm^3]	14.21 (<i>vertical</i>)
		14.26 (<i>horizontal</i>)

^a [Simonneau *et al.*, 1998]^b Lr , radial hydraulic conductivity; Kx , axial hydraulic conductance [Doussan *et al.*, 1998b]

3.2.4 Scenarios

The relations between transpiration, root zone water potential and fraction of roots in dry soil obtained from numerical simulations and from approximate direct relations were compared for H+C and C plants and for three potential transpiration rates. Each numerical setup consisted of 12 individual runs (4 vertical + 8 horizontal splits).

The parameters for the direct relations were equal to the parameters used in the numerical model. As the value for the sensitivity to leaf pressure s_p was chosen in a way that $1/s_p > \psi_{lim}$, the hormone production and stomatal closure due to hormone concentration starts at higher pressures than the amplification of the hormonal signal by the leaf pressure. The only parameter that could not be directly transferred to the theoretical model was the signal production a . The numerical model uses a production rate at each segment, a , while in the theoretical model a^* refers to a global signal production rate (Table 3.3). In theory $a^* = m a$. With a total root mass of 14.2 g this would lead to a value of $a^* = 3.85 \cdot 10^{-11}$ (mol hPa⁻¹ d⁻¹). However, using this value led to a too strong reduction in transpiration predicted by the direct relations. A first reason is that due to transport limitations part of the produced mass was trapped in the root system. A second reason is that the simulated $\psi_{x,dry}$ were still considerably larger than the ψ_{leaf} so that the production of chemical signal was overestimated when $\psi_{x,dry}$ was assumed to be equal to ψ_{leaf} . Especially for the H+C case, in which signal is only produced when $\psi_{x,dry} < \psi_{lim}$, this had an important impact. Therefore, a^* was manually adjusted to match the transpiration reduction. It must be noted though that the same a^* was used for all scenarios with different f_{dry} and T_{pot}

3.3 Results and Discussion

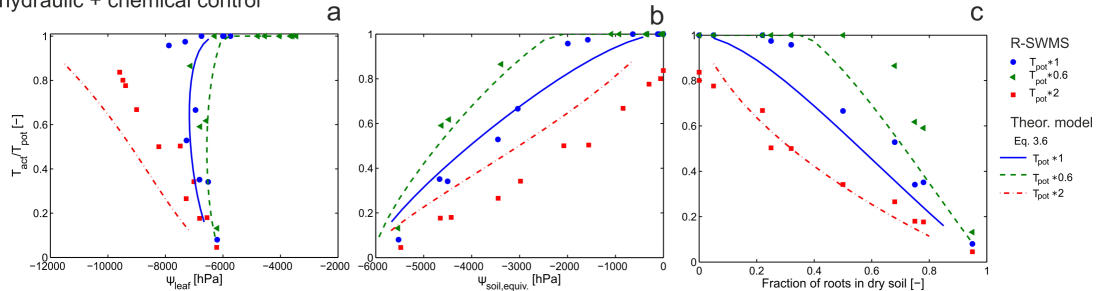
3.3.1 Comparison of the direct and the numerical relations

The numerical simulations indicated that responses for the vertical and the horizontal splits were comparable so that all simulation results were combined and compared with the direct relations (Figure 3.3) between T_{act}/T_{pot} , leaf and soil water pressure, and the fraction of roots in dry soil. The results from the numerical model refer to the states after a maximum of 100 days simulation time. Most of the runs established a steady state; however, 17 of the 72 runs did not reach steady state.

For illustration, distributions of water potential in the root xylem and soil water contents at steady state and the time course of root water uptake from each soil compartment are given for the 50% splits (2 x horizontal, 1 x vertical) in Appendix B.1.

For H+C control the direct relations (Eq. 3.6) match the numerical results qualitatively (Figure 3.3 a-c). When plotted versus ψ_{leaf} , the relative transpiration rate T_{act}/T_{pot} remains equal to one with decreasing ψ_{leaf} until a critical leaf pressure head is reached. Since ψ_{leaf} is approximately equal to the root water potential in the dry zone, $\psi_{root,dry}$, no signal is produced and no reduction in transpiration takes place as long as $\psi_{root,dry}$ and ψ_{leaf} are larger than ψ_{lim} . In this range, ψ_{leaf} decreases due to a decreasing fraction of roots in the wetted zone and therefore a lower effective hydraulic conductivity of the root system ($(1-f_{dry}) K_{root}$) so that a larger gradient between the wetted root zone and the shoot is required to sustain the potential transpiration. When $\psi_{root,dry}$ and ψ_{leaf} become smaller than ψ_{lim} , hormone production in the dry root zone is triggered, stomatal conductance decreases and T_{act} becomes smaller than T_{pot} . According to Eq. 3.2, the reduction depends on the hormone concentration which in turn depends on the hormone production rate and the transpiration rate. For a higher transpiration rate, the dilution of the produced hormone concentrations is larger and ψ_{lim} is reached for a smaller fraction of roots in the dry zone. Consequently ψ_{leaf} must be smaller for a high than for a low potential transpiration to achieve the same hormone concentration and consequently the same transpiration reduction (Figure 3.3 a).

hydraulic + chemical control



chemical control

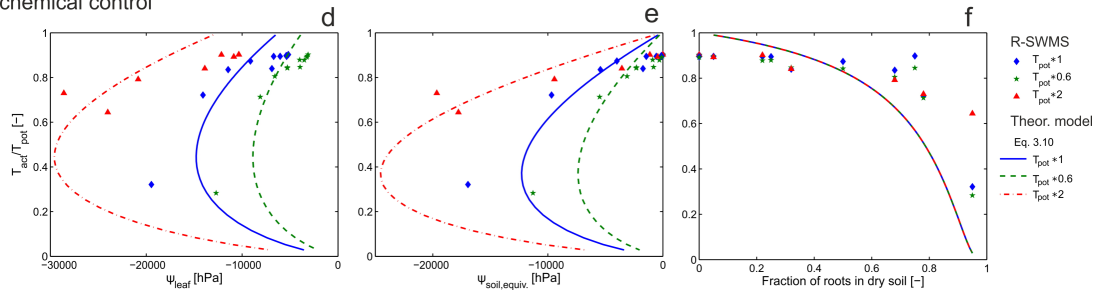


Figure 3.3 Relative transpiration rates at steady state for hydraulic + chemical (a-c) and chemical control (d-f) over leaf water potential (a, d), effective soil water potential (b, e), and fractions of roots in dry soil (c, f). The numerical results (R-SWMS) are depicted as symbols and the corresponding theoretical results that were derived either by Eq. 3.6 or Eq. 3.10 are shown as lines.

The relation between T_{act}/T_{pot} and ψ_{leaf} is non-monotonous. For high T_{act}/T_{pot} , T_{act}/T_{pot} decreases with decreasing ψ_{leaf} until a minimal ψ_{leaf} is reached after which T_{act}/T_{pot} decreases with increasing ψ_{leaf} . In our model setup, T_{act} decreases since a larger part of the root zone is in the dry soil compartment. When f_{dry} increases, the effective hydraulic conductivity of the root system $(1-f_{dry})K_{root}$ decreases and the fraction of the root system in which chemical signals are produced increases, which leads to a reduction in stomatal conductance. When f_{dry} is small, i.e. for high T_{act}/T_{pot} , besides an increase in the fraction of roots that produce hormones, also increase in production rate due to a decrease in $\psi_{root,dry}$ or ψ_{leaf} is required to reduce T_{act}/T_{pot} . For larger f_{dry} , the increase in hormone production and decrease of the dilution when T_{act}/T_{pot} decreases is large enough to decrease the stomatal conductance so that the production rate may decrease and hence $\psi_{root,dry}$ and ψ_{leaf} may increase with decreasing T_{act}/T_{pot} . Although the non-monotonic behaviour may be observed for the different transpiration rates, except for the highest one, the difference between the minimally reached ψ_{leaf} and ψ_{lim} is not so large. This implies that a quasi isohydric behaviour of the H+C plant emerges with a more or less constant $\psi_{leaf} = \psi_{lim,H}$ when $T_{act} < T_{pot}$. Figure 3.3 illustrates that, for the scenarios considered, this constant ψ_{leaf} or $\psi_{lim,H}$ was almost equal to the threshold root water pressure ψ_{lim} that triggered hormonal production (-6000 hPa, Table 3.3). The relation between T_{act}/T_{pot} and $\psi_{soil,eff}$ that is derived from the numerical simulations and the approximate direct relations for the H+C control is monotonous. Opposite to the relation between T_{act}/T_{pot} and ψ_{leaf} , $\psi_{soil,eff}$ is for the same T_{act}/T_{pot} lower for a low than a high T_{pot} . This is in line with relations that were derived for isohydric plants [see e.g. *Couvreur et al.*, 2012; *Javaux et al.*, 2013]. T_{act}/T_{pot} remains equal to one with decreasing $\psi_{soil,eff}$ until a critical $\psi_{soil,eff}$ is reached. This critical $\psi_{soil,eff}$ is smaller (more negative) for smaller transpiration rates. For smaller $\psi_{soil,eff}$, T_{act}/T_{pot} decreases and for a constant K_{root} and ψ_{leaf} , a linear decrease of T_{act}/T_{pot} with a decrease in $\psi_{soil,eff}$ emerges from the hydraulics of the soil-plant system [*Couvreur et al.*, 2012]. The plot of T_{act}/T_{pot} versus f_{dry} is a mirror image of the response of T_{act}/T_{pot} to $\psi_{soil,eff}$.

For the C controlled plant, the direct relations between T_{act}/T_{pot} and ψ_{leaf} are also non-monotonic and for the same T_{act}/T_{pot} more negative ψ_{leaf} are obtained for higher than for lower T_{pot} . Again, the relations between T_{act}/T_{pot} and ψ_{leaf} that were derived from numerical simulations corresponded fairly well with the direct relations. However, the range of T_{act}/T_{pot} that was simulated by the numerical model was not large enough to validate the non-monotonic behaviour. The numerical simulations only indicated that ψ_{leaf} decreased with increasing transpiration reduction or decreasing T_{act}/T_{pot} . The relation between T_{act}/T_{pot} and ψ_{leaf} for the H+C and C controlled plants are qualitatively similar. However, for the C plant, the leaf water potentials were more negative, and varied more with T_{act}/T_{pot} and with T_{pot} which is typical of anisohydric behaviour.

Despite the qualitative similarities in the relations between T_{act}/T_{pot} and ψ_{leaf} for the H+C and C controlled plants, the different sensitivities to production of signalling chemicals in the root zone (only after a certain root zone pressure, ψ_{lim} , was reached with a high sensitivity to signal concentrations for H+C or production for all negative root zone pressures and a low sensitivity to signal concentrations for C) the relations between root zone conditions, $\psi_{soil,eff}$ and f_{dry} , potential transpiration, T_{pot} , and transpiration reduction, T_{act}/T_{pot} were completely different. The C parameterisation leads to a unique relation between T_{act}/T_{pot} and f_{dry} , which is independent of T_{pot} (Figure 3.3 f) and in which T_{act}/T_{pot} decreases monotonously with increasing f_{dry} (Eq. 3.10). For the same f_{dry} and the same T_{act}/T_{pot} , the leaf water pressure must be lower for a larger T_{pot} to sustain a larger transpiration flux. This leads to a lower water pressure in the dry root zone and a higher production in signal rate. Since for the C-parameterization both T_{act} (Eq 3.5 a for $\psi_{leaf} \ll \psi_{root,wei}$) and the signal production rate (Eq. 3.1 with $\psi_{lim} = 0$) are proportional to ψ_{leaf} , which is equal to $\psi_{soil,dry}$, the higher production rate is offset by a higher dilution so that the hormone concentration and consequently T_{act}/T_{pot} do not depend on T_{pot} . The lower sensitivity of the stomatal closure to hormone concentrations in the C-parameterization led to a small sensitivity of T_{act}/T_{pot} to f_{dry} for f_{dry} smaller than 0.6. The fact that T_{act}/T_{pot} was not dependent on T_{pot} and did not vary a lot with f_{dry} for $f_{dry} < 0.6$ explains why the leaf water potentials decreased considerably with decreasing T_{act}/T_{pot} before they reached their minimum and were much smaller for larger T_{pot} . The non-monotonic relation between T_{act}/T_{pot} and ψ_{leaf} and the large differences in these relations for different T_{pot} are translated into the relation between T_{act}/T_{pot} and $\psi_{soil,eff}$. Opposite to the H+C parameterization, the relation between T_{act}/T_{pot} and $\psi_{soil,eff}$ is non-monotonic and the same reduction in T_{act}/T_{pot} occurs for higher T_{pot} at lower $\psi_{soil,eff}$.

The good comparison between numerical simulation results and direct relationships suggest that the direct relationships can be used to predict plant transpiration as a function of the water status in the root zone for different parameterizations of stomatal regulation by plant hormones that lead to either isohydric or anisohydric plant behaviour. Isohydric behaviour may be described by Eq. 3.9 with $\psi_{leaf} = \psi_{lim,H} \approx \psi_{lim}$, whereas anisohydric behaviour, which implies additional chemical signalling, can be explained by Eq. 3.9 in combination with Eq. 3.12. However, to derive these relationships several assumptions were made that are discussed in more detail in the following.

3.3.2 Verification of the assumptions

Part of the assumptions that were made to derive the approximate direct relations were taken over in the setup of the numerical simulations. Two isolated soil compartments between which no water flow can take place and a steady state condition with a soil compartment that is kept wet were also implemented in the numerical simulations. The distribution of roots and their hydraulic properties were defined so that also assumption (vi) was satisfied in the numerical simulations.

Assumption (i) soil is constituted of two isolated compartments and plant roots do not cross the compartment boundaries

Splitting up the root network in two separated parts was the basis to link the root water potential in the dry soil part to the leaf water potential (assumption iii). This assumption was violated in the horizontal split setups in which the root system crossed the different compartments. However, according to the results shown in Figure 3.3, this violation did not affect the agreement between the outcome of the numerical simulations and the predictions using the direct relations.

Assumption (ii), $\psi_{\text{root,wet}} \approx 0$

The root water pressure at the root-soil interface of the irrigated compartment was never lower than -450 hPa (data not shown). Thus assumption (ii) is valid. The water pressure in the xylem, $\psi_{x,\text{wet}}$, however, was always lower than -2000 hPa (Figure 3.4), which is due to the radial hydraulic resistance of the root system. While the vertical splits show a marked difference between dry and irrigated xylem water pressure (Figure 3.4 b, d), the xylem water pressures in the two compartments were very close for the horizontally split domains (Figure 3.4 a, c). Since there was almost no radial flow in the roots in the dry part, the water pressure in the xylem of the dry part of the root system was nearly equal to the water pressure at the root-soil interface: $\psi_{x,\text{dry}} \approx \psi_{\text{root,dry}}$ (data not shown).

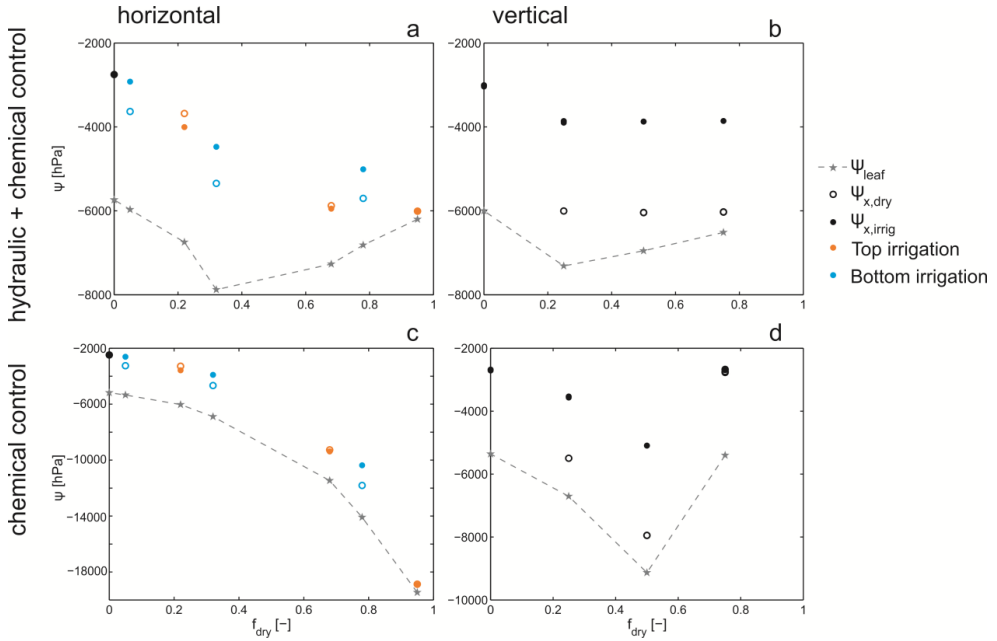


Figure 3.4 Comparison of leaf and root xylem water potential of the dry and irrigated compartment for (a, b) the H+C and (c, d) the C control and T_{pot}^*1 for (a, c) the horizontal splits where the boundary condition is indicated for each f_{dry} in orange for top irrigation and blue for bottom irrigation, respectively; (b, d) depict the vertical splits.

Assumption (iii), $\psi_{leaf} = \psi_{root,dry}$

Figure 3.4 illustrates that this assumption is not fully correct. Although the difference between $\psi_{x,dry} \approx \psi_{root,dry}$ and ψ_{leaf} is decreasing with larger root fractions in dry soil, a small difference between the dry roots and the leaf water potential remains. For the vertical splits, this difference is due to a small uptake from the dry root zone because equilibrium between the dry root zone and the shoot was not yet reached at the end of the simulations. However, the uptake was smaller than 5% of the total water uptake (data not shown). Especially for H+C controlled horizontal splits, the assumption is much less well met for small f_{dry} . In contrast to the vertical split scenarios, the shoot segment is not connected in parallel but in series to the dry and wet soil. As a consequence, the xylem root water potentials in the dry and wet compartments are similar for the horizontal splits. When water flows from the wet compartment through root segments in the dry compartment to the shoot (i.e. when irrigation is from the bottom), the water potentials in the dry compartment are closer to the potential in

the shoot. However, when the dry compartment is below the wet compartment (irrigation from the top), the water potentials in the shoot are closer to the potentials in the wet root segments, which can especially be observed for higher transpiration rates (Appendix B.2).

Assumption (iv), signal production only at the dry side of the root system

For the vertical split, there is a considerable difference between $\psi_{x,dry}$ and $\psi_{x,wet}$ (see Figure 3.4 b and d). For the H+C case, in which chemical production starts for $\psi_x < \psi_{lim}$, no signal is produced in the wet zone whereas nearly all root segments in the dry zone produce signal (Appendix B.3). For the C case, all root segments produce signal but since $\psi_{x,dry} < \psi_{x,wet}$, most of the signal is produced in the dry zone. For the vertical splits assumption (iv) can be considered valid.

For the horizontal splits, $\psi_{x,dry}$ and $\psi_{x,wet}$ are similar and for irrigation from the top, $\psi_{x,wet}$ is even smaller than $\psi_{x,dry}$ (Figure 3.4 a and c). Assumption (iv) is therefore clearly violated for the horizontal split experiments. Because the pressure heads are similar in both compartments, it could be assumed that the production of chemical signal takes place in both compartments so that instead of using Eq. 3.3, the concentration in the leaves could be calculated as:

$$c_{leaf} = \frac{a^* |\psi_{leaf} - \psi_{lim}|}{T_{act}} \quad 3.15$$

Deriving direct relations between transpiration reduction and soil and plant parameters using Eq. 3.15 is straightforward. An evaluation of these functions indicated that the direct relations showed a similar behaviour as shown in Figure 3.4 but that an adjustment of the a^* parameter might be required. Therefore, we continued to use the equations that were derived based on Eq. 3.3.

Assumption (v), immediate effect of chemical signal (no transport limitation)

A previous study showed the impact of transport of chemical signalling on transpiration reduction (Huber et al., 2014). Due to transport limitations (when uptake is close to zero) chemicals can be trapped in the roots in dry zones, which can lead to a reduction by an order of magnitude of chemical signal arriving at the leaves. Transport limitation can further result in a slight re-opening of stomata during prolonged drying as the trapped signal cannot be effective in stomatal closure. These simulations showed that the effective signal was around 60 % of the total signal produced. This transport related effects are quite minor in comparison to the actual stomatal response and might be accounted for by the adjustment of a^* .

3.3.3 Sensitivity analysis

Figure 3.5 shows the sensitivities of Eq. 3.6 and 3.10 with respect to the parameters K_{root} and s_c . Both were varied separately by one order of magnitude. For the H+C parameterisation the slope between relative transpiration and $\psi_{soil,eff}$ is influenced by K_{root} . Further, for a given T_{act}/T_{pot} , the difference between soil and leaf water pressure is decreasing with higher K_{root} . The parameter s_c affects slope as well as curvature of the relation between relative transpiration and water potentials. As noted before, for high values of s_c this relationship becomes almost linear and has a response comparable to Eq. 3.9 (isohydric behaviour) whereas for low s_c , the variation of ψ_{leaf} with T_{act}/T_{pot} increases and the relation between T_{act}/T_{pot} and $\psi_{soil,eff}$ becomes more nonlinear, and even non monotonous. This resembles more an anisohydric behaviour.

In the C cases the relation between T_{act}/T_{pot} to $\psi_{soil,eff}$ is independent of K_{root} and non-monotonous. The parameter s_c is highly sensitive and responsible for the slope and curvature of T_{act}/T_{pot} ($\psi_{soil,eff}$). For lower values of s_c the response of stomatal closure to soil drying is almost negligible.

The sensitivity of Eq. 3.6 to ψ_{lim} on $\psi_{soil,eff}$ and ψ_{leaf} is shown in Appendix Figure B. 4.

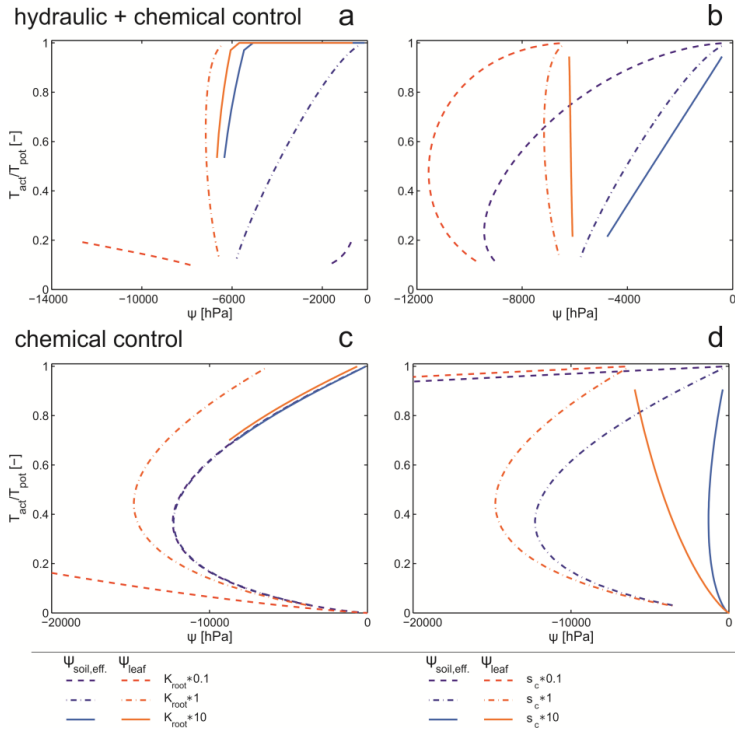


Figure 3.5 Sensitivity analysis for the two parameters K_{root} (a, c) and s_c (b, d) as a function of effective soil water potential (in blue) or leaf potential (in red) for hydraulic + chemical (a, b, Eq. 3.6) and chemical control (c, d, Eq. 3.10)

3.3.4 Applicability of these approaches

For H+C parameterisation a reduction in T_{act} occurs for higher $\psi_{soil,eff}$ when T_{pot} is higher and the relation between T_{act}/T_{pot} versus $\psi_{soil,eff}$ may be approximated by a piecewise linear relation. This type of apparent isohydric behaviour is assumed in many soil hydrological models (e.g. [Feddes *et al.*, 1978]). Couvreur *et al.* [2012; 2014] used this approach to describe root water uptake as a function of the hydraulic conductivity of the root system and assumed a fixed leaf water potential. The relations predicted by this approach (Eq. 3.9 with $\psi_{leaf} = \psi_{lim}$) are given by dashed lines in Figure 3.6. If stomatal regulation leads to a more or less constant ψ_{leaf} with decreasing T_{act}/T_{pot} , the approach reproduces the course of T_{act}/T_{pot} versus $\psi_{soil,eff}$ relatively well. However, with increasing T_{pot} , and for the considered parameterisation of the stomatal conductance, the stomatal regulation was not ‘able’ to

maintain the leaf water potential close to ψ_{lim} but led to considerably smaller ψ_{leaf} values. Consequently, the ratio of T_{act}/T_{pot} was for the same $\psi_{soil,eff}$ considerably larger than predicted assuming that $\psi_{leaf} = \psi_{lim}$. These results indicate that despite the fact that the transpiration reduction as a function of $\psi_{soil,eff}$ for different T_{pot} shows a behaviour that points at an anisohydric behaviour, the transpiration reduction cannot be predicted well using a model that assumes a perfect isohydric behaviour (Eq. 3.9 with constant $\psi_{leaf} = \psi_{lim}$ and constant K_{root}). Further, the sensitivity analysis revealed that with decreasing sensitivities to chemical signalling simulated T_{act}/T_{pot} correspond more to apparent anisohydric behaviour (Figure 3.5 b). Thus even if the plant is controlled by hydraulic as well as chemical signalling, it does not necessarily have to result in an isohydric behaviour.

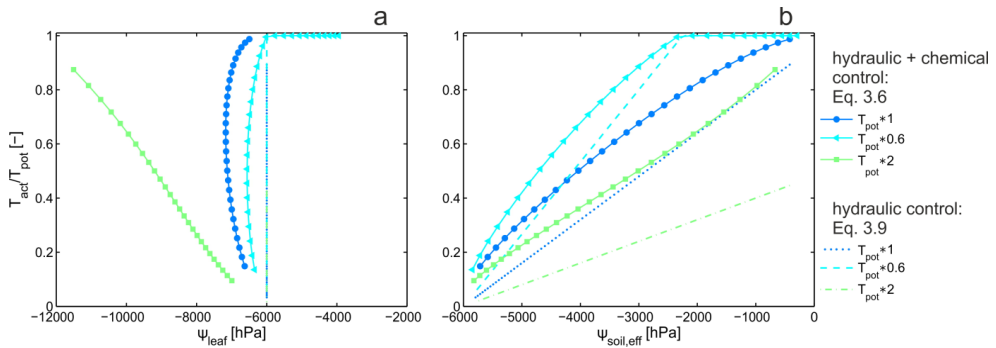


Figure 3.6 Comparison between the two theoretical models with either hydraulic + chemical (Eq. 3.6, lines with symbols) or hydraulic control (Eq. 3.9, lines): Relative transpiration rates as a function of Ψ_{leaf} (a) and $\Psi_{soil,eff}$ (b) for three different transpiration demands.

C control predicts that the relative transpiration reduction in relation to f_{dry} is independent of T_{pot} . This behaviour was observed by *Tardieu and Simonneau* [1998] for sunflower, where the relation between stomatal conductance and the concentration of ABA was independent of vapour pressure deficit, which for the conditions in their experiment was linearly related to the potential transpiration. Several species are known to exhibit anisohydric behaviour with different intensities of stomatal closure: sunflower with a low sensitivity [*Tardieu and Simonneau*, 1998], or *Eucalyptos gomphocephala* [*Franks et al.*, 2007] and an anisohydric cultivar of grapevine [*Rogiers et al.*, 2012] which show pronounced stomatal closure but still high variations in leaf water potential.

As f_{dry} can be directly related to the bulk soil water content, model approaches that relate stomatal closure to bulk soil water content like the FAO approach [*Allen*, 1998], might be valid to describe anisohydric plant behaviour.

A recent study suggests that plant behaviour cannot be strictly classified as either anisohydric or isohydric, but rather in between [Klein, 2014], which also emerged from the H+C simulations. The behaviour might also change during the lifetime of a plant with changing root architectural conductivity [Sade and Moshelion, 2014]. The direct relation shows that smaller K_{root} led to a more anisohydric behaviour (see Figure 3.5 a). It will be of interest how these relationships change dynamically, as K_{root} depends on root hydraulic conductivities, which change with age but also with environmental conditions in time-scales as fast as hours [Chaumont and Tyerman, 2014], and on root architecture.

3.4 Conclusion

Two simple equations were derived to describe transpiration of plants of which stomata are controlled by hydraulic and/or chemical signalling. Both are in good agreement with relations derived from simulations with a numerical mechanistic model, which solved the plant hydraulics as well as chemical signalling and transport explicitly.

The results indicate that a completely different relation between the reduction of plant transpiration, soil water status and potential transpiration rate is obtained depending on how the production of hormonal signals in the root zone and the sensitivity of stomatal closure to hormone concentrations are parameterized.

The commonly used piece-wise linear relationship between the ratio of the actual to the potential transpiration and the effective water potential at the soil root interface is based on the assumption of a constant leaf water potential when transpiration is reduced due to low soil water availability. H+C controlled plants can keep leaf water potential constant when T_{pot} is not too large and the conductivity of the root system (K_{root}) and the sensitivity to chemical concentrations (s_c) are sufficiently large. Otherwise, leaf water potential depends strongly on the effective soil water potential at the soil root interface and the potential transpiration.

A simplified equation relating actual and potential transpiration for C controlled plants was derived by omitting the water pressure threshold for signal production and stomatal regulation. Contrasting to H+C controlled plants, for C-controlled plants the ratio of the actual to the potential transpiration rate is a unique function of the fraction of roots in dry soil. This emerging behaviour is to some extent analogous to eco-hydrological models that describe root water uptake only as function of the lumped soil water content in the root zone [Rodriguez-Iturbe and Porporato, 2005]. It implies that for the same soil water availability or the same amount of roots in dry soil, the actual transpiration is larger with a lower leaf water potential for a high than for a low potential transpiration rate.

Based on this theoretical study, it could be concluded that datasets in which the transpiration rates and leaf water potentials are measured for the same soil water availability but with different potential transpiration offer great potential to discriminate between contrasting plant behaviour and parameterize their control mechanisms. A next step would be to investigate the impact of different control mechanisms on total water uptake, plant growth, and field water balances over an entire growing season. This would require simulations that consider more realistic spatial and temporal distributions of the soil water content.

CHAPTER 4

MEASURING AND MODELLING THREE-DIMENSIONAL WATER UPTAKE OF GROWING BROAD BEANS (*VICIA FABA L.*) WITHIN SPLIT COLUMNS

This chapter is based on a journal article in preparation:

Koebnick, N., K. Huber*, E. Kerkhofs, J. Vanderborght, M. Javaux, H. Vereecken, and D. Vetterlein, Measuring and modeling three-dimensional water uptake of growing broad beans (*Vicia faba L.*) within split-soil columns, *Frontiers in Plant Science* (in preparation).

* shared first co-authorship

4.1 Introduction

Water scarcity is an important abiotic limitation to plant growth and agricultural productivity. Under water limited conditions, the evolution of root system architecture (RSA) plays a major role for reaching locations where water is still present, which is often the subsoil. There is no simple relationship between the amounts of roots present in certain locations and the actual root water uptake (RWU) from these sites [Pohlmeier *et al.*, 2008]. RWU is repeatedly described as a sink moving down the profile with time, only weakly related to root length density in a certain depth [Garrigues *et al.*, 2006; Hainsworth and Aylmore, 1986; 1989; Pierret *et al.*, 2003]. In many of these studies change in soil water content in a certain depth is assumed to be synonymous with root water uptake. The simple Martini glass analogy first used by Zwieniecki *et al.* [2002] illustrates that this assumption is too simple. When drinking a sip of Martini with a straw, the Martini is taken up from the bottom of the glass, but a change in “Martini content” is only observed in the upper layer of the glass due to the very high hydraulic conductivity within the glass. Roots and soil matrix are much more complex than the Martini-glass system; however, in soil-plant system soil hydraulic conductivity and resulting soil hydraulic redistribution also obstruct the view on the site of root water uptake and its temporal dynamics.

This has been known for a long time and a number of strategies have been developed to overcome this problem.

An experimental strategy to prevent soil hydraulic redistribution is to divide the root zone into different compartments, which prevent water flow between compartments to permit controlled heterogeneous distribution of soil moisture [Drew, 1975; Herkelrath *et al.*, 1977]. In case of horizontal splits, the split layers should additionally be penetrable by roots, which can be, for example, achieved by applying wax. When roots take up water in a given compartment the change in water content can be directly related to root water uptake from this compartment. This assumption can, however, only be drawn if the split layers are completely hydraulically isolated (not leaking). If there is significant hydraulic redistribution either through the soil or the roots between the soil compartments, local water content changes do not correspond to RWU [Neumann and Cardon, 2012; Vandoorne *et al.*, 2012].

A second experimental strategy is to directly observe water flux in soil as it has been successfully demonstrated by Zarebanadkouki *et al.* [2012]. They imaged water flow into roots using neutron imaging of deuterated water. However, this method is hitherto either constrained to quasi two-dimensions (rhizotrons) or very small root systems and to short time scales.

An alternative approach is to quantify the amount of water being translocated by root or soil hydraulic redistribution. Mechanistic root water uptake models that describe water flow in soil, into, and within roots allow quantifying and locating root water uptake and redistribution of water within the soil and root system. The use of mechanistic models, like R-SWMS [Javaux *et al.*, 2008], has two prerequisites: (i) that the dominant processes are known and (ii) that the required input parameters are available. To fulfil the latter, dynamic information about RSA as well as hydraulic properties of individual root segments has to be available.

RSA has been obtained in the past by root growth models, i.e. RSA is artificially created based on a set of crop specific parameters and rules (branching rules, growth rates, etc.) derived from experiments [Clausnitzer and Hopmans, 1994; Leitner *et al.*, 2010a; Lynch *et al.*, 1997; Pagès *et al.*, 2004]. Mostly, one or several typical realizations of RSA obtained from such models for a plant of a certain age have been used to calculate different scenarios, like root water uptake from saline soils [Schröder *et al.*, 2013], performance of varying root architectural traits under different soil moisture regimes [Leitner *et al.*, 2014], or the impact of stomatal regulation type on root water uptake [Huber *et al.*, 2014].

Root growth models have been used as an alternative to 3D-data of root systems as these were not available in the past. However, such data are now becoming increasingly accessible with non-invasive methods reaching a level of resolution which is sufficient to visualize most or all of the root system. The most advanced techniques for imaging soil-grown roots include X-ray computed tomography [Koebernick *et al.*, 2014; Mooney *et al.*, 2012], neutron radiography [Oswald *et al.*, 2008], magnetic resonance imaging [Pohlmeier *et al.*, 2008], or transparent soils [Downie *et al.*, 2012]. First modelling approaches based on the use of RSA from non-invasive imaging are available [Stingaciu *et al.*, 2013].

The second challenge remains, i.e. the scarcity of data on root hydraulic properties. Measured data are primarily from hydroponically grown very young root systems. Certain assumptions have to be made to separate radial and axial conductivity during the measurements. Nevertheless, there is a wealth of information on how conductivity changes during root development and these have been used by Doussan *et al.* [1998a]; [2006] to scale the conductivity of individual root segments. As roots age the resistance in the axial pathway typically decreases due to the maturation of xylem vessels, while in the radial pathway resistance increases with the development of apoplastic barriers [Bramley *et al.*, 2009; Frensch and Steudle, 1989].

In order to avoid confounding root water uptake and hydraulic redistribution by the interpretation of local changes in soil water content two of the above strategies were chosen: (i) an experimental

approach of introducing barriers to avoid soil hydraulic redistribution; (ii) a modelling approach which takes soil and root hydraulic redistribution into account.

The objective of the current study is to compare experimental (introducing barriers to avoid soil hydraulic redistribution) and modelling approaches (calculation of soil and root water flow) in respect to their capacity to localize root water uptake. Local changes in soil water content will be compared to measured/modelled root water uptake.

For the experimental approach a classical set up using wax barriers [Drew, 1975] was combined with quantitative measurement of RSA over time via X-ray CT.

For the modelling approach the mechanistic 3D model R-SWMS [Javaux *et al.*, 2008] was used, which enables a detailed description of soil and root water flow. While R-SWMS so far has only been applied for static (non-growing) root systems, mostly created by root architectural models, the existing model was extended by an additional root development module, which uses the measured CT-data of RSA over time. Doussan's concept of changing axial and radial conductivity with age [Doussan *et al.*, 2006] was included by using his root hydraulic parameterization by assigning these parameters to root age classes derived from the 4D RSA CT-Data.

Apart from modelling the actual experimental setup, experiments with split layers were simulated as having none and vice versa.

This approach allowed us to (i) reinterpret measurement results, (ii) show the influence of split layers on plant water potentials that could be linked to differences in on plant/root growth and eventually on root water uptake and (iii) show where soil water is taken up during root growth.

4.2 Materials and Methods

4.2.1 Experiments

Two subsequent experiments under the same environmental conditions (growth chamber, 23° C day / 18° C night, 65 % relative humidity, photoperiod of 14 hours, photon-flux density of 350 $\mu\text{mol m}^{-2} \text{s}^{-1}$) were conducted with *Vicia faba* L. cv. Fuego.

The first experiment (3 replications), which will be referred to as “NoSplit” in the following, was conducted with homogeneously filled soil columns with unrestricted soil water flow. The second (4 replications), referred to as “Split” was similar to the first one, but paraffin layers at 5, 10, and 15 cm height were established to interrupt soil water redistribution. This method was adopted from *Drew* [1975], who showed that root growth was unaffected by such layers. Both experiments were conducted consecutively, which explains the differences in the second setup.

Experimental setup

“NoSplit” (without Paraffin layers)

The porous substrate was prepared by mixing quartz particles of different size classes, consisting of 85 % sand, 10 % silt, and 5 % clay [*Vetterlein et al.*, 2007]. Additionally 50 g kg^{-1} of gravel (2-3 mm \varnothing) and 20 g kg^{-1} of plastic beads (polypropylene, 2-3 mm \varnothing) were added to the substrate as internal reference for digital image analysis.

PVC cylinders ($\varnothing = 12.5$ cm, $h = 21.5$ cm) were filled up with the substrate by passing it through two sieves of 4 mm mesh size separated by a distance of 10 cm. This procedure was chosen to avoid particle size separation during filling. Resulting bulk density of the substrate was 1.52 ± 0.01 g cm^{-3} . The cylinders had porous plates at the lower end (Figure 4.1 a), which were connected with plastic tubing to a water source. The soil was gently watered with a nutrient solution (modified from *Römheld and Marschner* [1990]) by capillary rise from the bottom of the sample (soil water potential $\psi = 0$ hPa at $z = -21.5$ cm). Average volumetric soil water content (θ) at the start of the experiment was 31.1 ± 1 %. *Vicia faba* seeds were surface sterilised in 10 % H_2O_2 solution for 10 minutes, thoroughly rinsed in deionised water and subsequently imbibed for one hour in a saturated CaSO_4 solution. Seeds were placed on wet blotting paper and placed in a dark cabinet at room temperature for 2 days. For each cylinder, one pre-germinated seed was carefully placed in a prepared cavity in the soil at a depth of 1 cm. The soil surface was covered by a 2 cm layer of fine quartz gravel. Until shoot emergence columns were covered with aluminium foil to further minimize evaporation. With the removal of aluminium foil the drying period was initiated (Day 6).

“Split” (with Paraffin layers)

The substrate was the same as in the “NoSplit” experiment, however, without the addition of plastic beads as these caused problems in the segmentation procedure (see below). Soil bulk density was slightly higher ($\Delta = 0.12 \text{ g/cm}^3$).

For the split layers, molten paraffin was casted and flattened to a thickness of approximately 0.5 mm and cut into a circular shape. At -5, -10, and -15 cm depth a layer of paraffin was placed on top of the soil and sealed to the cylinder walls using molten paraffin (Figure 4.1 b). For initial irrigation, rhizon soil moisture samplers (Eikelkamp, Giesbeek, NL) were placed in each soil compartment. Those were connected over night to bottles filled with 150 ml nutrient solution each. Volumetric water content at the start of the experiment was $23.8 \pm 0.5 \%$ in each compartment. Seed preparation was the same as in the “NoSplit” experiment. To avoid the formation of cracks in the soil due to the placement of large *Vicia faba* seeds, these were planted in a separate seed compartment: a cylinder ($\varnothing = 6 \text{ cm}$, $h = 3 \text{ cm}$) filled with the soil mixture and 20 ml of water. When the roots emerged through the paraffin layer at the bottom of the seed compartment, the small cylinder was placed on the topsoil. The remaining bare topsoil was covered with gravel to reduce evaporation. The split samples were initially also covered with aluminium foil, which was removed on Day 4 to start the drying period.

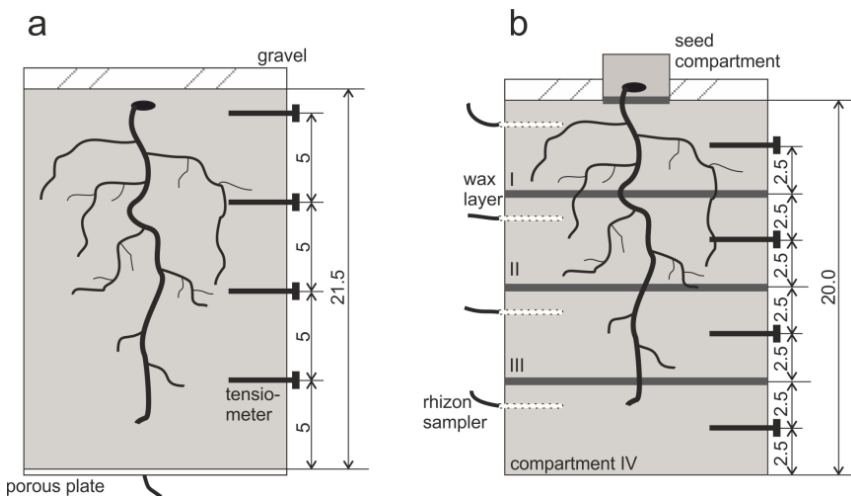


Figure 4.1 Schematic view of the experimental setup with locations for tensiometers and paraffin layers. (a): NoSplit setup (b): Split setup

Transpiration and soil matric potential

The PVC cylinders were placed on weighing cells (KERN 572 ,Kern & Sohn GmbH, Balingen, Germany), and grown for 30-36 days with no additional watering. Weight data were recorded every 10 minutes throughout the experimental period. Four micro-tensiometers [Vetterlein *et al.*, 1993] were inserted horizontally through sealed boreholes (“NoSplit”: -1.5, -6.5, -11.5, and -16.5 cm soil depth; “Split”: -2.5, -7.5, -12.5, -17.5 cm, Figure 4.1) to monitor the soil matric potential (ψ_m), during drying.

The daily transpiration rate was calculated from weight differences between two subsequent days. Evaporation was assumed to be negligible due to the layer of coarse gravel on the surface and as surface was never rewetted during the experiment. Relative humidity was constant day and night hence dew formation could also be excluded. Only for the seed compartment used in “Split” experiment, there was no gravel layer and hence water applied initially (20 ml) was assumed to be lost by evaporation uniformly within the first 7 days.

Leaf area development was estimated by daily measuring the length and width of the lamina of each leaflet and using the linear model of *Peksen* [2007]:

$$LA = 0.919 + 0.682 LW \quad 4.1$$

where LA [cm²] is the one-sided leaf area, L [cm] is the length of the lamina, and W [cm] is the width of the lamina. Stomatal conductance was measured at the end of each day using a steady-state porometer (SC-1 Leaf Porometer, Decagon Devices, Inc., Pullman, WA, USA). Two measurements per plant were taken on the abaxial side of the youngest unfolded leaf pair and the mean value of the two measurements was stored.

CT Scanning and image analysis

One sample from the “NoSplit” experiment and all the samples from the “Split” experiment were scanned every second day during the night phase with an industrial X-ray micro-CT scanner (X-Tek HMX 225) with a fine focus X-ray tube. The scanning parameters are summarized in Table 4.1. Due to the height of the cylinders separate scans of the upper and the lower part of the sample had to be performed. In the NoSplit setup the mechanism for attaching the porous plate to the soil cylinder at the bottom required an additional plastic ring for sealing reasons which caused photon starvation at the lower end (7 cm), thus not the entire root system could be imaged.

Table 4.1 X-ray settings for the different experimental setups

	NoSplit	Split
Voltage [kV]	200	210
Current [μ A]	250	500
Number of Projections	800	2000
Exposure time [ms]	200	200
Resolution [μ m]	245	277

After alignment of the images and combination of the upper and lower half, the raw images were filtered with a total variation (TV) filter [Rudin *et al.*, 1992], to remove small scale noise while preserving edges. Additionally a pseudomedian filter [Pratt, 1991] was used to enhance the contrast between roots and soil and to remove beam hardening artefacts. Roots were segmented from the background using a region growing algorithm. A more detailed description of the technical procedure can be found in [Koebernick *et al.*, 2014].

For the subsequent simulations, a connected root structure was required. Thus, the binary images had to be manually reconstructed using a three-dimensional virtual reality system (for a detailed description of this method see Stingaciu *et al.* [2013]). The average length of the reconstructed root segments was 0.087 ± 0.008 cm. Due to the labour-intensive manual reconstruction only one replication of “NoSplit” (NoSplit 2) and two replications of the “Split” (Split 1 and Split 3) experiment were reconstructed. Split 1 and Split 3 were chosen to cover the contrasting root architectures in the “Split” experiment.

For the determination of root age of each segment at each time step, the reconstructed and stored root system of the precedent scan was opened simultaneously with the image of the subsequent scan. Using the overlay of both scans newly grown roots could be identified and added to the existing root structure. The temporal resolution of the growing root architecture was limited by the time interval between two CT scans (2 days). To obtain smoother root growth, the origination time of a segment s , t_s , grown between times t_i and t_{i+1} when a CT scan was made, was calculated as Eq. 4.2:

$$t_s = t_i + \frac{l_s}{\Delta l_s} (t_{i+1} - t_i) \quad 4.2$$

where Δl_s [L] is the length of all segments that grew between time t_i [T] and t_{i+1} and that are connected to the same connection point of the root system at time t_i as the root segment s , and l_s is the length of the segments that emerged before segment s and that are closer to the connection point than segment s .

Destructive measurements

Roots were extracted from the soil by washing using sieves of 3 and 2 mm mesh size successively. In the “Split” experiment, compartments were analysed separately. In the “NoSplit” experiment, the roots grown into the lower 7 cm of the cylinder that could not be imaged were harvested separately. Roots were stored in Rotisol and subsequently scanned on a flatbed scanner (EPSON Perfection V700 PHOTO). The images were analysed with WinRHIZO 2009b (Regent Instruments, Inc., Quebec, Canada) to obtain total root lengths.

4.2.2 Modelling of RWU

For the simulation of RWU the model R-SWMS was used. R-SWMS is a numerical model solving the water flow equation in the root network and in the soil [Javaux *et al.*, 2008]. The numerical solution of the Richards equation [Richards, 1931] with a sink term (soil water flow) is based on SWMS_3D [Simunek *et al.*, 1995]. The finite mesh for soil is made of rectangular voxels which are automatically subdivided into 6 tetrahedral elements. A Galerkin finite element approach is applied which uses tetrahedral elements for its spatial discretization. The time component is incorporated using an implicit backward finite difference method. A solver based on a conjugate gradient method is integrated and the solution is obtained from a Picard iterative numerical scheme.

The water flow equation for the root network is solved based on the radial and axial flow equations and the mass balance at each root node, resulting in a system of linear equations for h_x , the xylem water potential. The system is solved with a biconjugated gradient method.

The root and the soil water flow equations are coupled through the definition of the sink term of the Richards equation and of the water potential at the soil-root interface for the Doussan equation [Doussan *et al.*, 2006]. The sink term of the Richards equation is defined as the sum of all radial root flow located within a cuboid divided by the cuboid volume. The soil-root interface water potential at each root node is defined as the distance weighted average of the water potential at the soil voxel nodes.

Model setup

The samples NoSplit 2 from “NoSplit” experiment and Split 1 and Split 3 from “Split” experiment, with fully reconstructed root architectures, were used for the setup of virtual experiments in R-SWMS. In the following when referring to modelled data names of samples will be written in italics.

Soil domain

Domains were defined rectangular with a discretization of $0.5 \times 0.5 \times 0.25 \text{ cm}^3$. The domain size was $14 \times 14 \times 21.5 \text{ cm}^3$ for the “NoSplit” experiment. The domains of the “Split” experiment differed in the z-direction ($z=20 \text{ cm}$ for Split 1; $z=20.25 \text{ cm}$ for Split3, Figure 4.2). The cylindrical geometry of the soil columns was approximated using Pythagoras’ Theorem with a cylinder radius of 7 cm. Voxels belonging to this cylinder were defined as soil material; voxels on the outside were defined as wall material. The water retention characteristic was described by a bimodal Mualem - van Genuchten expression [Durner, 1994; Van Genuchten, 1980]. The soil hydraulic parameters were derived from separate HyProp measurements [Peters and Durner, 2008] (

Table 4.2). Paraffin layers were defined as 0.5 cm thick layers within the cylinder. All soil boundary conditions were defined as zero flux. Initial conditions were defined according to the initial conditions at the start of the drying period in the experiments. Soil matric potential was in hydraulic equilibrium in the NoSplit and in the Split setup, soil water content was equal in each compartment.

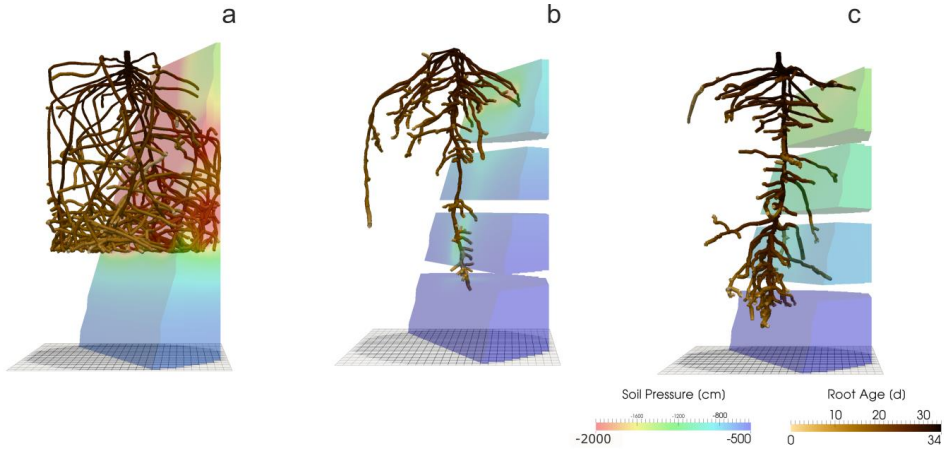


Figure 4.2 Root system architectures at the end of the experiment within their respective soil domains for a) *NoSplit* after 32 days, b) *Split 1* after 30 days, and c) *Split 3* after 34 days of growth. Root systems are colored according to root age and the soil according to soil water pressure.

Table 4.2 Soil hydraulic parameters for the Mualem-van Genuchten expression. Saturated and residual water content, θ_s and θ_r , respectively; van Genuchten shape parameters, α and n ; pore connectivity parameter λ ; and saturated hydraulic conductivity, K_s . For the soil, a bimodal $\theta(\psi)$ relation (Durner, 1994) was used.

Material	θ_r [cm ³ cm ⁻³]	θ_s [cm ³ cm ⁻³]	α [cm ⁻¹]	n [-]	w_2 [-]	α_2 [cm ⁻¹]	n_2 [-]	λ [-]	K_s [cm d ⁻¹]
<i>Soil</i>	0.01	0.35	0.05	4	0.35	0.0033	1.3	0.5	170
<i>Wall</i>	0.01	0.35	0.000003	1.5	-	-	-	0.5	0
<i>Paraffin</i>									
<i>non-conductive</i>	0.01	0.35	0.000003	1.5	-	-	-	0.5	0
<i>semi-conductive</i>	0.01	0.35	0.000003	1.5	-	-	-	0.5	0.001

Root architecture

The root architectures for the simulations were obtained from the manually reconstructed CT images. Root hydraulic properties were based on an age dependent parameter set by *Doussan et al.* [2006] for *Lupinus angustifolius*. Radial conductivity of roots was given a constant value of $8.64 \times 10^{-4} \text{ cm d}^{-1} \text{ hPa}^{-1}$. The axial conductance increased stepwise with segment age and are summarized in Table 4.3. In Doussan et al. (2006) axial conductance (i.e. xylem conductance) of lateral roots increased with age, whereas taproot axial conductance increased with distance to the tip. Thus for the tap root the age information needed to be converted to distance information. For this the given distances were divided by the mean measured elongation rate of the taproot (0.7 cm d^{-1}) to translate distances to ages.

Table 4.3 Age dependent root axial conductance for the taproot and lateral roots (changed after Doussan, 2006)

Taproot		Lateral roots	
<i>Age [d]</i>	<i>Axial conductance</i> <i>[cm⁴ d⁻¹ hPa⁻¹]</i>	<i>Age [d]</i>	<i>Axial conductance</i> <i>[cm⁴ d⁻¹ hPa⁻¹]</i>
0	0.000864	0	0.002376
2.85	0.01728	8	0.00864
14.28	0.11232	11	0.01296
28.58	0.2592		

To allow root growth in the model the most recent root architecture including the origination times for each root segment were used. At a given simulation time only the root segments with an origination time smaller than the actual simulation time were taken into account. The root system was updated at each further run-time step thus enabling predefined root growth over time.

The measured daily transpiration rates of each sample were converted to a periodic step function with zero flow during the night and so defined the root flow boundary conditions in the model at the root collar

Scenarios

Each of the three samples was exposed to two or three scenarios to analyse the effect of paraffin layers on RWU. In the first scenario (*A*), a continuous soil domain without any split layers was used. In the second scenario (*B*), three non-conductive paraffin layers were defined. Finally, the third scenario (*C*), aimed to achieve best agreement to measured data for “Split” experiment by including the possibility of leaking paraffin layers. The leakage was simulated by assigning a low hydraulic conductivity of 0.001 cm d^{-1} (Table 4.2) to the split layers. Sample Split 1 was simulated with three slightly conductive layers, and Split 3 with a non-conductive layer at -5 cm and two remaining slightly conductive layers.

4.3 Results

4.3.1 Experimental results

As expected, plant performance differed markedly between the two experiments (Figure 4.3). In the “NoSplit” experiment plants were bigger and had a larger leaf area (Figure 4.3 a). Leaf growth was initially the same in both experiments, but after Day 15 leaf area increased more in the “NoSplit” experiment. A similar pattern could be observed for total root lengths obtained from CT images over time (Figure 4.3 c). Root elongation was similar for both, “Split” and “NoSplit” experiment, until Day 10. Afterwards elongation rate was higher for “NoSplit”. Root length estimations from destructively harvested roots using WinRHIZO were on average higher than estimations from CT (Table 4.4).

The vertical root length distribution over depth in the “Split” experiment differed between Split 1 and the remaining samples. Compartment I in Split 1 contained about 3/4 of the total root length, while the distribution for the other replications of the “Split” experiment was more even (Table 4.4).

In both experiments transpiration rate initially increased with leaf area (Figure 4.3 b). In “NoSplit” a sharp decrease in transpiration rate was seen at Days 23, 25, and 28, respectively for the different samples. Transpiration reduction occurred earliest in NoSplit 3, which was also the largest plant with the highest transpiration rate up to that day. In the “Split” experiment, transpiration reduction could be observed earlier, although the reduction in transpiration was not as strong as in the “NoSplit” experiments. The lower leaf areas and smaller transpiration rates in the “Split” experiment were accompanied by lower stomatal conductance of the youngest unfolded leaves in comparison to the “NoSplit” experiments (Figure 4.3 d). Stomatal conductance decreased already from the first measurement, i.e. Day 10, in the “Split” experiment. In the “NoSplit” experiment the variability of stomatal conductance in the different samples was very high, but low values were not measured until Days 23/24.

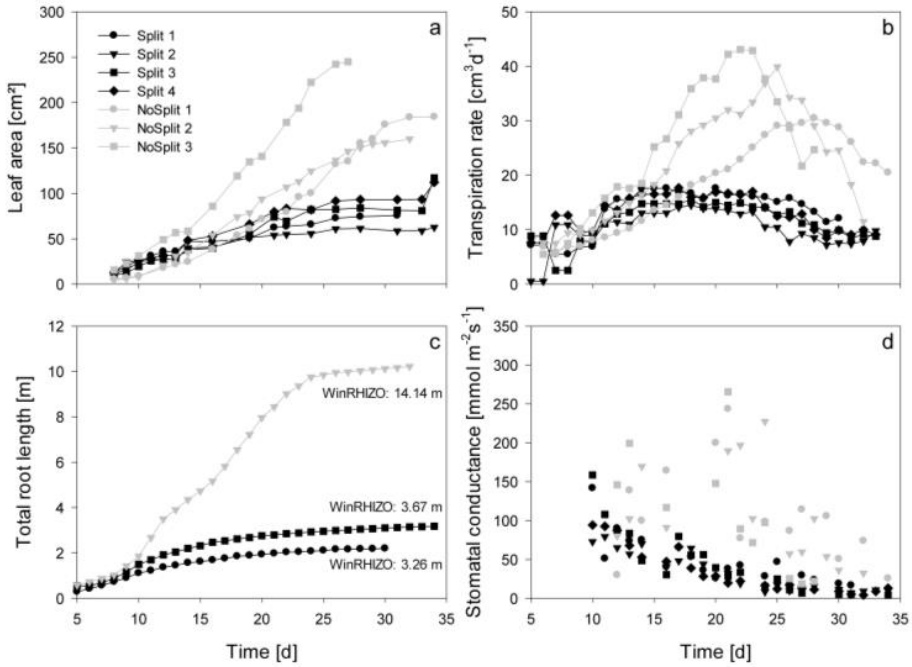


Figure 4.3 Measured plant traits over time from day 5 until day 35. Gray symbols represent traits from the NoSplit setup, black symbols the traits from the Split setup, respectively. Different symbols represent replications. a) One-sided leaf area, b) Evapotranspiration rate, c) total estimated root length of the samples used for modelling, d) axial stomatal conductance of the youngest unfolded leaves, data points represent the mean of $n=2$ measurements.

Table 4.4 Root length estimations from CT images and from destructive measurements at the end of each experiment.

	Length CT [cm]	Length WinRhizo [cm]	(WinRhizo-CT)/WinRhizo [-]
NoSplit 1	-	1504	-
NoSplit 2	1022	1414	0.27
NoSplit 3	-	2023	-
Split 1	Total	326	0.17
	Comp. I	240	0.18
	Comp. II	48	0.08
	Comp. III	27	0.26
	Comp. IV	11	0.10
Split 3	Total	335	-
	Comp. I	79	-
	Comp. II	-	-
	Comp. III	213*	-
	Comp. IV	43	-
Split 4	Total	368	0.13
	Comp. I	132	0.05
	Comp. II	69	0.07
	Comp. III	125	0.28
	Comp. IV	41	0.07
Split 5	Total	573	-
	Comp. I	143	-
	Comp. II	234	-
	Comp. III	158	-
	Comp. IV	38	-

* Value for Compartment II and III combined

The addition of paraffin layers (“Split” experiment) also had a pronounced effect on the temporal development of the soil matric potentials in the different soil compartments (Figure 4.5 a-c). For the sake of brevity only the results of the samples that were later used for modelling are presented (the remaining samples behaved similarly, see Appendix C.1). In NoSplit 2, soil matric potential remained high during a long period (approximately until 25 days after the start of the experiment) and there were only small differences between the matric potentials at different depths. After 25 days, the time at which the transpiration in the no-split experiment started to decrease (Figure 4.3 b), the matric potentials decreased strongly and more or less simultaneously at different depths in the column. For the “Split” experiments, the matric potentials started to decrease much earlier (from Day 10 onwards) and sequentially from the top towards the bottom compartments. Except for the upper compartment in Split 3, the decrease of matric potential was more gradual and less abrupt than in the “NoSplit” experiments. The tensiometer readings for the “Split” experiment showed a pronounced day-night cycle in the upper and a more damped diurnal signal in the lower compartments.

Water depletion from each compartment was calculated from measured tensiometer values assuming a uniform matric potential within a layer and using the substrate specific water retention curve (Table 4.2). These data were compared to total water loss derived from weighing cells (Figure 4.4). When air bubbles started to form in the tensiometers no further water content change could be calculated. The calculated water content at this point was 10.5% (for $h = -450$ hPa) in both Compartments I and II of Split 1, and 9.8 % (for $h = -649$ hPa) in Compartment I of Split 3. While the difference between calculated and measured cumulative water depletion converged to below 10 % (+9 % Split4, -5 % Split1) at the end of the experiment, comparison of the slopes over time indicates a poor fit of the dynamics. Calculated water depletion was clearly overestimated in the moist range and underestimated in the dry range, especially in Split 3.

The arrival times of roots in Compartment III and IV in Split 1 were Day 12 and 18, respectively, nonetheless there was significant (even if overestimated) water depletion from both compartments before these dates.

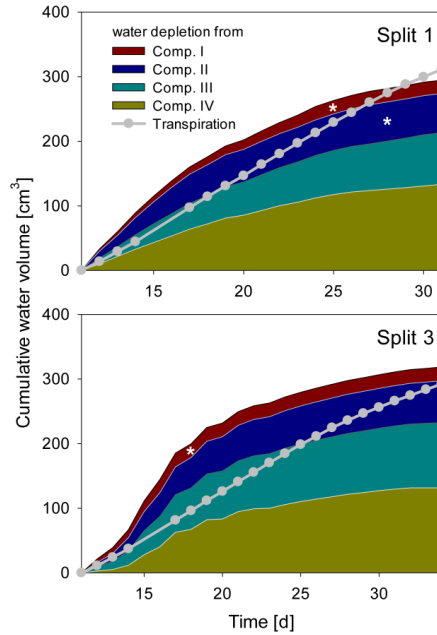


Figure 4.4 Cumulative water depletion from each compartment over time compared to cumulative transpiration from day 11 until the end of the experiment. Filled areas represent cumulative water content change in the different compartments calculated from tensiometer measurements. Gray line and scatters represent cumulative transpiration measured with balances. White asterisks denote the point, when the tensiometer in the compartment showed air bubbles.

4.3.2 Simulation results

The three samples (NoSplit 2, Split 1 and Split 3) representing different RSA were subjected to three different scenarios: (A), a continuous, unrestricted soil domain, (B) a soil domain with non-conductive split layers, and (C) with semi-conductive split layers. Mean simulated soil matric potentials in four layers were compared to the measured tensiometer values (Figure 4.5).

Choice of scenario

In scenario (A) (continuous soil domain) (Figure 4.5 d - f), the simulated matric potentials in the different soil layers started declining strongly and nearly simultaneously only towards the end of the simulation period. The simulated decline occurred the earliest and was the strongest in the “NoSplit” experiment reflecting the larger cumulative transpiration from this experiment.

For the “NoSplit” experiment, the simulated matric potentials for scenario (A) showed a similar behaviour as the measurements (Figure 4.5 d). The timing and the slope of decrease fitted the experimental data well. The lowest tensiometer (-16.5 cm) was an exception, probably due to the fact, that the deep roots could not be detected in the CT and were missing in the model.

For both samples of the “Split” experiment (Figure 4.5 e, f), the measured matric potentials of the upper two tensiometers started decreasing much earlier than the simulated matric potentials in scenario (A) of these tensiometers. This illustrates the effect of the paraffin layers on the soil water distribution in the “Split” experiment which is ignored in scenario (A).

Scenario (B) with non-conductive paraffin layers was simulated only for the “Split” experiment (Figure 4.5 g, h). The simulated matric potentials of the tensiometers decreased also sequentially from top to bottom but the time lag between these decreases was much larger than in scenario (A) for the same samples. The simulated water potentials started to decrease shortly after roots arrived in a compartment. In *Split 3* (Figure 4.5 h), simulated average water potential in Compartment I decreased to about -2000 hPa until Day 15 and remained at this level thereafter only showing pronounced diurnal fluctuations thereafter until the end of the simulation run. In both samples of the “Split” experiment (Figure 4.5 g, h) for scenario (B) the simulated changes in water potential in Compartment IV were very small due to the small fraction of roots in these compartments.

Scenario (B) was not able to reproduce the measured dynamics of soil matric potentials of the “Split” samples. Measured matric potentials did not show a sequential stepwise decrease but a more gradual decrease that started earlier than the simulated decrease and sometimes even earlier than the root arrival time in a compartment. One exception was the matric potential in Compartment I of the *Split 3* sample. Scenario (B) produced large water potential differences between the different compartments, which were not in agreement with the measurements.

The previously described results indicate that paraffin layers were not perfectly isolating, but that there must have been water redistribution between neighbouring compartments, albeit at a lower rate than in completely unrestricted soil. Thus, scenario (C) was applied.

For Sample *Split 1* in scenario (C) (Figure 4.5 j), the simulated matric potentials of Compartment I showed a slower decrease than those obtained with scenario (B) or (A). At the same time scenario (C) resulted in an earlier decrease of matric potential in the lowest compartment compared to scenario (B). The pronounced measured diurnal pattern of soil matric potential in compartment I was successfully reproduced in scenario (C).

Likewise, for Sample *Split 3* simulated matric potentials of scenario (C) showed the best agreement with measured tensiometer data. Here the assumption that all layers except the top layer were leaking was important for obtaining the good agreement.

As expected, for the sample *NoSplit 2* from “NoSplit” experiment (Figure 4.5 i), agreement between measured soil matric potentials and those simulated with scenario (C) was very poor. However it is interesting to note the influence of, albeit leaking, hydraulic barriers to soil water potentials.

In contrast to experimental approaches which can only detect changes in soil matric potential, the simulation results allow disentangling the different fluxes which contribute to local changes in matric potential and soil water content. The evaluation of fluxes was restricted to those simulations which showed the best agreement between measured matric potentials and simulated once, i.e. scenario (A) for sample *NoSplit 2*, scenario (C) for samples *Split 1* and *Split 3*.

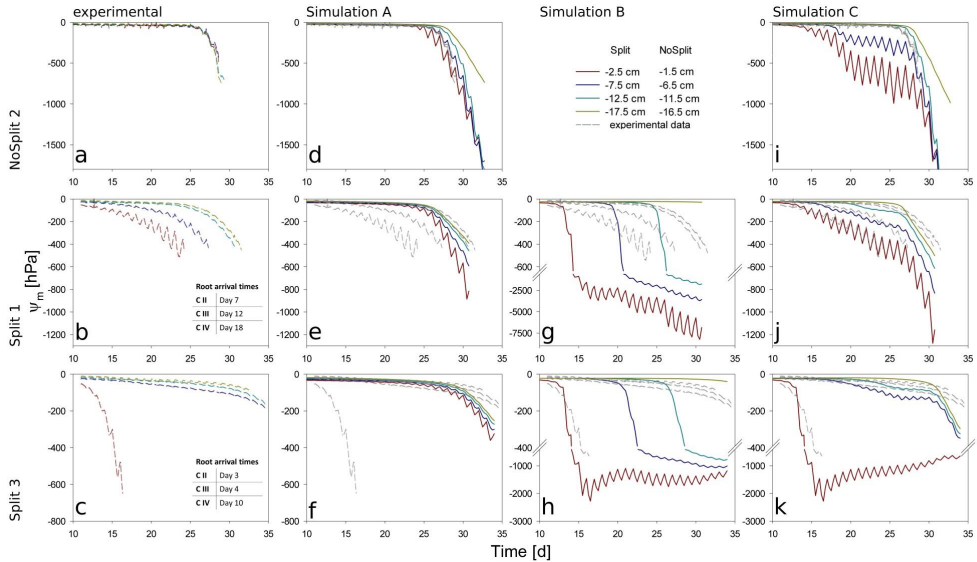


Figure 4.5 Soil matric potentials for the three samples (top to bottom) within the different compartments. (a) – (c): Values measured by the tensiometers in the experiments. (d) – (k): Comparison of different scenarios with the measured values, repeated in dashed, grey lines. (d) – (f): Simulation A – unrestricted soil domain, (g) – (h): Simulation B – impermeable layers, (i) – (k): Simulation C – semipermeable layers.

Simulated flow dynamics

The water balances of the single soil compartments are depicted in Figure 4.6. In case of impermeable split layers, the storage change within one soil compartment should equal root water uptake. However, if the split layers are leaking, which is the case for most of the layers, the net flow through the split layers in addition to the storage change equals root water uptake.

For sample *NoSplit 2* (Figure 4.6 a) simulation showed that RWU was largest in the upper compartment, where it started to decrease from Day 25 onward. The 5-10 cm layer only started to significantly contribute to RWU from Day 17 onward and the 10-20 cm layer only after Day 20, which is related to root arrival time.

It is interesting to note that “early morning values” of RWU in the 0-5 cm layer remained higher than those in the other layers even after 25 days i.e. during a period where overall contribution of the lower layers to RWU had increased and total transpiration rate was reduced in the experiment.

Simulations showed soil hydraulic redistribution of water from the lower layers to the top 0-5 cm, with higher flow rates during day than during night. At 5-10 cm depth inflows from the deepest soil layer and outflows to the 0-5 cm layer were almost of the same magnitude, so the resulting net flow oscillated around zero. Soil hydraulic redistribution started to decrease after Day 25 and ceased after Day 31.

Since RWU from a layer corresponds to the sum of the net water flow into and the decrease of the water storage in a soil compartment, it is evident that RWU in a soil layer cannot be derived from water storage changes in that layer. In 0-5 cm layer RWU is considerably larger than the changes in water storage whereas the opposite is true for the 10 to 15 cm layer. It is clearly visible that RWU and storage change didn't correspond to each other as long as there was significant hydraulic redistribution.

Substantial soil hydraulic redistribution occurred also in the samples *Split 1 (C)* and *Split 3 (C)*, although K_s values of paraffin layers were only 0.001 cm d^{-1} (Figure 4.6 b, c). In both simulations RWU did not correspond to water storage change with the exception of Compartment I in *Split 3*, which was assumed to be separated by a non-conductive split layer. RWU from Compartment IV was very small in both cases while the change in soil water content was substantially higher due to flow across the split layer. The same pattern was observed in Compartment III, but net outflow of water started earlier and was eventually compensated by inflow from Compartment IV. Compartment II showed a contrasting behaviour between the two samples of the “Split” experiment. In *Split 3* the non-

conductive layer at the top prevented water movement in the soil to Compartment I, and the fraction of RWU from compartment II was considerably higher in *Split 3* than in *Split 1*.

In both simulations of the “Split” experiment, there was significant hydraulic redistribution via deep roots into Compartment I. Root hydraulic redistribution was much more pronounced in *Split 3*. According to the simulations the redistribution occurred during night and the water was taken up by the roots during the next day.

The comparison of cumulative root water uptake from the different compartments with cumulative water depletion at the end of the simulations highlights the importance of including soil hydraulic redistribution when analysing the pattern of RWU (Table 4.5). This is most obvious in the unrestricted example of *NoSplit 2*, where 69% of RWU occurred in the 0-5 cm layer, while the water depletion in this layer was only 16% of total water depletion. But even in Compartment I of *Split 3*, which was assumed to be perfectly isolated, RWU and water depletion are slightly different, which is probably due to the discretization of the simulation outputs and rounding errors.

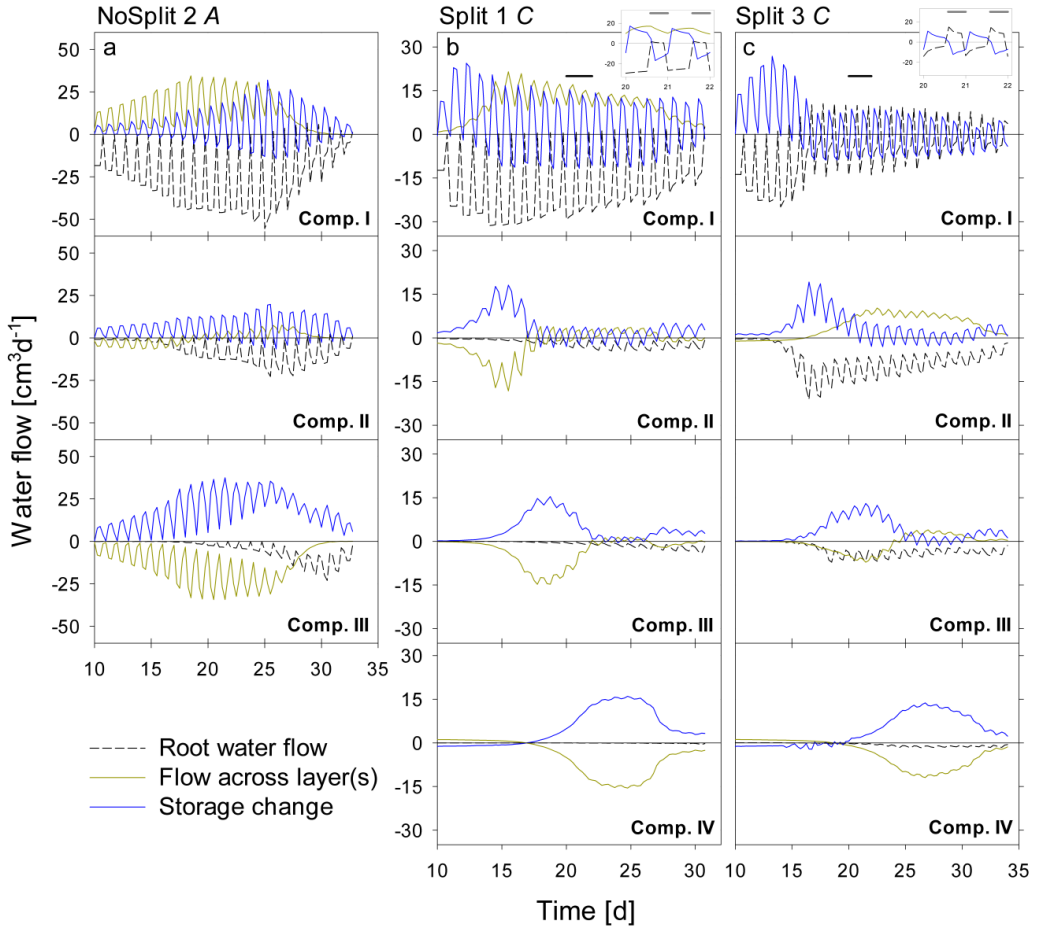


Figure 4.6 Modelled water flow dynamics over time in the a) NoSplit *A*, b) Split1 *C*, and c) Split3 *C* scenarios. Dashed black lines represent root water flow. Dark yellow lines represent the net flow across the paraffin layers from neighboring compartments. Negative values indicate water removal, positive values water addition to a compartment, respectively. Blue lines represent the resulting change of soil water content in the compartment with positive values denoting a decrease in water storage and negative values and increase in storage. Plotted values are flow rates at four discrete times per day. Because there is only one value for the night phase, flows at night appear as single peaks. The inlays at the top show the dynamics in Compartment I between Days 20-22 (as indicated by the black bars) at a higher temporal resolution (10/d), showing the dynamics of RWU and hydraulic redistribution.

Table 4.5 Total root water uptake and water depletion in each soil compartment at the end of each simulation.

Simulation		RWU [cm ³]	Water depletion [cm ³]
NoSplit A	Total	660.4	657.4
	Comp. I	456.2	105.8
	Comp. II	124.3	139.6
	Comp. III	79.9	412
Split 1 C	Total	387.7	386.7
	Comp. I	336.8	121.6
	Comp. II	32.2	82.4
	Comp. III	17.2	84.6
	Comp. IV	1.5	98.2
Split 3 C	Total	358.4	358.2
	Comp. I	101.8	97.8
	Comp. II	175.5	87.8
	Comp. III	66.7	81.9
	Comp. IV	14.4	90.6

Pre-dawn water potential at the root collar

Simulated pre-dawn water potential at the root collar (ψ_{pd}) was used as an indicator for plant water status (Figure 4.7). ψ_{pd} is independent of actual transpiration rates and can therefore be used to compare different samples. ψ_{pd} is generally thought to be in equilibrium with the soil water potential provided that night induced interruption of transpiration is long enough and flow rates in soil root systems are high enough to reach this equilibrium [Donovan *et al.*, 2003]. However, the soil matric potentials, simulated in this study were clearly not in equilibrium, especially for the two split samples.

In sample *NoSplit 2*, simulated predawn ψ_{pd} decreased only slowly until Day 25 and was in equilibrium with soil matric potential in the topsoil (-1.5 cm depth). From Day 25 onwards there was a strong decrease of topsoil matric potential and an according decrease of ψ_{pd} . After Day 30, ψ_{pd} was more negative than the topsoil matric potential. The disequilibrium increased until the end of the experiment. ψ_{pd} was more negative than the wettest soil accessible to the plant (i.e. the soil at maximum rooting depth) over the entire drying period.

In both split samples ψ_{pd} was more negative than the matric potential at maximum rooting depth but less negative than the topsoil matric potential, indicating that the system did not reach equilibrium at the end of the night. ψ_{pd} in *Split 1* was closer to the matric potential in the topsoil, reflecting the higher redistribution through the split layers in *Split 1*.

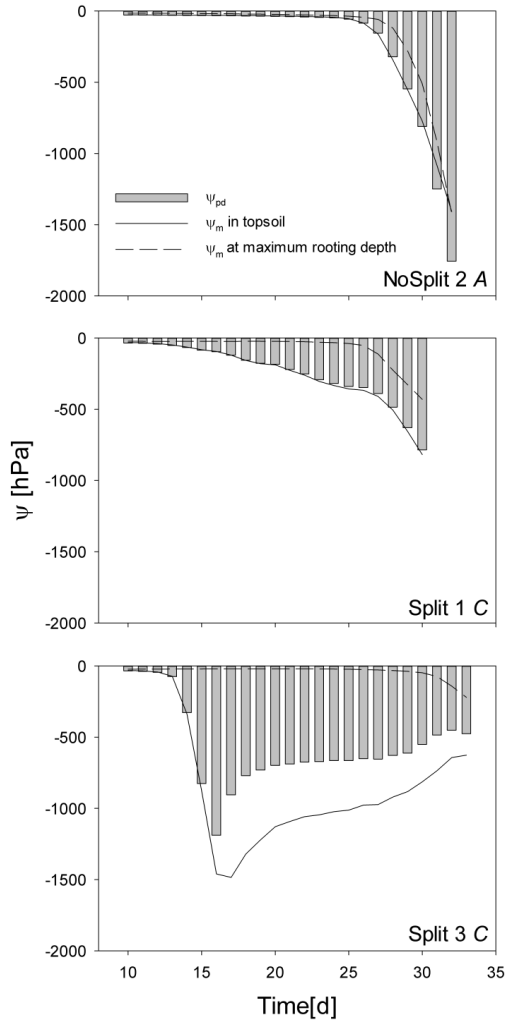


Figure 4.7 Predawn water potential at the root collar (ψ_{collar}) over time. Gray bars represent ψ_{collar} . The solid line represents soil matric potential (ψ_m) in the top 5 cm of the soil, the dashed line represents ψ_m at maximum rooting depth.

To illustrate the impact of the split layers on plant water status, predawn water potentials of the different scenarios with and without paraffin layers (*C* vs. *A*) for each sample were compared. The difference of absolute collar water potentials for the two contrasting soil environments was calculated ($\Delta|\psi_{pd}| = |\psi_{pd}|_C - |\psi_{pd}|_A$) (Figure 4.8). As expected, collar potential was constantly more negative in scenario *C* than in scenario *A*. $\Delta\psi_{pd}$ in *Split 1* and in *NoSplit 2* had the same magnitude and dynamics, while in *Split 3*, where the upper paraffin layer was non-conductive, it increased more rapidly and had a higher magnitude, indicating an effect of the degree of hydraulic isolation.

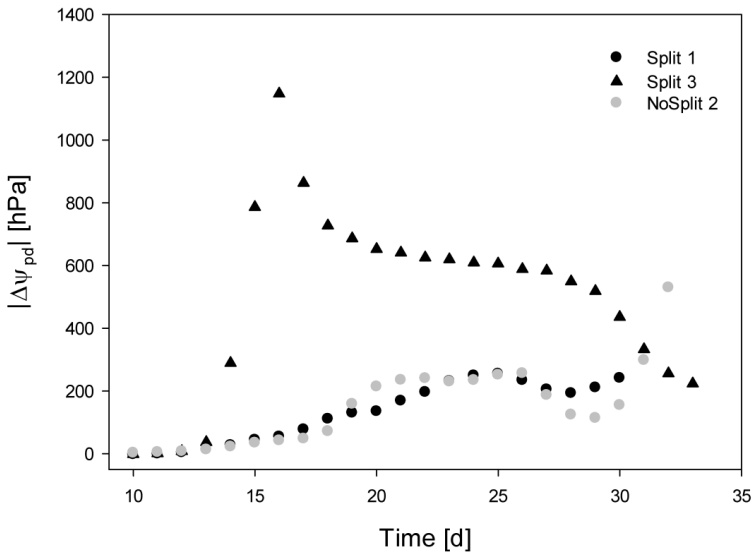


Figure 4.8 Influence of split layers on collar water potential. Difference of absolute predawn collar water potentials for each root system subjected to different scenarios; $\Delta|\psi_{PD}| = |\psi_{PD,C}| - |\psi_{PD,A}|$

4.4 Discussion

The available data set was ideally suited for the applied model. The combination of these two methods allowed to get a more in depth understanding of the processes within the soil-root system and also to reinterpret the measurement results.

4.4.1 Influence of paraffin layers on plant growth

CT measurements could give insight into the changes of growth behaviour caused by the addition of wax layers. However, the mechanisms behind these changes remain unclear. Use of the model could bridge the gap to internal plant water potentials. This enables an interpretation of plant water stress.

Experimental results as well as simulations suggested strongly that most of the paraffin layers were not perfectly hydraulically isolating. Tomographic images and visual inspection after destructive harvest showed, however, no evidence of cracks or holes in the wax layers. It is possible that there were cracks at the container walls that were formed due to shearing of the paraffin caused by the weight of the soil in the upper compartments. The only paraffin layers that were evidently tight were consequently the uppermost layers in the samples Split 3-5. *Drew* [1975] suggested the use of layers as thin as 0.2 mm, which is even thinner than the layers that were used in this study.

Roots easily penetrated the paraffin and grew into the lower compartments. However, a few roots continued to grow horizontally within the soft paraffin layers (see Appendix C.2). Taproots and vertically oriented laterals were not affected by paraffin layer. While the paraffin had only a small effect on root morphology, it did affect the extent of the root system.

The plants in the “Split” experiment were overall smaller with lower root densities. Inserting additional split layers generated a substantial resistance to vertical water flow within the soil or water redistribution in the soil column. A restriction of this redistribution led to lower simulated predawn root and collar water potentials, which were related to lower measured stomatal conductance. The lower predawn water potentials pointed at plant stress that resulted in a restriction of root and shoot growth. Even though the root-shoot ratio was shown to increase in *Vicia faba* in dryer environments [*El Nadi et al.*, 1969], this could not be observed in this experiment.

4.4.2 Relation between measured water loss and RWU

The simulations showed the location of root water uptake, which clarifies that measured changes of water content cannot be readily interpreted as root water uptake, which has mainly two reasons: First,

the relation between pressure head and water content is non-linear, which forbids the extrapolation of a single tensiometer reading to the total soil compartment without knowing the gradients. The development of gradients around root water uptake can be seen in Appendix C.3. And, second, hydraulic redistribution in the soil but also in the roots mean that the measured change in water content or storage change within one soil compartment is not equal to water uptake. Even a small conductivity of the split layer can lead to considerable hydraulic redistribution of soil water. Using Hagen-Poiseuille values from the simulation, an approximation of the size of the rupture can be calculated:

$$Q = \frac{\pi r^4}{8\eta} \frac{\Delta\psi}{l} \quad 4.3$$

In *Split 1* between Compartment 1 and 2 (first paraffin layer) on Day 23 the water flow through the soil layer Q is approximately $10 \text{ cm}^3 \text{ d}^{-1}$ ($1.157 \text{ m}^3 \text{ s}^{-1}$), the viscosity of water η is 0.001 Pa s , the gradient in soil water potential between the compartments $\Delta\psi$ is approximately 200 cm ($\approx 2 \cdot 10^4 \text{ Pa}$), and l is the length of the paraffin layer with 0.5 cm ($5 \cdot 10^{-3} \text{ m}$). Using all these rough estimations, this would result in a radius of $2.92 \cdot 10^{-5} \text{ m}$ ($30 \text{ }\mu\text{m}$).

Even if the vertical soil flow is restricted, the hydraulic redistribution through the roots might still be a substantial amount of water that is exchanged between the roots and the soil in the drier regions of the root zone. The amount of water that can be redistributed depends on soil type as well as root properties (architecture, hydraulic conductivities) [Neumann *et al.*, 2014]. In this case, however, the net root water uptake should correspond to soil water depletion.

4.4.3 Predawn collar potential:

Simulation results suggest that predawn collar water potential is not related to the water potential in the wettest but in the driest part of the root zone and that in case water redistribution in the soil is restricted, there are large differences of water potentials in the root system. Disequilibrium between plant and soil water potentials was caused by the heterogeneity of soil water potential. In the simulations of the “Split” experiment the heterogeneity of soil water potential led to hydraulic redistribution via the root system during the night. Water was taken up in the lower, wetter compartments and was released by the roots in the drier top compartment. This leads potentially to the equilibration of the system but is ultimately limited by the soil-root resistance to water flow. The

largest redistribution, however, takes place through the leaking split layers. For this reason, ψ_{pd} of *Split 1* where the complete soil domain was drying more or less simultaneously, was very close to the potential of the dry topsoil, while in *Split 3*, with Compartment I being perfectly hydraulically isolated, ψ_{pd} was between the potentials of the topsoil and the soil at maximum rooting depth.

4.4.4 Determination of RSA with CT

Compared to subsequent WinRhizo scans CT imaging lost up to 27 % of the total root length (Table 4.4). One reason is the coarse resolution of the CT scans that enables to visualize only roots with a diameter larger than twice the resolution of 245 μm or 277 μm , respectively. Due to their hydraulic properties, however, these undetected roots contribute largely to root water uptake [Eshel and Beeckman, 2013]. The average root diameter measured with WinRHIZO was 1.07 ± 0.13 mm and roots with a diameter below 0.5 mm amounted to only 3.5 % of total root length. As in some of the experiments the soil started to form cracks during desiccation, roots growing into these cracks could not be detected by the CT scanner. Further roots that grew along the cylinder walls are often lost in the course of data processing, when edges of the domain have to be removed. In the split setup, roots sometimes remained within the soft paraffin layers, which were eventually undetectable with X-ray CT as there is no contrast between paraffin and roots.

4.4.5 Parameterization of root hydraulic conductivity

The root hydraulic parameters were derived from literature data and could not be validated by direct measurements or simulation results. Measurements of pressure heads in the collar or the leaves would be needed to evaluate the root hydraulic properties and/or to optimize these properties. However, for known root architecture and transpiration rates, the order of the collar water potentials that were simulated for the different experiments will remain the same if it is assumed that the hydraulic properties of the root segments and how they depend on age does not differ between the different experiments.

4.5 Conclusion and Outlook

- 1) Plants grown in split experiments with paraffin layers developed less than plants grown under the same conditions in no-split experiments.
- 2) Using a simulation model in combination with data of the root architecture development, it was found that the split layers generated an important resistance to vertical water flow or water redistribution in the soil column. Vertical redistribution of water was an important process to provide the root system with sufficient water for uptake. A restriction of this redistribution led to lower simulated predawn root and collar water potentials which were related to lower measured stomatal conductance. The lower predawn collar water potentials pointed at plant stress that resulted in a restriction of root and shoot growth.
- 3) Vertical water redistribution makes it impossible to link root water uptake to soil water depletion.
- 4) If vertical redistribution of water through the soil is restricted, there may be nevertheless a substantial amount of water that is exchanged between the roots and the soil in the drier regions of the root zone.
- 5) Simulation results suggest that predawn collar water potential is not related to the water potential in the wettest but in the driest part of the root zone and that in case water redistribution in the soil is restricted, there are large differences of water potentials in the root system.
- 6) Paraffin layers are not perfectly hydraulically isolating different soil compartments.
- 7) Conclusions 2-6 could not have been made without soil and root water flow simulations. To setup the model, data on the dynamic root architecture was essential. The agreement between measured and simulated soil water potentials and their dynamics for the different root architectures and experimental conditions (scenarios for the different soil setup) while making use of the same set of root hydraulic and soil parameters for all the simulated experiments indicates that the flow processes in the coupled soil-plant systems were well represented in the model.

CHAPTER 5

GENERAL CONCLUSIONS AND OUTLOOK

5.1 Conclusion

The question how to incorporate short term plant responses to soil heterogeneity in existing models, was targeted by implementing hormonal signalling for stomatal closure into an explicit soil and root water flow model.

A root originated hormonal signal can lead to significant oscillations in stomatal aperture, an effect that was previously observed in several species. With the additional implementation of a buffer, representing the plant's shoot volume, these oscillations could be suppressed. The simulated hormone concentration, arriving at the leaves, was within the range of measured ABA concentrations. The transport of the hormonal signal within the plant can play a significant role, as in dry zones of the roots, when water uptake cannot be upheld anymore, the hormones can be trapped. Re-irrigation of these parts of the root zone can then lead to a flush of the accumulated signal and an initially larger stomatal closure, even if water availability is, after irrigation, in a more favourable state. However, for the presented scenario, the response of an additional hormonal signalling was only slightly different from a system with hydraulic control.

In the next chapter a theoretical framework was built to determine in which cases (additional) hormonal signalling has to be taken into account to disentangle the influence of hormonal and hydraulic stomatal control. A theoretical relationship for steady state conditions was derived to account for plants that are additionally to hydraulics also or only controlled by hormonal signals. Depending on the mode of control, fundamentally different behaviour of stomata in case of heterogeneously distributed water availability was observed. Hydraulic and chemical control resulted in a piece-wise linear relationship between soil hydraulic potential and stomatal regulation, similar to isohydric behaviour and also similar to stress functions implemented in hydrological models. Chemical control alone, on the other hand, resulted in leaf water potentials that depended strongly on soil water potential: a behaviour which has previously been shown for anisohydric plant species. Chemical control further implies that for the same water availability, the actual transpiration is increasing with potential transpiration rate: A relationship, which is, to some extent, used in eco-hydrological models. The theoretical relationships were compared with the numerical solutions and were in good agreement. Even though the theoretical framework hinges on several assumptions and simplifications, most of these were shown to be justifiable. This study enables to identify different plant behaviour and to study their control mechanisms.

The next part was related to long-term plant adaptations and was investigated by using numerical simulations to analyse an experimental data set of plants that were grown under permanently restricted soil water availability.

In experiments, where bean plants were grown in vertically unrestricted soil columns and in soil columns with additional horizontal split layers, it was shown that plants developed less in respect to overall size, stomatal conductance, and transpiration rate in case of restricted water availability. Time series of the CT scanned root systems were reconstructed to gain digitized dynamic root architectures for the subsequent numerical simulations. Comparing measured with modelled soil water potentials showed that most of the split layers were not perfectly hydraulically isolating and a considerable amount of water was redistributed between the individual soil compartments. The vertical water redistribution made it impossible to link root water uptake to water depletion from one soil compartment. Regardless of the redistribution, the split layers still resulted in lower predawn root and collar water potentials, which can be related to a reduction in stomatal conductance.

5.2 Outlook

The presented model for hormonal signalling might prove useful to investigate the influence of soil properties on stomatal behaviour and, in conjunction with experiments, might allow the optimization of irrigation strategies, such as the already applied alternated partial root zone drying.

The theoretical relationships between effective soil water potential and transpiration rate could be of use to determine the underlying control mechanisms of stomata in different plant species. This would require an experimental data set with measured leaf water potentials and transpiration rates for the same soil water status and varying potential transpiration. It would be further interesting to investigate the impact of different stomatal control mechanisms on plant growth and uptake on the field scale.

The combination of experimental data and numerical simulations offers more than the previously described synergetic effects. A new approach to determine dynamic root growth responses in a heterogeneous soil environment would be to link measured local root growth parameters to simulated local soil water potentials. In contrast to commonly used rhizotron experiments, this would offer an in-situ method to quantify root growth within a rather unrestricted soil environment.

Plant transpiration rate depends not only on the soil state, i.e. water availability, but also on atmospheric conditions, like radiation intensity or vapour pressure deficit. To describe the complete soil-plant-atmosphere continuum, the coupling to simulation modules that represent the above ground part of the plant and the atmosphere, i.e. crop growth models, would be the next logical step. The description of the full soil-plant atmosphere continuum would enable to replace the upper boundary condition for root water uptake with a dynamic stomatal model that depends on plant size and atmospheric conditions. This would also allow to determine carbon uptake by the stomata and to calculate carbon allocation within the plant.

Appendix A

A.1 Influence of shoot volume (buffer size) on transpiration reduction

When shoot volume was smaller than $0.5 \cdot V_{\text{Root}}$, multi-frequency oscillations in simulated transpiration occurred (Figure A. 1) for all scenarios which included chemical signalling. When averaged over time, the trend of transpiration and the signal concentrations (data not shown), were independent of buffer size. Oscillations in stomatal conductance have been observed in several plant species [Buckley, 2005], including cotton (with frequencies ranging from $1.3 - 1.8 \text{ h}^{-1}$) [Farquhar and Cowan, 1974; Marengo *et al.*, 2006; Passioura and Tanner, 1985] and citrus trees when exposed to high vapour pressure deficits (mandarin tree, frequency ca. 1.8 h^{-1}) [Dzikiti *et al.*, 2010]. Regardless of the physiological explanation (and site) of this buffer, simulations revealed that, stomatal conductance can oscillate due to a chemical signal arriving from the roots.

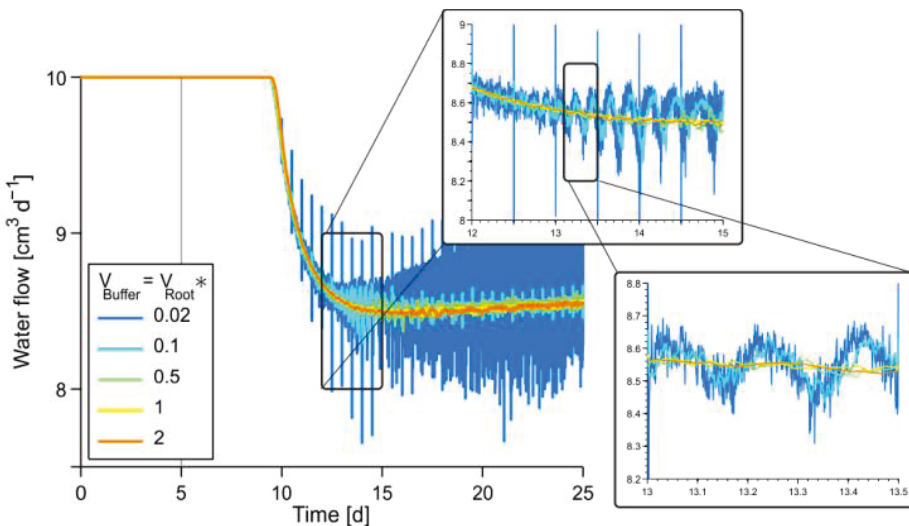


Figure A. 1 Influence of buffer size: Oscillations in transpiration rates are related to buffer size. A buffer size of $1 \cdot V_{\text{Root}}$ corresponds to an average residence time of 0.1 days and a root:shoot ratio of 1.

Appendix B

B.1 Time courses of water uptake depending on the boundary conditions

Three simulations with the same fraction (50%) of dry *soil* domain were chosen to compare the influence of the boundary conditions on the transpiration regulation. As the root length density profile was not uniform over depth this results, for the horizontal splits, to an f_{dry} (fraction of *roots* in dry soil) of 0.32 for the bottom irrigation and 0.68 for the top irrigation respectively.

In Figure B. 1 the root systems are depicted at the end of the simulations, after 100 days (a, c, e). It might be worth noting that the most negative xylem water potential and the smallest transpiration rate is found in the horizontal split with top irrigation, this, however is not due to the boundary condition but rather to the highest f_{dry} . Nevertheless, the differences can be compared by looking at the right panel of Figure B. 1 (b, d, f). The uptake is largely compensated by the irrigated compartments.

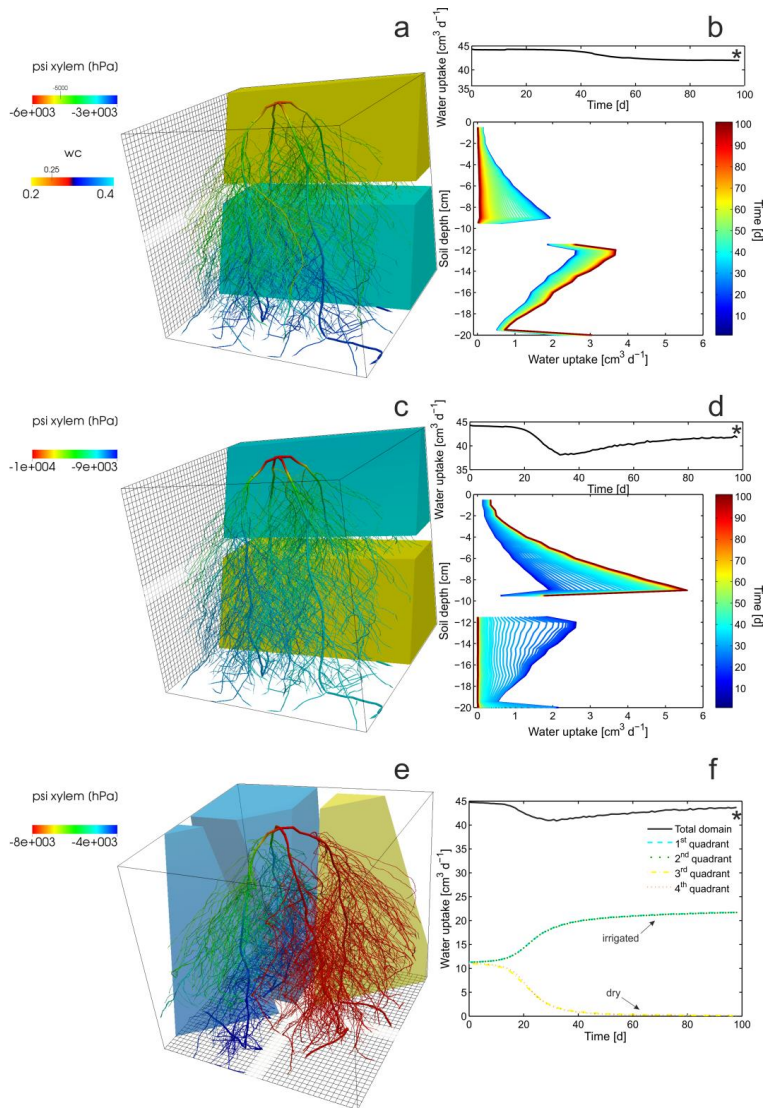


Figure B.1 Simulation domain for horizontal and vertical split setup with 50% of irrigated soil domain, which shows the water content from blue (= high water content) to yellow (=low water content). The root system is coloured by the xylem water potential from red (=low water potential) to blue (=high water potential). a) horizontal split with bottom irrigation and b) the water uptake over the soil depth and over the duration of the simulation (100 days), small panel at the top shows total root water uptake over time c) horizontal split with top irrigation and d) water uptake over the soil depth for this simulation, small panel at the top shows total root water uptake over time e) vertical split with the two compartments on the left irrigated and f) water uptake from the four soil compartments and the total uptake. Asterisks indicate values taken for the comparison to the direct model. $T_{pot} = 50 \text{ cm}^3 \text{ d}^{-1}$, C controlled plant.

B.2 Gradients between leaf and root water potential

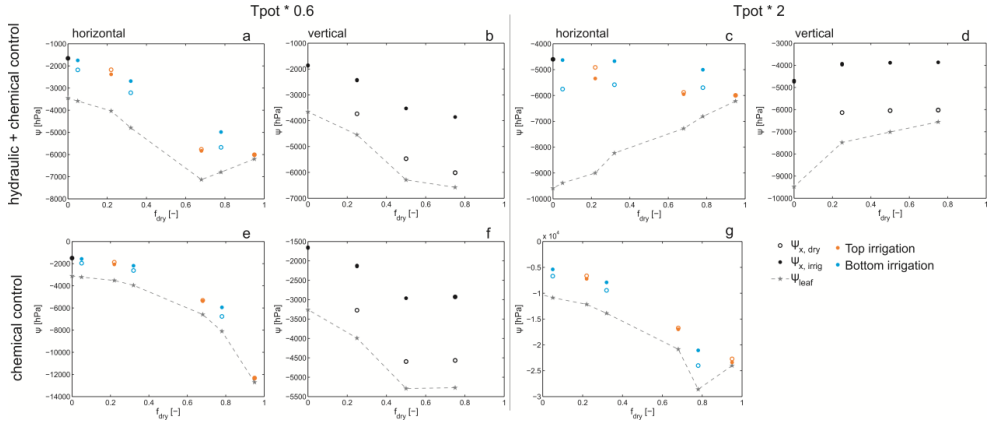


Figure B. 2 Gradients between leaf and root water potential for H+C control (top panel) and C control (bottom) over different transpiration rates (a, b, e, f: $T_{pot} = 30 \text{ cm}^3 \text{ d}^{-1}$, and c, d, g: $T_{pot} = 100 \text{ cm}^3 \text{ d}^{-1}$). The boundary condition of the horizontal splits is indicated in a) for each f_{dry} in blue for bottom irrigation and orange for top irrigation, respectively.

B.3 Signal production for H+C

Signal production for H+C control. For the vertical split root system the signal is produced only in and throughout the dry compartments. The horizontal splits show that only a small amount of roots are contributing to signal production.

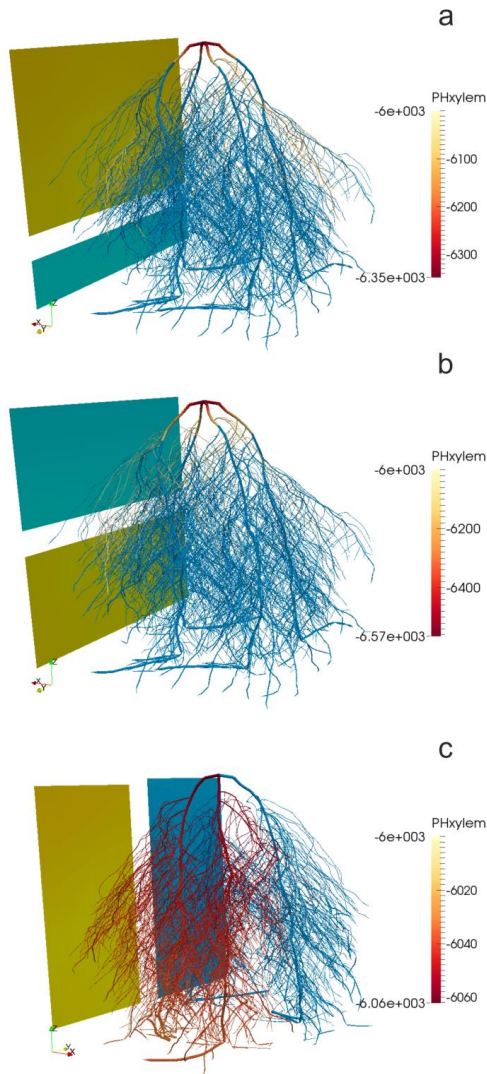


Figure B. 3 Signal production in the root system for horizontal split with a) bottom irrigation ($f_{\text{dry}} = 0.78$) and b) top irrigation ($f_{\text{dry}} = 0.68$) and for vertically split domain ($f_{\text{dry}} = 0.5$). The soil is coloured in blue = high and yellow = low soil water

content; the roots are coloured according to the water potential in the xylem in blue for $\psi_{\text{xyl}} > \psi_{\text{lim}}$ and in red for $\psi_{\text{xyl}} \leq \psi_{\text{lim}}$, i.e. for roots that produce chemical signal.

B.4 Sensitivity analysis for ψ_{lim}

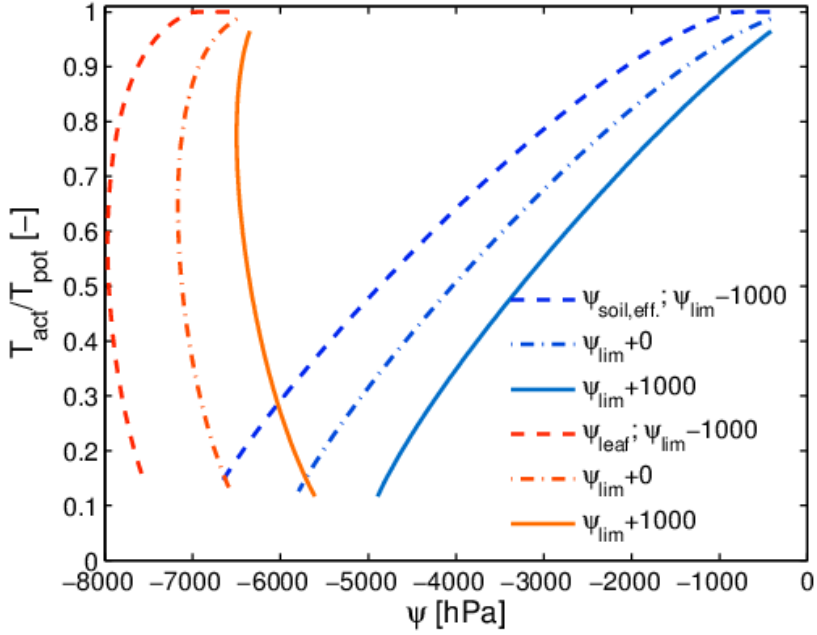


Figure B. 4 Influence of ψ_{lim} on leaf and soil water potentials for H+C control.

Appendix C

C.1 Soil matric potentials of the remaining experimental samples

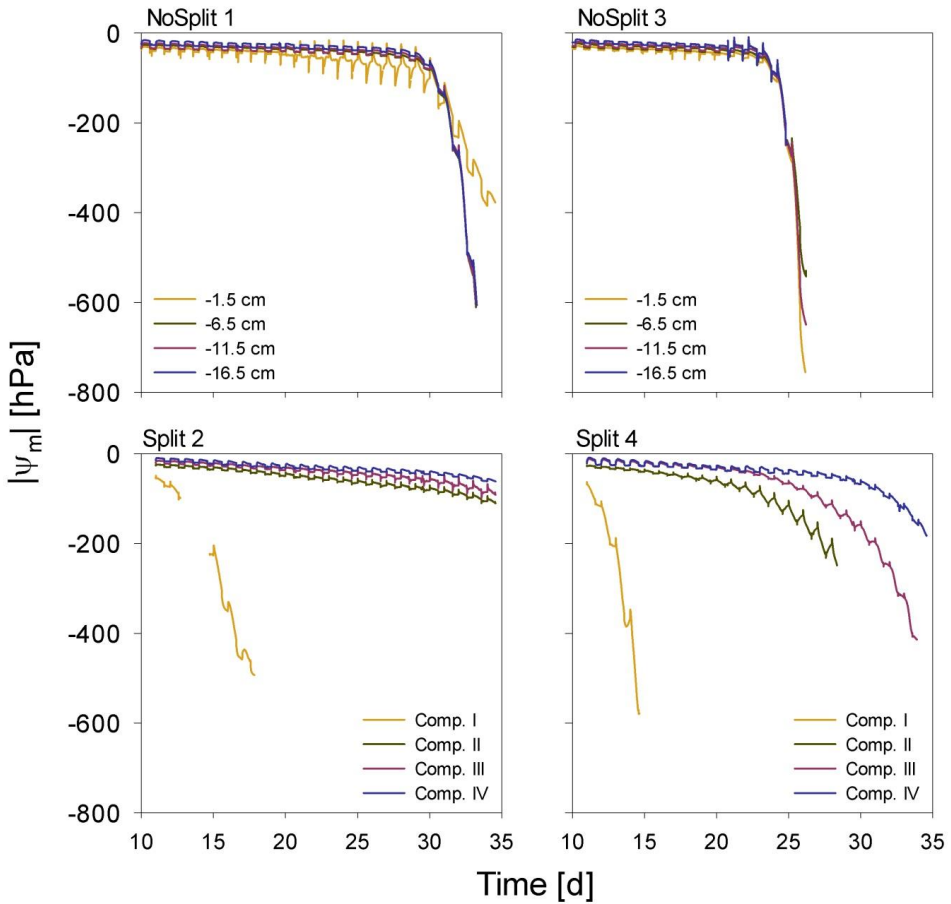


Figure C. 1 Development of soil water pressure ψ_m over time of the samples not used for modelling. Different colors represent measurements in different depths / compartments

C.2 *Roots growing through paraffin layer*

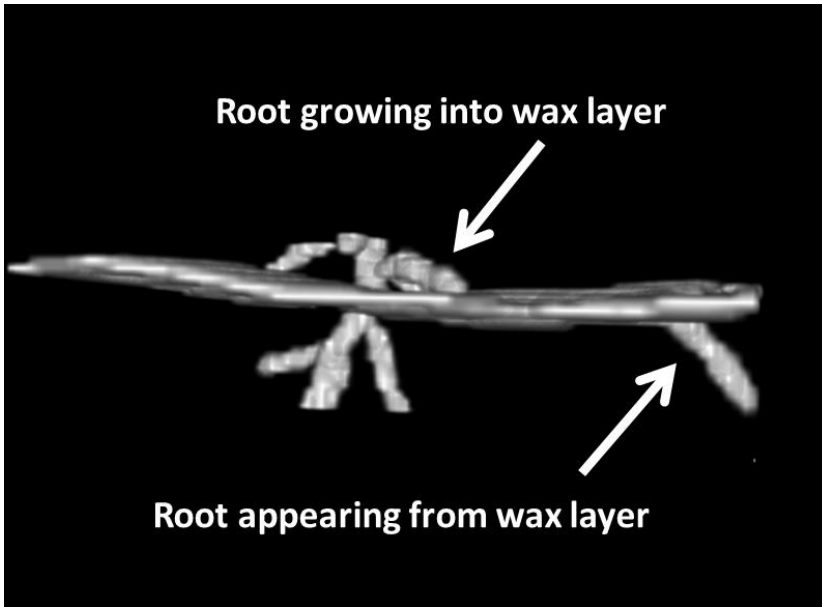


Figure C. 2 Influence of paraffin layer on root growth: roots grow either unimpeded (left), but can also be deflected within the soft paraffin and later re-penetrate the soil. Split 1, Day 12, Layer at -5 cm, Height of image section: 13.5 mm

C.3 Gradients of soil water pressure around the roots

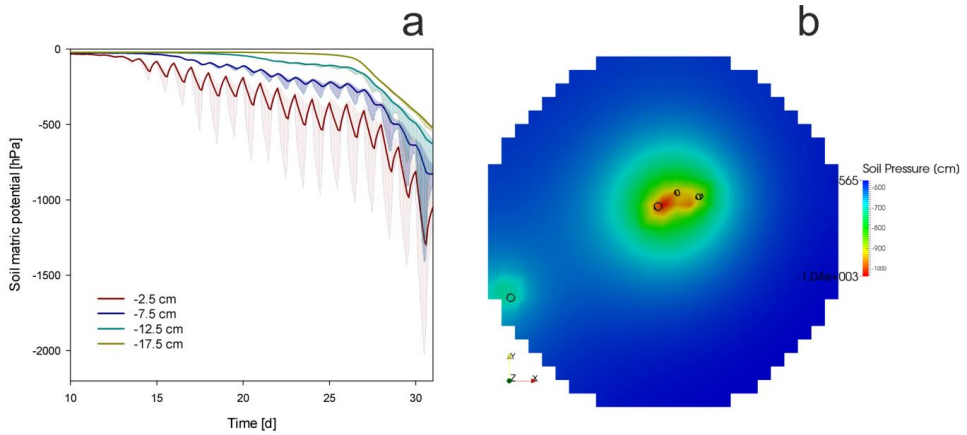


Figure C. 3 Water potential gradients gradient around the roots: (a) Plane spans the range (min - max) of water pressures within each of the four soil compartments, line shows the mean (b) slice at $z=-12$ cm showing gradients of soil water pressure around the roots (black circles); *Split 1* scenario

ACKNOWLEDGEMENTS

I am particularly obliged to my supervisor and mentor Jan Vanderborgh who was always willing to think his way through each and every one of my ‘products’, be it figure, sentence, or equation, and to find, mostly to my great surprise, either a way to cut the Gordian knot or to prove its utter nonsense. Thanks Jan, for patiently showing me the core of research: being exact and, luckily, never finished!

To Mathieu, who was the restless and enthusiastic motivator who could clear the skies when I could not see the horizon where all these hormones were driving me: merci bien!

Thanks to Harry Vereecken for keeping up-to-date with, not only, my work and to provide me with new articles until the end.

I also want to thank TR32 for funding and allowing me as the student representative to peak a little behind the curtains of such a large research project.

Grrreat Scottish thanks to Glyn Bengough for letting me stay in Dundee during three, most pleasant, winter months in 2014 at the James Hutton Institute! Thanks to all of the colleagues and friends there!

Another warm thanks to Ian Dodd from Lancaster, who believed in our modelling activities, which was great motivation for me.

I am duly grateful for the chance to meet and work with people from the UFZ in Halle, who provided valuable ‘plant knowledge’ as well as *the* supplementary data set to our model: Nico Koebernick and Doris Vetterlein.

My father used to tell me that in the end it might not matter what I would end up doing in my life but rather the people I worked with. He was, like so often, right. Luckily I not only found an inspiring profession but also great colleagues. Being at my wits end, I found open ears, smart discussions, coffee and loads of cookies, cakes (may they have fallen to the ground or not, I loved each piece!), and chocolate. Big thanks to my big office and your good humor regarding some of life’s bad humor! Markus, Seb, Wei, Sayeh, and Betiglu! Also many thanks to all the other colleagues at the institute that were usually not disinclined to Friday night beers, BBQs or other mischief: Anja, Daniela, Kathrina, Inge, Maria, Hanna, Nina, Steffen...

My first steps in programming would not have been possible without Natalie. Thanks for explaining and explaining and explaining everything all over again!

During my first two years I found a great friend in Laura and a home, where I would have never expected it, in Düren. Thank you for cycling with me, head or tail wind, and for a good time!

Weil ich jetzt quasi Experte bin für Wurzeln möchte ich meine eigenen nicht unerwähnt lassen. Meinem Papa, der immer hinter mir steht und mich mit festen Stützen ins Leben gestellt hat: Danke, du bist der Beste!

Und weil gute Freunde wie Anker sind, einen Riesendank an meine liebe Isi, die mich vielleicht immer noch am besten versteht von allen!

The last year I’ve learned the hardships of long-distance commuting, but was rewarded a warm and lively home with music, laughter, love, and understanding. Weil’st a Herz host wia a Bergwerk...Danke Denner!

BIBLIOGRAPHY

- Allen, R. G. (1998), *Crop evapotranspiration : guidelines for computing crop water requirements / by Richard G. Allen*, XXVI, 300 S. pp., Food and Agriculture Organization of the United States, Rome.
- Barigah, T. S., O. Charrier, M. Douris, M. Bonhomme, S. Herbette, T. Améglio, R. Fichot, F. Brignolas, and H. Cochard (2013), Water stress-induced xylem hydraulic failure is a causal factor of tree mortality in beech and poplar, *Annals of Botany*, 112(7), 1431-1437.
- Bramley, H., N. C. Turner, D. W. Turner, and S. D. Tyerman (2009), Roles of Morphology, Anatomy, and Aquaporins in Determining Contrasting Hydraulic Behavior of Roots, *Plant Physiol.*, 150(1), 348-364.
- Bravdo, B. A. (2005), Physiological mechanisms involved in the production of non-hydraulic root signals by partial rootzone drying - A review, in *Proceedings of the Seventh International Symposium on Grapevine Physiology and Biotechnology*, edited by L. E. Williams, pp. 267-276, International Society Horticultural Science, Leuven 1.
- Brodribb, T. J., and S. A. M. McAdam (2011), Passive Origins of Stomatal Control in Vascular Plants, *Science*, 331(6017), 582-585.
- Buckley, T. N. (2005), The control of stomata by water balance, *New Phytologist*, 168(2), 275-291.
- Caldwell, M. M., T. E. Dawson, and J. H. Richards (1998), Hydraulic lift: consequences of water efflux from the roots of plants, *Oecologia*, 113(2), 151-161.
- Carsel, R. F., and R. S. Parrish (1988), DEVELOPING JOINT PROBABILITY-DISTRIBUTIONS OF SOIL-WATER RETENTION CHARACTERISTICS, *Water Resources Research*, 24(5), 755-769.
- Chaumont, F., and S. D. Tyerman (2014), Aquaporins: Highly Regulated Channels Controlling Plant Water Relations, *Plant Physiol.*, 164(4), 1600-1618.
- Christmann, A., E. Grill, and J. Huang (2013), Hydraulic signals in long-distance signaling, *Current Opinion in Plant Biology*, 16(3), 293-300.
- Christmann, A., E. W. Weiler, E. Steudle, and E. Grill (2007), A hydraulic signal in root-to-shoot signalling of water shortage, *Plant J.*, 52(1), 167-174.
- Clausnitzer, V., and J. W. Hopmans (1994), Simultaneous modeling of transient three-dimensional root growth and soil water flow, *Plant and Soil*, 164(2), 299-314.
- Couvreur, V., J. Vanderborght, and M. Javaux (2012), A simple three-dimensional macroscopic root water uptake model based on the hydraulic architecture approach, *Hydrol. Earth Syst. Sci.*, 16(8), 2957-2971.
- Couvreur, V., J. Vanderborght, L. Beff, and M. Javaux (2014), Horizontal soil water potential heterogeneity: simplifying approaches for crop water dynamics models, *Hydrology and Earth System Sciences*, 18(5), 1723-1743.
- Cowan, I. (1965), Transport of water in the soil-plant-atmosphere system, *Journal of Applied Ecology*, 221-239.
- Damour, G., T. Simonneau, H. Cochard, and L. Urban (2010), An overview of models of stomatal conductance at the leaf level, *Plant, Cell & Environment*, 33(9), 1419-1438.
- Davies, W., S. Wilkinson, and B. Loveys (2002), Stomatal control by chemical signalling and the exploitation of this mechanism to increase water use efficiency in agriculture, *NEW PHYTOLOGIST; MAR, 2002*, 153 3, p449-p460, 12p., 153(3), Start Page: 449.
- Davies, W. J., and J. H. Zhang (1991), ROOT SIGNALS AND THE REGULATION OF GROWTH AND DEVELOPMENT OF PLANTS IN DRYING SOIL, *Annu. Rev. Plant Physiol. Plant Molec. Biol.*, 42, 55-76.
- Dixon, H., and J. Joly (1894), On the Ascent of Sap, *Philosophical Transactions of the Royal Society of London. B, Biological Sciences*, 186.
- Dodd, I. C. (2009), Rhizosphere manipulations to maximize 'crop per drop' during deficit irrigation, *Journal of Experimental Botany*, 60(9), 2454-2459.

- Dodd, I. C., G. Egea, and W. J. Davies (2008a), Abscisic acid signalling when soil moisture is heterogeneous: decreased photoperiod sap flow from drying roots limits abscisic acid export to the shoots, *Plant Cell Environ.*, 31(9), 1263-1274.
- Dodd, I. C., G. Egea, and W. J. Davies (2008b), Accounting for sap flow from different parts of the root system improves the prediction of xylem ABA concentration in plants grown with heterogeneous soil moisture, *Journal of Experimental Botany*, 59(15), 4083-4093.
- Dodd, I. C., J. C. Theobald, M. A. Bacon, and W. J. Davies (2006), Alternation of wet and dry sides during partial rootzone drying irrigation alters root-to-shoot signalling of abscisic acid, *Funct. Plant Biol.*, 33(12), 1081-1089.
- Dodd, I. C., G. Egea, C. W. Watts, and W. R. Whalley (2010), Root water potential integrates discrete soil physical properties to influence ABA signalling during partial rootzone drying, *Journal of Experimental Botany*, 61(13), 3543-3551.
- Donovan, L. A., J. H. Richards, and M. J. Linton (2003), MAGNITUDE AND MECHANISMS OF DISEQUILIBRIUM BETWEEN PREDAWN PLANT AND SOIL WATER POTENTIALS, *Ecology*, 84(2), 463-470.
- Doussan, C., L. Pagès, and G. Vercambre (1998a), Modelling of the Hydraulic Architecture of Root Systems: An Integrated Approach to Water Absorption--Model Description, *Annals of Botany*, 81(2), 213-223.
- Doussan, C., G. Vercambre, and L. Pagès (1998b), Modelling of the Hydraulic Architecture of Root Systems: An Integrated Approach to Water Absorption—Distribution of Axial and Radial Conductances in Maize, *Annals of Botany*, 81(2), 225-232.
- Doussan, C., A. Pierret, E. Garrigues, and L. Pages (2006), Water uptake by plant roots: II - Modelling of water transfer in the soil root-system with explicit account of flow within the root system - Comparison with experiments, *Plant and Soil*, 283(1-2), 99-117.
- Downie, H., N. Holden, W. Otten, A. J. Spiers, T. A. Valentine, and L. X. Dupuy (2012), Transparent Soil for Imaging the Rhizosphere, *PLoS One*, 7(9).
- Drew, M. C. (1975), COMPARISON OF THE EFFECTS OF A LOCALISED SUPPLY OF PHOSPHATE, NITRATE, AMMONIUM AND POTASSIUM ON THE GROWTH OF THE SEMINAL ROOT SYSTEM, AND THE SHOOT, IN BARLEY, *New Phytologist*, 75(3), 479-490.
- Dunbabin, V. M., J. A. Postma, A. Schnepf, L. Pages, M. Javaux, L. H. Wu, D. Leitner, Y. L. Chen, Z. Rengel, and A. J. Diggle (2013), Modelling root-soil interactions using three-dimensional models of root growth, architecture and function, *Plant and Soil*, 372(1-2), 93-124.
- Dupuy, L., M. Vignes, B. M. McKenzie, and P. J. White (2010), The dynamics of root meristem distribution in the soil, *Plant, Cell & Environment*, 33(3), 358-369.
- Durner, W. (1994), HYDRAULIC CONDUCTIVITY ESTIMATION FOR SOILS WITH HETEROGENEOUS PORE STRUCTURE, *Water Resources Research*, 30(2), 211-223.
- Dzikiti, S., J. S. Verreyne, J. Stuckens, A. Strever, W. W. Verstraeten, R. Swennen, and P. Coppin (2010), Determining the water status of Satsuma mandarin trees Citrus Unshiu Marcovitch using spectral indices and by combining hyperspectral and physiological data, *Agricultural and Forest Meteorology*, 150(3), 369-379.
- El Nadi, A. H., R. Brouwer, and J. T. Locher (1969), SOME RESPONSES OF THE ROOT AND THE SHOOT OF VICIA-FABA-D PLANTS TO WATER STRESS, *Netherlands Journal of Agricultural Science*, 17(2), 133-142.
- Eshel, A., and T. Beekman (2013), *Plant roots : the hidden half* 4th ed. ed., Getr. Pag. pp., CRC Press, Boca Raton, Fla.
- Farquhar, G. D., and I. R. Cowan (1974), OSCILLATIONS IN STOMATAL CONDUCTANCE - INFLUENCE OF ENVIRONMENTAL GAIN, *Plant Physiol.*, 54(5), 769-772.
- Feddes, R. A., P. J. Kowalik, and H. Zaradny (1978), *Simulation of field water use and crop yield*, 189 pp., Pudoc, Wageningen, The Netherlands.
- Foley, J. A., et al. (2005), Global Consequences of Land Use, *Science*, 309(5734), 570-574.
- Foley, J. A., et al. (2011), Solutions for a cultivated planet, *Nature*, 478(7369), 337-342.

- Franks, P. J., P. L. Drake, and R. H. Froend (2007), Anisohydric but isohydrodynamic: seasonally constant plant water potential gradient explained by a stomatal control mechanism incorporating variable plant hydraulic conductance, *Plant Cell Environ.*, 30(1), 19-30.
- Frensch, J., and E. Steudle (1989), AXIAL AND RADIAL HYDRAULIC RESISTANCE TO ROOTS OF MAIZE (ZEA-MAYS-L), *Plant Physiol.*, 91(2), 719-726.
- Gardner, W. R., and C. F. Ehlig (1963), INFLUENCE OF SOIL WATER ON TRANSPIRATION BY PLANTS, *Journal of Geophysical Research*, 68(20), 5719-&.
- Garrigues, E., C. Doussan, and A. Pierret (2006), Water Uptake by Plant Roots: I – Formation and Propagation of a Water Extraction Front in Mature Root Systems as Evidenced by 2D Light Transmission Imaging, *Plant and Soil*, 283(1-2), 83-98.
- Gowing, D. J. G., W. J. Davies, and H. G. Jones (1990), A POSITIVE ROOT-SOURCED SIGNAL AS AN INDICATOR OF SOIL DRYING IN APPLE, MALUS X DOMESTICA-BORKH, *Journal of Experimental Botany*, 41(233), 1535-1540.
- Hainsworth, J. M., and L. A. G. Aylmore (1986), Water Extraction by Single Plant Roots, *Soil Sci. Soc. Am. J.*(4), 841-848.
- Hainsworth, J. M., and L. A. G. Aylmore (1989), Non-uniform soil water extraction by plant roots, *Plant and Soil*, 113(1), 121-124.
- Hartung, W., and A. A. Aboumandour (1980), ABSCISIC-ACID IN ROOT CULTURES OF PHASEOLUS-COCCINEUS L, *Zeitschrift Fur Pflanzenphysiologie*, 97(3), 265-269.
- Herkelrath, W. N., E. E. Miller, and W. R. Gardner (1977), WATER-UPTAKE BY PLANTS .1. DIVIDED ROOT EXPERIMENTS, *Soil Science Society of America Journal*, 41(6), 1033-1038.
- Holbrook, N. M., V. R. Shashidhar, R. A. James, and R. Munns (2002), Stomatal control in tomato with ABA-deficient roots: response of grafted plants to soil drying, *Journal of Experimental Botany*, 53(373), 1503-1514.
- Huber, K., J. Vanderborght, M. Javaux, N. Schröder, I. Dodd, and H. Vereecken (2014), Modelling the impact of heterogeneous rootzone water distribution on the regulation of transpiration by hormone transport and/or hydraulic pressures, *Plant and Soil*, 1-20.
- Jarvis, N. J. (1989), A simple empirical model of root water uptake, *Journal of Hydrology*, 107(1-4), 57-72.
- Javaux, M., T. Schröder, J. Vanderborght, and H. Vereecken (2008), Use of a Three-Dimensional Detailed Modeling Approach for Predicting Root Water Uptake, *Vadose Zone Journal*, 7(3), 1079-1079.
- Javaux, M., V. Couvreur, J. Vanderborght, and H. Vereecken (2013), Root Water Uptake: From Three-Dimensional Biophysical Processes to Macroscopic Modeling Approaches, *Vadose Zone Journal*, 12(4).
- Kang, S. (2004), Controlled alternate partial root-zone irrigation: its physiological consequences and impact on water use efficiency, *Journal of Experimental Botany*, 55(407), 2437-2446.
- Khalil, A. A. M., and J. Grace (1993), DOES XYLEM SAP ABA CONTROL THE STOMATAL BEHAVIOR OF WATER-STRESSED SYCAMORE (ACER-PSEUDOPLATANUS L) SEEDLINGS, *Journal of Experimental Botany*, 44(264), 1127-1134.
- Klein, T. (2014), The variability of stomatal sensitivity to leaf water potential across tree species indicates a continuum between isohydric and anisohydric behaviours, *Functional Ecology*, n/a-n/a.
- Koeberner, N., U. Weller, K. Huber, S. Schlüter, H.-J. Vogel, R. Jahn, H. Vereecken, and D. Vetterlein (2014), In Situ Visualization and Quantification of Three-Dimensional Root System Architecture and Growth Using X-Ray Computed Tomography, *Vadose Zone J.*(8).
- Kuhlmann, A., I. Neuweiler, S. E. A. T. M. van der Zee, and R. Helmig (2012), Influence of soil structure and root water uptake strategy on unsaturated flow in heterogeneous media, *Water Resources Research*, 48(2), W02534.
- Kutschera, L. (1960), *Wurzelatlas mitteleuropäischer Ackerunkräuter und Kulturpflanzen*.
- Kutschera, L., and E. Lichtenegger (2002), *Wurzelatlas mitteleuropäischer Waldbäume und Sträucher*, 2. Auflage ed., Stocker Verl., Graz.

- Lambers, H., F. S. Chapin, and T. L. Pons (2008), *Plant Physiological Ecology by Hans Lambers, F. Stuart Chapin, Thijs L. Pons. [E-Book]*, Second Edition. ed., online resource pp., Springer-Verlag New York, New York, NY.
- Leitner, D., S. Klepsch, G. Bodner, and A. Schnepf (2010a), A dynamic root system growth model based on L-Systems, *Plant and Soil*, 332(1-2), 177-192.
- Leitner, D., A. Schnepf, S. Klepsch, and T. Roose (2010b), Comparison of nutrient uptake between three-dimensional simulation and an averaged root system model, *Plant Biosyst.*, 144(2), 443-447.
- Leitner, D., F. Meunier, G. Bodner, M. Javaux, and A. Schnepf (2014), Impact of contrasted maize root traits at flowering on water stress tolerance – A simulation study, *Field Crops Research*, 165(0), 125-137.
- Li, B., Z. Feng, M. Xie, M. Sun, Y. Zhao, L. Liang, G. Liu, J. Zhang, and W. Jia (2011), Modulation of the root-sourced ABA signal along its way to the shoot in *Vitis riparia* × *Vitis labrusca* under water deficit, *Journal of Experimental Botany*, 62(6), 1731-1741.
- Liang, J. S., J. H. Zhang, and M. H. Wong (1997), How do roots control xylem sap ABA concentration in response to soil drying?, *Plant Cell Physiol.*, 38(1), 10-16.
- Liu, F. L., C. R. Jensen, and M. N. Andersen (2005), A review of drought adaptation in crop plants: changes in vegetative and reproductive physiology induced by ABA-based chemical signals, *Aust. J. Agric. Res.*, 56(11), 1245-1252.
- Liu, F. L., R. Song, X. Y. Zhang, A. Shahnazari, M. N. Andersen, F. Plauborg, S. E. Jacobsen, and C. R. Jensen (2008), Measurement and modelling of ABA signalling in potato (*Solanum tuberosum* L.) during partial root-zone drying, *Environ. Exp. Bot.*, 63(1-3), 385-391.
- Lynch, J. P., K. L. Nielsen, R. D. Davis, and A. G. JablOKow (1997), SimRoot: Modelling and visualization of root systems, *Plant and Soil*, 188(1), 139-151.
- Marengo, R. A., K. Siebke, G. D. Farquhar, and M. C. Ball (2006), Hydraulically based stomatal oscillations and stomatal patchiness in *Gossypium hirsutum*, *Funct. Plant Biol.*, 33(12), 1103-1113.
- Martin-Vertedor, A. I., and I. C. Dodd (2011), Root-to-shoot signalling when soil moisture is heterogeneous: increasing the proportion of root biomass in drying soil inhibits leaf growth and increases leaf abscisic acid concentration, *Plant Cell Environ.*, 34(7), 1164-1175.
- Molz, F. J. (1981), MODELS OF WATER TRANSPORT IN THE SOIL-PLANT SYSTEM - A REVIEW, *Water Resources Research*, 17(5), 1245-1260.
- Mooney, S. J., T. P. Pridmore, J. Helliwell, and M. J. Bennett (2012), Developing X-ray Computed Tomography to non-invasively image 3-D root systems architecture in soil, *Plant and Soil*, 352(1-2), 1-22.
- Mualem, Y. (1976), NEW MODEL FOR PREDICTING HYDRAULIC CONDUCTIVITY OF UNSATURATED POROUS-MEDIA, *Water Resources Research*, 12(3), 513-522.
- Neumann, R. B., and Z. G. Cardon (2012), The magnitude of hydraulic redistribution by plant roots: a review and synthesis of empirical and modeling studies, *New Phytologist*, 194(2), 337-352.
- Neumann, R. B., Z. G. Cardon, J. Teshera-Levy, F. E. Rockwell, M. A. Zwieniecki, and N. M. Holbrook (2014), Modelled hydraulic redistribution by sunflower (*Helianthus annuus* L.) matches observed data only after including night-time transpiration, *Plant Cell Environ.*, 37(4), 899-910.
- North, G. B., and P. S. Nobel (1991), Changes in Hydraulic Conductivity and Anatomy Caused by Drying and Rewetting Roots of *Agave deserti* (Agavaceae), *American Journal of Botany*, 78(7), 906-915.
- Oswald, S. E., M. Menon, A. Carminati, P. Vontobel, E. Lehmann, and R. Schulin (2008), Quantitative Imaging of Infiltration, Root Growth, and Root Water Uptake via Neutron Radiography, *Vadose Zone J.*, 7(3), 1035-1047.
- Pagès, L., G. Vercambre, J.-L. Drouet, F. Lecompte, C. Collet, and J. Le Bot (2004), Root Typ: a generic model to depict and analyse the root system architecture, *Plant and Soil*, 258(1), 103-119.
- Pantin, F., T. Simonneau, and B. Muller (2012), Coming of leaf age: control of growth by hydraulics and metabolics during leaf ontogeny, *New Phytologist*, 196(2), 349-366.
- Parent, B., C. Hachez, E. Redondo, T. Simonneau, F. Chaumont, and F. Tardieu (2009), Drought and Abscisic Acid Effects on Aquaporin Content Translate into Changes in Hydraulic Conductivity and Leaf Growth Rate: A Trans-Scale Approach, *Plant Physiol.*, 149(4), 2000-2012.

- Passioura, J. B., and C. B. Tanner (1985), OSCILLATIONS IN APPARENT HYDRAULIC CONDUCTANCE OF COTTON PLANTS, *Aust. J. Plant Physiol.*, 12(5), 455-461.
- Peksen, E. (2007), Non-destructive leaf area estimation model for faba bean (*Vicia faba* L.), *Sci. Hortic.*, 113(4), 322-328.
- Peters, A., and W. Durner (2008), Simplified evaporation method for determining soil hydraulic properties, *Journal of Hydrology*, 356(1-2), 147-162.
- Pierret, A., M. Kirby, and C. Moran (2003), Simultaneous X-ray imaging of plant root growth and water uptake in thin-slab systems, in *Roots: The Dynamic Interface between Plants and the Earth*, edited by J. Abe, pp. 361-373, Springer Netherlands.
- Pohlmeier, A., A. Oros-Peusquens, M. Javaux, M. I. Menzel, J. Vanderborght, J. Kaffanke, S. Romanzetti, J. Lindenmair, H. Vereecken, and N. J. Shah (2008), Changes in Soil Water Content Resulting from Ricinus Root Uptake Monitored by Magnetic Resonance Imaging *Vadose Zone J.*, 7(3), 1010-1017.
- Pratt, W. K. (1991), *Digital Image Processing*, John Wiley & Sons, Inc., New York.
- Prusinkiewicz, P., A. Lindenmayer, and J. Hanan (1990), *The Algorithmic beauty of plants* 228 pp., Springer-Verlag, New York.
- Puértolas, J., R. Alcobendas, J. J. Alarcón, and I. C. Dodd (2013), Long-distance abscisic acid signalling under different vertical soil moisture gradients depends on bulk root water potential and average soil water content in the root zone, *Plant, Cell & Environment*, 36(8), 1465-1475.
- Richards, L. A. (1931), Capillary conduction of liquids through porous mediums, *Physics-a Journal of General and Applied Physics*, 1(1), 318-333.
- Rockwell, F. E., J. K. Wheeler, and N. M. Holbrook (2014), Cavitation and Its Discontents: Opportunities for Resolving Current Controversies, *Plant Physiol.*, 164(4), 1649-1660.
- Rodriguez-Iturbe, I., and A. Porporato (2005), *Ecohydrology of water-controlled ecosystems : soil and moisture and plant dynamics*, XVIII, 442 S. pp., Cambridge Univ. Press, Cambridge.
- Rodriguez-Iturbe, I., A. Porporato, F. Laio, and L. Ridolfi (2001), Plants in water-controlled ecosystems: active role in hydrologic processes and response to water stress: I. Scope and general outline, *Advances in Water Resources*, 24(7), 695-705.
- Rogiers, S. Y., D. H. Greer, J. M. Hatfield, R. J. Hutton, S. J. Clarke, P. A. Hutchinson, and A. Somers (2012), Stomatal response of an anisohydric grapevine cultivar to evaporative demand, available soil moisture and abscisic acid, *Tree Physiol.*, 32(3), 249-261.
- Romero, P., I. C. Dodd, and A. Martinez-Cutillas (2012), Contrasting physiological effects of partial root zone drying in field-grown grapevine (*Vitis vinifera* L. cv. Monastrell) according to total soil water availability, *Journal of Experimental Botany*, 63(11), 4071-4083.
- Römheld, V., and H. Marschner (1990), Genotypical differences among graminaceous species in release of phytosiderophores and uptake of iron phytosiderophores, *Plant and Soil*, 123(2), 147-153.
- Rudin, L. I., S. Osher, and E. Fatemi (1992), Nonlinear total variation based noise removal algorithms, *Physica D: Nonlinear Phenomena*, 60(1-4), 259-268.
- Sade, N., and M. Moshelion (2014), The dynamic isohydric-anisohydric behavior of plants upon fruit development: taking a risk for the next generation, *Tree Physiol.*
- Schneider, C. L., S. Attinger, J. O. Delfs, and A. Hildebrandt (2010), Implementing small scale processes at the soil-plant interface - the role of root architectures for calculating root water uptake profiles, *Hydrology and Earth System Sciences*, 14(2), 279-289.
- Schroder, N., M. Javaux, J. Vanderborght, B. Steffen, and H. Vereecken (2012), Effect of Root Water and Solute Uptake on Apparent Soil Dispersivity: A Simulation Study, *Vadose Zone Journal*, 11(3).
- Schröder, N., N. Lazarovitch, J. Vanderborght, H. Vereecken, and M. Javaux (2013), Linking transpiration reduction to rhizosphere salinity using a 3D coupled soil-plant model, *Plant and Soil*, 1-17.
- Schroder, T., M. Javaux, J. Vanderborght, B. Korfgem, and H. Vereecken (2009), Implementation of a Microscopic Soil-Root Hydraulic Conductivity Drop Function in a Three-Dimensional Soil-Root Architecture Water Transfer Model, *Vadose Zone Journal*, 8(3), 783-792.

- Schurr, U., T. Gollan, and E. D. Schulze (1992), Stomatal response to drying soil in relation to changes in the xylem sap composition of *helianthus-annuus* .2. Stomatal sensitivity to abscisic-acid imported from the xylem sap, *Plant Cell Environ.*, 15(5), 561-567.
- Simonneau, T., P. Barrieu, and F. Tardieu (1998), Accumulation rate of ABA in detached maize roots correlates with root water potential regardless of age and branching order, *Plant Cell Environ.*, 21(11), 1113-1122.
- Simunek, J., K. Huang, and M. T. Van Genuchten (1995), The SWMS-3D code for simulating water flow and solute transport in three-dimensional variably-saturated media. US Salinity Laboratory, *Agricultural Research Service, US Department of Agriculture, Riverside, California*.
- Somma, F., J. W. Hopmans, and V. Clausnitzer (1998), Transient three-dimensional modeling of soil water and solute transport with simultaneous root growth, root water and nutrient uptake, *Plant and Soil*, 202(2), 281-293.
- Stedle, E. (2000), Water uptake by plant roots: an integration of views, *Plant and Soil*, 226(1), 45-56.
- Stedle, E., and C. A. Peterson (1998), How does water get through roots?, *Journal of Experimental Botany*, 49(322), 775-788.
- Stingaciu, L., H. Schulz, A. Pohlmeier, S. Behnke, H. Zilken, M. Javaux, and H. Vereecken (2013), In Situ Root System Architecture Extraction from Magnetic Resonance Imaging for Water Uptake Modeling, *Vadose Zone Journal*, 12(1).
- Stoll, M., B. Loveys, and P. Dry (2000), Hormonal changes induced by partial rootzone drying of irrigated grapevine, *Journal of Experimental Botany*, 51(350), 1627-1634.
- Taiz, L., and E. Zeiger (2006), *Plant physiology / Lincoln Taiz ; Eduardo Zeiger*, 4th ed. ed., XXVI, 764 S. pp., Sinauer, Sunderland, Mass.
- Tardieu, F., and W. J. Davies (1993), INTEGRATION OF HYDRAULIC AND CHEMICAL SIGNALING IN THE CONTROL OF STOMATAL CONDUCTANCE AND WATER STATUS OF DROUGHTED PLANTS, *Plant Cell Environ.*, 16(4), 341-349.
- Tardieu, F., and T. Simonneau (1998), Variability among species of stomatal control under fluctuating soil water status and evaporative demand: modelling isohydric and anisohydric behaviours, *Journal of Experimental Botany*, 49, 419-432.
- Tardieu, F., J. Zhang, and D. J. G. Gowing (1993), STOMATAL CONTROL BY BOTH ABA IN THE XYLEM SAP AND LEAF WATER STATUS - A TEST OF A MODEL FOR DROUGHTED OR ABA-FED FIELD-GROWN MAIZE, *Plant Cell Environ.*, 16(4), 413-420.
- Tyree, M. T. (1997), The Cohesion-Tension theory of sap ascent: current controversies, *Journal of Experimental Botany*, 48(315), 1753-1765.
- van den Honert, T. (1948), Water transport in plants as a catenary process, *Discussions of the Faraday Society*, 3, 146-153.
- Van Genuchten, M. T. (1980), A CLOSED FORM EQUATION FOR PREDICTING THE HYDRAULIC CONDUCTIVITY OF UNSATURATED SOILS, *Soil Science Society of America Journal*, 44(5), 892-898.
- van Lier, Q. d. J., K. Metselaar, and J. C. van Dam (2006), Root Water Extraction and Limiting Soil Hydraulic Conditions Estimated by Numerical Simulation, *Vadose Zone Journal*, 5(4), 1264-1264.
- Vandoorne, B., L. Beff, S. Lutts, and M. Javaux (2012), Root Water Uptake Dynamics of *Cichorium intybus* var. *sativum* Under Water-Limited Conditions, *Vadose Zone Journal*, 11(3).
- Vereecken, H., J. A. Huisman, H. Bogena, J. Vanderborght, J. A. Vrugt, and J. W. Hopmans (2008), On the value of soil moisture measurements in vadose zone hydrology: A review, *Water Resources Research*, 44(4), W00D06.
- Vetterlein, D., H. Marschner, and R. Horn (1993), Microtensiometer technique for in situ measurement of soil matric potential and root water extraction from a sandy soil, *Plant and Soil*, 149(2), 263-273.
- Vetterlein, D., K. Szegedi, J. Ackermann, J. Mattusch, H.-U. Neue, H. Tanneberg, and R. Jahn (2007), Competitive Mobilization of Phosphate and Arsenate Associated with Goethite by Root Activity All rights reserved. No part of this periodical may be reproduced or transmitted in any form or by any means, electronic or mechanical, including photocopying, recording, or any information storage and

- retrieval system, without permission in writing from the publisher, *J. Environ. Qual.*, 36(6), 1811-1820.
- Wan, X. C., and J. J. Zwiazek (2001), Root water flow and leaf stomatal conductance in aspen (*Populus tremuloides*) seedlings treated with abscisic acid, *Planta*, 213(5), 741-747.
- Weaver, J. E., J. Kramer, and M. Reed (1924), Development of Root and Shoot of Winter Wheat Under Field Environment, *Ecology*, 5(1), 26-50.
- Wilkinson, S., and W. J. Davies (1997), Xylem sap pH increase: A drought signal received at the apoplastic face of the guard cell that involves the suppression of saturable abscisic acid uptake by the epidermal symplast, *Plant Physiol.*, 113(2), 559-573.
- Wilson, J. B. (1988), A Review of Evidence on the Control of Shoot: Root Ratio, in Relation to Models, *Annals of Botany*, 61(4), 433-449.
- Wolf, O., W. D. Jeschke, and W. Hartung (1990), LONG-DISTANCE TRANSPORT OF ABSCISIC-ACID IN NaCl-TREATED INTACT PLANTS OF LUPINUS-ALBUS, *Journal of Experimental Botany*, 41(226), 593-600.
- Yin, X., and H. H. van Laar (2005), *Crop systems dynamics : an ecophysiological simulation model for genotype-by-environment interactions / Xinyou Yin ; H. H. van Laar*, 155 S. pp., Academic Publishers, Wageningen.
- Zarebanadkouki, M., and A. Carminati (2014), Reduced root water uptake after drying and rewetting, *Journal of Plant Nutrition and Soil Science*, 177(2), 227-236.
- Zarebanadkouki, M., Y. X. Kim, A. B. Moradi, H. J. Vogel, A. Kaestner, and A. Carminati (2012), Quantification and Modeling of Local Root Water Uptake Using Neutron Radiography and Deuterated Water, *Vadose Zone Journal*, 11(3).
- Zimmermann, U., H. Schneider, L. H. Wegner, and A. Haase (2004), Water ascent in tall trees: does evolution of land plants rely on a highly metastable state?, *New Phytologist*, 162(3), 575-615.
- Zwieniecki, M. A., M. V. Thompson, and N. M. Holbrook (2002), Understanding the hydraulics of porous pipes: Tradeoffs between water uptake and root length utilization, *Journal of Plant Growth Regulation*, 21(4), 315-323.

LIST OF TABLES

Table 2.1 Parameters for Eq. 2.1a - 2.3a and root hydraulic conductivities.....	23
Table 2.2 Parameters that were varied in the sensitivity analysis	23
Table 2.3 Soil hydraulic parameters of the Mualem van Genuchten equations	24
Table 3.1 Model setups, the sketches for the setup show the irrigated compartments.....	50
Table 3.2 Soil hydraulic parameters of the Mualem van Genuchten equation.....	51
Table 3.3 Parameterization for C and H+C controlled stomata	54
Table 4.1 X-ray settings for the different experimental setups	76
Table 4.2 Soil hydraulic parameters for the Mualem-van Genuchten expression.....	79
Table 4.3 Age dependent root axial conductance for the taproot and lateral roots	80
Table 4.4 Root length estimations from CT images and from destructive measurements	84
Table 4.5 Total root water uptake and water depletion in each soil compartment.....	93

LIST OF FIGURES

Figure 1.1 Water flow in the soil-plant-atmosphere continuum (SPAC)..... 4

Figure 1.2 Typical R-SWMS setup with a root grown within a cylindrical domain..... 6

Figure 1.3 Root growth adaptations 7

Figure 2.1 General behaviour of Eq. 2.2a over varying leaf water potentials..... 17

Figure 2.2 3D distribution of soil water content within the soil domain..... 25

Figure 2.3 Responses of the soil-root system..... 28

Figure 2.4 Concentration effect..... 29

Figure 2.5 Comparison of root xylem and soil water pressure heads..... 30

Figure 2.6 Transport effect..... 31

Figure 2.7 Sensitivity analysis of the parameters of Eq.2.2a 32

Figure 2.8 Partial rootzone drying with constant transpiration demand..... 34

Figure 2.9 Partial rootzone drying with transient transpiration demand 36

Figure 3.1 Schemes of the different split-root setups at steady state 44

Figure 3.2 Root length densities over depth of the domain..... 52

Figure 3.3 Relative transpiration rates at steady state 57

Figure 3.4 Comparison of leaf and root xylem water potential..... 61

Figure 3.5 Sensitivity analysis..... 64

Figure 3.6 Comparison between the two theoretical models 65

Figure 4.1 Schematic view of the experimental setup..... 74

Figure 4.2 Root system architectures at the end of the experiment..... 79

Figure 4.3 Measured plant traits over time..... 83

Figure 4.4 Cumulative water depletion from each compartment over time..... 86

Figure 4.5 Soil matric potentials for the three samples 89

Figure 4.6 Modelled water flow dynamics over time..... 92

Figure 4.7 Predawn water potential at the root collar 94

Figure 4.8 Influence of split layers on collar water potential 95

Figure A. 1 Influence of buffer size 105

Figure B. 1 Simulation domain for horizontal and vertical split setup..... 107

Figure B. 2 Gradients between leaf and root water potential 108

Figure B. 3 Signal production in the root system..... 109

Figure B. 4 Influence of ψ_{lim} on leaf and soil water potentials 110

Figure C. 1 Development of soil water pressure 111

Figure C. 2 Influence of paraffin layer on root growth 112

Figure C. 3 Water potential gradients gradient around the roots..... 113

Band / Volume 249

Quantitative Two-Layer Inversion and Customizable Sensor-Array Instrument for Electromagnetic Induction based Soil Conductivity Estimation

A. T. Mester (2015), viii, 119 pp

ISBN: 978-3-95806-035-7

Band / Volume 250

Partial Neutron Capture Cross Sections of Actinides using Cold Neutron Prompt Gamma Activation Analysis

C. Genreith (2015), vii, 166, XXXII pp

ISBN: 978-3-95806-036-4

Band / Volume 251

Long Term Aerosol Composition Measurements at the CESAR Tower at Cabauw, NL

P. Schlag (2015), iii, 228 pp

ISBN: 978-3-95806-037-1

Band / Volume 252

Modellbasierte Spezifikationsmethodik zur effizienten Systementwicklung von Brennstoffzellenantrieben

R. Biurrun Sotelo (2015), 255 pp

ISBN: 978-3-95806-038-8

Band / Volume 253

Three-dimensional ray-tracing simulations of convective gravity waves

S. Kalisch (2015), iii, 183 pp

ISBN: 978-3-95806-040-1

Band / Volume 254

First-Principles Study on Pyrites and Marcasites for Photovoltaic Application

T. Schena (2015), 206 pp

ISBN: 978-3-95806-041-8

Band / Volume 255

Glass-Ceramic Sealant Reinforcement for High-Temperature Applications

B. Cela Greven (2015), xi, 119 pp

ISBN: 978-3-95806-042-5

Band / Volume 256

Entwicklung planarer $\text{Ba}_{0,5}\text{Sr}_{0,5}\text{Co}_{0,8}\text{Fe}_{0,2}\text{O}_{3-\delta}$ -Membranmodule zur Sauerstoffabtrennung und Analyse ihres Transportverhaltens

P. Niehoff (2015), VIII, 134 pp

ISBN: 978-3-95806-044-9

Band / Volume 257

**Extension of the Reactor Dynamics Code MGT-3D
for Pebble-bed and Block-type High-Temperature-Reactors**

D. Shi (2015), x, 162 pp

ISBN: 978-3-95806-045-6

Band / Volume 258

Failure Analysis of Thin Film Solar Modules using Lock-in Thermography

M. Siegloch (2015), XIII, 131 pp

ISBN: 978-3-95806-047-0

Band / Volume 259

**Relation between growth rate, material quality, and device grade condition
for intrinsic microcrystalline silicon:**

From layer investigation to the application to thin-film tandem solar cells

S. Michard (2015), vi, 184 pp

ISBN: 978-3-95806-048-7

Band / Volume 260

**Quantitative analysis of spatially resolved electroluminescence
of Cu(In,Ga)Se₂ and a-Si:H thin-film solar cells and modules**

T. Tran (2015), iii, 161 pp

ISBN: 978-3-95806-050-0

Band / Volume 261

**Influence of the surface composition and morphology
on the reflectivity of diagnostic mirrors in a fusion reactor**

M. Matveeva (2015), 158 pp

ISBN: 978-3-95806-051-7

Band / Volume 262

**Very High Cycle Fatigue Behavior of Riblet Structured
High Strength Aluminum Alloy Thin Sheets**

S. Stille (2015), XII, 123 pp

ISBN: 978-3-95806-054-8

Band / Volume 263

**The role of soil heterogeneity on field scale evapotranspiration:
3D integrative modelling and upscaling of root water uptake**

K. Huber (2015), xii, 128 pp

ISBN: 978-3-95806-057-9